EVALUATION OF USING ECC AND CFRP FOR STRENGTHENING OF CONCRETE STRUCTURES

コンクリート構造物補強に ECC と CFRP を適用した場合の評価

By
Ahmed Mohamed Anwar Mahmoud

September 2009

EVALUATION OF USING ECC AND CFRP FOR STRENGTHENING OF CONCRETE STRUCTURES

コンクリート構造物補強に ECC と CFRP を適用した場合の評価

By

Ahmed Mohamed Anwar Mahmoud
September 2009

Thesis submitted to the United Graduate School of Agricultural Sciences for partial fulfillment of the requirements of the

Degree of Doctor of Philosophy
Production Environment Engineering – Concrete Technology
Bioenvironment Science course

Tottori University
Japan

<u>To Whom It May Concern</u>
We hereby certify that this is a typical copy of the original Thesis

OFFICIAL SEAL

Supervisor Professor
Professor Kunio HATTORI
Professor and Head of the Concrete Technology Laboratory

Professor Yoshinobu KITAMURA
Dean of the United Graduate School of Agricultural Sciences, Tottori University

EVALUATION OF USING ECC AND CFRP FOR STRENGTHENING OF CONCRETE STRUCTURES

コンクリート構造物補強に ECC と CFRP を適用した場合の評価

By

Ahmed Mohamed Anwar Mahmoud
September 2009

Thesis submitted to the United Graduate School of Agricultural Sciences for partial fulfillment of the requirements of the

Degree of Doctor of Philosophy
Production Environment Engineering – Concrete Technology
Bioenvironmental Science course

Tottori University
Japan

Approved by

Prof. Dr. Kunio HATTORI
Professor, Tottori University
(Main Supervisor)

Prof. Dr. Tsuguhiro NONAKA
Professor, Shimane University
(Examiner)

Prof. Dr. Isamu NATSUKA
Professor, Shimane University
(Examiner)

Dr. Hidehiko OGATA
Assoc. Professor, Tottori University
(Co-supervisor)

Dr. Masayuki ISHII
Assoc. Professor, Shimane University
(Co-supervisor)

Table of Contents

List of Figures and Photos

List of Tables

ACKNOWLEDGEMENT

Thanks equivalent to His supreme power, majesty, greatness, and sovereignty of ALLAH. Without the support and guidance of the Almighty ALLAH, the thesis would have never been finished and presented in a good shape. Thanks to Profit Mohammad – Peace be upon him for conveying the message of ALLAH that encourages people to perform their duties in the best way.

I would like to acknowledge and extend my heartfelt gratitude to ***Prof. Hattori Kunio***, not only for his fruitful suggestions, beneficial discussions, his proof reading of thesis, and for the much information I have gained from him, but also, because of his fatherhood, continuous support, invaluable guidance to all students in his laboratory.

My due respect goes to ***Dr. Ogata Hedihiko*** for his support in both theoretical and experimental work. His friendly behavior makes it easy to explore and exchange many ideas and clues that benefit me a lot. Thanks for his help and his extended inspiration.

Thanks form the bottom of my heart to ***Dr. Ishii Masayuki,*** his continuous support, nice ideas and discussions were giving me big potential to pursue my research in a good way. He was always providing me with constructive suggestions, and upholding my achievements during my study period.

It is also important to recognize the support provided by my Laboratory mates; ***Dr. Ashraf Muhammad***, ***Dr. Ajay Goyal, Dr. Mandula,*** and ***Mrs. Cleopatra*** for their sincere efforts, assistance during the experimental work, and for their vital encouragement and support.

Deep gratitude and best regards goes to my Egyptian former supervisor, ***Prof. Hesham Elshazly***, who always appear to be a man of principles. His guidance, advices and continuous support during being in either Egypt or Japan are really much appreciated. A lot of experience was gained on his hands.

I am immensely thankful to ***Mrs. Hayashi Asami*** for her exerted efforts and sincere help. In spite of her busy schedule, she was finding time to facilitate any kind of difficulties, affording help in communicating and dealing with Japanese people.

Gratitude to my late friend ***Dr. Khaled Hassan*** for his kind companionship on his occasionally stays in Tottori. Appreciation to ***Dr. Ahmed Khalil*** for his proof reading to parts of the thesis.

I would also wish to acknowledge all my Japanese colleagues, Egyptian and international friends in Tottori University for their continuous support and encouragements.

Respect and salute faced by all Tottori university staff were much appreciated. Thanks and gratitude goes to the **NIHON KOEI Ltd.** and **YONEYAMA Rotary club** for their partial financial support during my research period in Japan.

I won't forget to express my deep salutation to my institute in Egypt. I gained a lot of experience throughout participating in many local and international projects under its supervision. Of course, all these have influenced positively in my current research.

Special acknowledgement and deep thanks are due to my family, their continuous prayers, encouragements, inspiration were my real support during staying and studying in Japan.

To My Mother, Father, Sister, and to my beloved country Egypt

CHAPTER 1

1. INTRODUCTION AND GENERAL OVERVIEW

1.1 INTRODUCTION

Concrete is one of the most important materials being used in building industry. Recently, Egypt is suffering from the deterioration and aging problems of its concrete structures. Concrete is being used to serve a variety of structures such as hydraulic, residential, and industrial structures. Deterioration of hydraulic structures is one of the critical problems in Egypt (Tawfik A.E., 2003). This is due to the formation of hydraulic structures in big masses and along wide sections of the river Nile. Moreover, the presence of these structures in harmful atmosphere in addition to many structural and aging problems led the Egyptian government to further research in the field of protection, maintenance and rehabilitation of concrete structures in general and hydraulic structures in particular.

The thesis provides guidance on evaluating and identifying degradations in concrete as well as investigating and proposing some advanced techniques for strengthening and retrofitting of concrete structures. The following is a brief introduction about the main causes of deterioration in concrete as well as methods to increase its durability and consequently extend its life-span to a further longer time.

Deterioration of concrete is an extremely complex subject. It would be simplistic to suggest that it is impossible to identify a specific, single cause of deterioration for every symptom detected during an evaluation of a structure. In most cases, the damage detected will be the result of more than one mechanism. For example, corrosion of reinforcing steel may open cracks that allow moisture greater access to the interior of the concrete. This moisture could lead to additional damage by freezing and thawing. In spite of the complexity of several causes working simultaneously, given a basic understanding of the various damage causing mechanisms, it should be possible, in most cases, to determine the primary cause or causes of the damage seen on a particular structure and to make intelligent choices concerning selection of repair materials and methods.

Preventing concrete deterioration is much easier and more economical than repairing deteriorated concrete. Preventing concrete deterioration should actually begin with the selection of proper materials, mixture proportions, and placement and curing procedures. Of course, all potential hazards to concrete cannot always be predicted, and some well-engineered techniques and procedures may prove unsuccessful. Thus, there is generally a need for follow-up maintenance action. The primary types of maintenance for concrete include timely repair of cracks and spalls, cleaning of concrete to remove unsightly material, surface protection, and joint restoration.

Evaluation of concrete condition may include a review of design and construction documents, a review of structural instrumentation data, a visual examination, nondestructive testing (NDT), and laboratory analysis of concrete samples. Upon completion of the evaluation phase, personnel making the evaluation should have a thorough understanding of the condition of the concrete and may have insights into the causes of any deterioration noted. Once the evaluation of a structure has been completed, the visual observations and other supporting data must be related to the mechanism or mechanisms that caused the damage. Since many deficiencies are caused by more than one mechanism, a basic understanding of causes of deterioration of concrete is needed to determine the actual damage-causing mechanism for a particular structure.

Selection of appropriate repair materials and methods should be based and related to the mechanisms that caused the damage. The diversified amount of repairing materials, the experience of the engineer as well as the compatibility of the repair/strengthening material with the base substrates are factors affecting significantly the selection of repair method.

1.2 EVALUATION OF CONCRETE CONDITION

1.2.1 Laboratory Investigations

Once samples of concrete have been obtained, whether by coring or by other means, they should be examined in a qualified laboratory. In general, the examination should include petrographic, chemical, or physical tests. Each of these examinations is described as below:

a. Petrographic examination

Petrographic examination is the application of petrography, a branch of geology concerned with the description and classification of rocks, to the examination of hardened concrete, a synthetic sedimentary rock. Petrographic examination may include visual inspection of the samples, visual inspection at various levels of magnification using appropriate microscopes, X-ray diffraction analysis, and differential thermal Analysis, X-ray emission techniques, and thin section analysis. Petrographic techniques may be expected to provide information on the following (ACI 207.3R): (1) condition of the aggregate, (2) pronounced cement-aggregate reactions, (3) deterioration of aggregate particles in place, (4) denseness of cement paste, (5) homogeneity of the concrete, (6) occurrence of settlement and bleeding of fresh concrete, (7) depth and extent of carbonation, (8) occurrence and distribution of fractures, (9) characteristics and distribution of voids, and (10) presence of contaminating substances. Petrographic examination of hardened concrete should be performed in accordance with ASTM C 856 (CRD-C 57) by a person qualified by education and experience so that proper interpretation of test results can be made.

b. Chemical analysis

Chemical analysis of hardened concrete or of selected portions (paste, mortar, aggregate, reaction products, etc.) may be used to estimate the cement content, original water-cement ratio, and the presence and amount of chloride and other admixtures.

c. Physical analysis

The following physical and mechanical tests are generally performed on concrete cores:

(1) Density, (2) Compressive strength, (3) Modulus of elasticity, (4) Poisson's ratio, (5) Pulse velocity, (6) Direct shear strength of concrete bonded to foundation rock, (7) Friction sliding of concrete on foundation rock, (8) Resistance of concrete to deterioration caused by freezing and thawing, and (9) Air content and parameters of the air-void system.

Testing core samples for compressive strength and tensile strength should follow the method specified in ASTM C 42/42M-04 (CRD-C 27).

1.2.2 Analytical Investigations

Numerical methods are considered the fastest and cheapest analysis that could simulate the concrete structures. The simulation could show and illustrate the causes and expected locations of cracks as well as evaluating the enhancement and the feasibility of strengthening and rehabilitation process. Analytical methods are much effective in analyzing the behavior of the hydraulic structures under normal or excess load suggested by the engineer. For this reason, it is a powerful tool in the designing phase, and sometimes very good in showing the positions of cracks and weakness location caused by extra stresses. This kind of simulation requires a very good experience in judging the output results and comparing with the real condition.

1.2.3 Nondestructive Testing

The purpose of Nondestructive testing (NDT) is to determine the various relative properties of concrete such as strength, modulus of elasticity, homogeneity, and integrity, as well as conditions of strain and stress, without damaging the structure. Selection of the most applicable method or methods of testing will require good judgment based on the information needed, size and nature of the project, site conditions and risk to the structure (ACI 207.3R). Proper utilization of NDT requires a "toolbox" of techniques and someone with the expertise to know the proper tool to use in the various circumstances. In this paragraph, the commonly used nondestructive testing techniques for evaluating in situ concrete will be discussed. Malhotra (1991), Thornton and Alexander (1987), and Alexander (1993) provide additional information on NDT techniques. Also, recent advances in nondestructive testing of concrete are summarized by Carino (1992). Test methods are classified into those used to assess in-place strength and those used to locate hidden defects. In the first category, recent developments are presented on the pullout test, the break-off test, the torque test, the pull-off test, and the maturity method. In the second category, a review is presented of infrared thermography, ground penetrating radar, and several methods based upon stress wave propagation.

1.2.4 Field Inspection

A visual inspection of the exposed concrete is the first step in an on-site examination of a structure. The purpose of such an examination is to locate and define areas of distress or deterioration.

It is important that the conditions observed be described in unambiguous terms that can later be understood by others who have not inspected the concrete.

A thorough review of all of the pertinent data relating to a structure should be accomplished early in the evaluation process. To understand the current condition of the concrete in a structure, it is imperative to consider how design, construction, operation, and maintenance have interacted over the years since the structure was designed and constructed. Sources of engineering data which can yield useful information of this nature include project design memoranda, plans and specifications, construction history reports, as-built drawings, concrete report or concrete records (including materials used, batch plant and field inspection records, and laboratory test data), instrumentation data, operation and maintenance records, and periodic inspection reports. Instrumentation data and monument survey data to detect movement of the structure should be examined.

A condition survey involves visual examination of exposed concrete for the purpose of identifying and defining areas of distress. A condition survey will usually include a mapping of the various types of concrete deficiencies that may be found, such as cracking, surface problems (disintegration and spalling), and joint deterioration. Cracks are usually mapped on fold-out sketches of the monolith surfaces. Mapping must include inspection and delineating of pipe and electrical galleries, filling and emptying culverts (if possible), and other similar openings. Additionally, a condition survey will frequently include core drilling to obtain specimens for laboratory testing and analysis. Stowe and Thornton (1984), and American Concrete Institute (ACI) 207.3R provide additional information on procedures for conducting condition surveys.

1.2.6 Underwater Inspection

A variety of procedures and equipment for conducting underwater surveys are available (Popovics and McDonald 1989). Included are several nondestructive techniques which can be used in dark or turbid conditions that preclude visual inspection. Some techniques originally developed for other purposes have been adapted for application in underwater inspections. Prior to an underwater survey, it is sometimes necessary for the surface of the structure to be cleaned. A number of procedures and devices for underwater cleaning of civil works structures are described by Keeney (1987).

a. Visual inspection by divers

Underwater surveys by divers are usually either scuba or surface-supplied diving operations.

<u>(1) Advantages:</u> Underwater inspections performed by divers offer a number of advantages: they are (a) applicable to a wide variety of structures; (b) flexible inspection procedures; (c) simple (especially the scuba diver in shallow-water applications); and in most cases, (d) relatively

inexpensive. Also, a variety of commercially available instruments for testing concrete above water have been modified for underwater use by divers. These instruments include a rebound hammer to provide data on concrete surface hardness, a magnetic reinforcing steel locator to locate and measure the amount of concrete cover over the reinforcement, and direct and indirect ultrasonic pulse-velocity systems which can be used to determine the general condition of concrete based on sound velocity measurements (Malhotra, 1991).

(2) Limitations: Limitations on diver inspections include the regulations (EM 385-1-1) that restrict the allowable depths and durations of dives and the number of repeat dives in a given period. Also, in turbid water a diver's visibility may be reduced to only near distances. Also, cold climates tend to reduce the diver's ability to perform at normal levels. In any case, a diver's visual, auditory, tactile, and spatial perceptions are different underwater from what they are in air. Therefore, he is susceptible to making errors in observations and recording data.

b. Manned and unmanned underwater vehicles

Underwater vehicles can be thought of as platformed, underwater camera systems with manipulator and propulsion systems. They consist of a video unit, a power source for propulsion, vehicle controllers (referred to as "joysticks"), and display monitor. Available accessories which allow the vehicles to be more functional include angle lens, lighting components, and instrumentations for analyses, attachments for grasping, and a variety of other capabilities.

Underwater vehicles can compensate for the limitations inherent in diver systems because they can function at extreme depths, remain underwater for long durations, and repeatedly perform the same mission without sacrifice in quality. Also, they can be operated in environments where water temperatures, currents, and tidal conditions preclude the use of divers.

Underwater vehicles are being increasingly accepted as a viable means to effectively perform underwater surveys in practically all instances where traditional diver systems are normally used. Manned underwater vehicles have been used in the inspection of stilling basins, in direct support of divers, and in support of personnel maintaining and repairing wellheads. Applications include inspection of dams, breakwaters, jetties, concrete platforms, pipelines, sewers, mine shafts, ship hulls, etc. (Busby Associates, Inc. 1987). They have also been used in leak detection and structure cleaning.

c. High-resolution acoustic mapping system

Erosion and faulting of submerged surfaces have always been difficult to accurately map. To see into depressions and close to vertical surfaces requires a narrow beam. Also, there is a need to record exactly where a mapping system is located at any instant so that defects may be precisely located and continuity maintained in repeat surveys. The system can be broken into three main components: the acoustic subsystem, a positioning subsystem, and a compute-and-record subsystem. The acoustic subsystem consists of a boat-mounted transducer array and the signal processing electronics. During a survey, each transducer generates acoustic signals which are reflected from the bottom surface and received at the transducer array. The time of flight for the acoustic signal from the transducer to the bottom surface and back is output to a computer. The computer calculates the elevation of the bottom surface from this information, and the basic data are recorded on magnetic disks.

d. Side-scan sonar

The side-scan sonar, which evolved from the echo sounding depth finders developed during World War II, basically consists of a pair of transducers mounted in a waterproof housing referred to as a “fish,” a graphic chart-recorder set up for signal transmission and processing, and tow cable which connects the “fish” and recorder. The system directs sound waves at a target surface. The reflected signals are received by the transducers and transmitted to the chart-recorder as plotted images. The recorded image, called a sonograph, is characterized by various shades of darkened areas, or shadows, on the chart. Characteristics of the reflecting surface are indicated by the intensity of the reflected signals. Steel will reflect a more intense signal and produce a darker shaded area than wood, and gravel will reflect a more intense signal than sand. Acoustic shadows, shades of white, are projected directly behind the reflecting surface. The width of these shadows and the position of the object relative to the tow fish are used to calculate the height of the object. Electronic advances in the side-scan sonar have broadened its potential applications to include underwater surveying. In the normal position, the system looks at vertical surfaces. However, it can be configured to look downward at horizontal surfaces in a manner similar to that of the high-resolution acoustic mapping system. The side-scan sonar is known for its photograph-like image.

1.3 CAUSES OF DISTRESS AND DETERIORATION OF CONCRETE

1.3.1 Environmental

This section describes problems caused by water, wind, salt, biology, and environment as agents causing deterioration. Concrete may differ in nature from other materials like ceramic, brick, plastics and many other industrial materials. The reasons for that can be explained as follow; concrete as a material is pored and cured in nature, i.e. many environmental condition like temperature, humidity, and rains, …etc. can effect the final product and may cause a little drift than the target or the expected product (perhaps the quality control indoor is highly than outdoor), the second reason comes from the fact that concrete is left for many years in the surrounding condition whether it is harmful or not. So, such porous material could be affected by severe environment conditions; the following conditions are the most important : a) water, the depth of water varies from structure to another, either for small underground part only expressed in the foundation like residential building or a big part of the structure could be embedded like the case of hydraulic structures, and sometimes the whole structure is embedded in water like the case of tunnels that crosses under water, this water could have different characteristics varying from fresh water with small amount of salts and harmful materials to as much as the sea water or waste water that contains a lot of harmful diseases and much amount of dissolved salts. Water could easily penetrate to the concrete causing rusting of the reinforcement and consequently, damage to the cover. Also water containing harmful substances could harm the concrete itself causing deterioration and damage. Water also has a bad effect on concrete if its level is fluctuating continuously which will lead to several dry and wet cycle for the concrete causing corrosion of reinforcement as well as deterioration of concrete. b) Wind has a great effect on concrete structure, that is because the wind especially in arid and semi arid places where wind could easy carry small particles like sand, the problem is when these fine particles hit the concrete structure with high speed, small holes and cavitations might be found. By that way, the concrete cover will be damaged, and the concrete structure durability would be decreased. c) Dissolved salts and harmful particles dissolved in water, this kind of problems has a great and direct effect in the deterioration of the concrete structure; it can affect the steel bars causing rust to them and consequently decrease of the capacity of the structure which will lead to decrease the life time of the structure. The influence is also extended to the concrete as a material affected by the salts and sulfuric acid dissolved in water. d) Temperature; Most probably, hydraulic structures are characterized by its massive sections, thus it is very important to take the effect of the temperature into account, this is because the variation in temperature between the middle and the edge of big sections has great effect in formation of cracks, which will also lead to accelerate the speed of deterioration of that hydraulic structure. e) Water speed in the stream itself and the probability of occurring of cavitations could cause some erosion as well as some deterioration of the concrete cover which will finally lead to the corrosion of the reinforcement and the degradation of the structure integrity.

1.3.2 Structural

Deterioration of hydraulic structure might be caused due to structural reasons; this could be happened if the service load exceeds the maximum designed one, these could lead to formations of cracks and may cause collapse to the structure, this type of deterioration, might need a lot of studies, expenses for repairing to return the structure to its original state. Also, sometimes the need of making extensions or changing the purpose of the structure could make a lot of problems or troubles if not designed and constructed well.

1.3.4 Seismic

Seismic load is a very critical problem affecting the massive hydraulic structures, that is mainly because of the following reasons; a) the huge mass of those structures which will lead to increase the effect of the earthquake energy leading to high deformation and high straining actions, and b) the high aspect ratio between the length and the width of those structures, this is because the very long distance across the water stream to the small width of such structures, this geometry will lead to a very good resistance to the seismic forces in the longitudinal direction while a small resistance in the short direction due to the small inertia in that direction.

1.3.5 Chemical Attack

In general, deleterious chemical reactions may be classified as those that occur as the result of external chemicals attacking the concrete (acid attack, aggressive water attack, sulfate attack, and miscellaneous chemical attacks) or those that occur as a result of internal chemical reactions between the constituents of the concrete (alkali-silica and alkali-carbonate rock reactions). Examples of chemical reactions are described below:

i) Aggressive-water attack

Some waters have been reported to have extremely low concentrations of dissolved minerals. These soft or aggressive waters will leach calcium from cement paste or aggregates. This phenomenon has been infrequently reported in the United States. From the few cases that have been reported, there are indications that this attack takes place very slowly. For an aggressive water attack to have a serious effect on hydraulic structures, the attack must occur in flowing water. This keeps a constant supply of aggressive water in contact with the concrete and washes away aggregate particles that become loosened as a result of leaching of the paste.

ii) Alkali-carbonate rock reaction

Certain carbonate rock aggregates have been reactive in concrete. The results of these reactions have been characterized as ranging from beneficial to destructive. The destructive category is apparently limited to reactions with impure dolomitic aggregates and are a result of either dedolomitization or rim-silicification reactions. The mechanism of alkali-carbonate rock reaction is covered in detail in EM 1110-2-2002.

iii) Alkali-silica reaction

Some aggregates containing silica that is soluble in highly alkaline solutions may react to form a solid non-expansive calcium-alkali-silica complex or an alkali-silica complex which can imbibe considerable amounts of water and then expand, disrupting the concrete. Additional details may be found in EM 1110-2-2002.

iv) Sulfate attack

Naturally occurring sulfates of sodium, potassium, calcium, or magnesium are sometimes found in soil or in solution in ground water adjacent to concrete structures. The sulfate ions in solution will attack the concrete. There are apparently two chemical reactions involved in sulfate attack on concrete. First, the sulfate reacts with free calcium hydroxide which is liberated during the hydration of the cement to form calcium sulfate (gypsum). Next, the gypsum combines with hydrated calcium aluminate to form calcium sulfoaluminate (ettringite). Both of these reactions result in an increase in volume. The second reaction is mainly responsible for most of the disruption caused by volume increase of the concrete (ACI 201.2R). In addition to the two chemical reactions, there may also be a purely physical phenomenon in which the growth of crystals of sulfate salts disrupts the concrete.

v) Miscellaneous chemical attack

Concrete will resist chemical attack to varying degrees, depending upon the exact nature of the chemical. ACI 515.1R includes an extensive listing of the resistance of concrete to various chemicals. To produce significant attack on concrete, most chemicals must be in solution that is above some minimum concentration. Concrete is seldom attacked by solid dry chemicals. Also, for maximum effect, the chemical solution needs to be circulated in contact with the concrete. Concrete subjected to aggressive solutions under positive differential pressure is particularly vulnerable. The pressure gradients tend to force the aggressive solutions into the matrix. If the low-pressure face of the concrete is exposed to evaporation, a concentration of salts tends to accumulate at that face, resulting in increased attack. In addition to the specific nature of the chemical involved, the degree to which concrete resists attack depends upon the temperature of the aggressive solution, the w/c of the concrete, the type of cement used (in some circumstances), the degree of consolidation of the concrete, the permeability of the concrete, the degree of wetting and drying of the chemical on the concrete, and the extent of chemically induced corrosion of the reinforcing steel.

1.4 REPAIR AND STRENGTHENING OF CONCRETE

This section contains description of various materials and methods that are available for repair and strengthening of concrete structures. Emmons (1993) provides a discussion of materials and methods for concrete repair with extensive, detailed illustrations. The following are among the main considerations before starting the repair phase; 1) the condition of the substrate concrete surface, whether it is smooth or rough, wet or dry, 2) making sure that the inferior concrete surface has been removed, and 3) the damaged or deteriorated material embedded in concrete should also be removed and the concrete surface should be well cleaned. The following are among the most used materials for repair or strengthening of concrete structures:

1.4.1 Additional Reinforcement

Additional reinforcement is the provision of additional reinforcing steel, either conventional reinforcement or prestressing steel, to repair a cracked concrete section. In either case, the steel that is added is to carry the tensile forces that have caused cracking in the concrete. For example, cracked reinforced concrete bridge girders have been successfully repaired by use of additional conventional reinforcement (EM 1110-2-2002, 1995). Post tensioning is often the desirable solution when a major portion of a member must be strengthened or when the cracks that have formed must be closed. For the post tensioning method, some form of abutment is needed for anchorage, such as a strong back bolted to the face of the concrete, or the tendons can be passed through and anchored in connecting framing.

1.4.2 Conventional Concrete Placement

This method consists of replacing defective concrete with a new conventional concrete mixture of suitable proportions that will become an integral part of the base concrete. The concrete mixture proportions must provide for good workability, strength, and durability. The repair concrete should have a low w/c ratio and a high percentage of coarse aggregate to minimize shrinkage cracking. If the defects in the structure go entirely through a wall or if the defects go beyond the reinforcement and if the defective area is large, then concrete replacement is the desired method. Replacement is sometimes necessary to repair large areas of honeycomb in new construction.

Conventional concrete should not be used for replacement in areas where an aggressive factor which has caused the deterioration of the concrete being replaced still exists.

1.4.3 Crack Arrest Techniques

Crack arrest techniques are those procedures that may be used during the construction of a massive concrete structure to stop crack propagation into subsequent concrete lifts. These techniques should be used only for cracking caused by restrained volume change of the concrete. They should not be used for cracking caused by excessive loading.

The simplest technique is to place a grid of reinforcing steel over the cracked area. The reinforcing steel should be surrounded by conventional concrete rather than the mass concrete being used in the structure.

1.4.4 Drilling and Plugging

Drilling and plugging a crack consists of drilling down the length of the crack and grouting it to form a key. This technique is applicable only where cracks run in reasonably straight lines and are accessible at one end. This method is most often used to repair vertical cracks in walls.

1.4.5 Dry Packing

Dry packing is a process of ramming or tamping into a confined area a low water-content mortar. Because of the low w/c material, there is little shrinkage, and the patch remains tight and is of good quality with respect to durability, strength, and water tightness. This technique has an advantage in that no special equipment is required. However, the method does require that the craftsman making the repair be skilled in this particular type of work. Dry packing can be used for patching rock pockets, form tie holes, and small holes with a relatively high ratio of depth to area. It should not be used for patching shallow depressions where lateral restraint cannot be obtained, for patching areas requiring filling in back of exposed reinforcement, nor for patching holes extending entirely through concrete sections. Dry packing can also be used for filling narrow slots cut for the repair of dormant cracks. The use of dry pack is not recommended for filling or repairing active cracks.

1.4.6 Fiber-Reinforced Concrete

Fiber-reinforced concrete is composed of conventional Portland-cement concrete containing discontinuous discrete fibers. The fibers are added to the concrete in the mixer. Fibers are made of steel, plastic, glass, and other natural materials. A convenient numerical parameter describing a fiber is its aspect ratio, defined as the fiber length divided by an equivalent fiber diameter. Fiber-reinforced concrete has been used extensively for pavement repair. Fiber-reinforced concrete has been used to repair erosion of hydraulic structures caused by cavitation or high velocity flow and impact of large debris. However, laboratory tests and field experience show that the abrasion-erosion resistance of fiber-reinforced concrete is significantly less than that of conventional concrete with the same w/c and aggregate type (EM 1110-2-2002).

1.4.7 Flexible Sealing

Flexible sealing involves routing and cleaning the crack and filling it with a suitable field molded flexible sealant. This technique differs from routing and sealing in that, in this case, an actual joint is constructed, rather than a crack simply being filled. Flexible sealing may be used to repair major, active cracks. It has been successfully used in situations in which there is a limited water head on the crack. This repair technique does not increase the structural capacity of the cracked section.

1.4.8 Grouting (Chemical)

Chemical grouts consist of solutions of two or more chemicals that react to form a gel or solid precipitate as opposed to cement grouts that consist of suspensions of solid particles in a fluid. The reaction in the solution may be either chemical or physicochemical and may involve only the constituents of the solution or may include the interaction of the constituents of the solution with other substances encountered in the use of the grout. The reaction causes a decrease in fluidity and a tendency to solidify and fill voids in the material into which the grout has been injected. Cracks in concrete as narrow as 0.05 mm (0.002 in.) have been filled with chemical grout. The advantages of chemical grouts include their applicability in moist environments, wide limits of control of gel time, and their application in very fine fractures. Disadvantages are the high degree of skill needed for satisfactory use, their lack of strength, and, for some grouts, the requirement that the grout not dry out in service. Also some grouts are highly inflammable and cannot be used in enclosed spaces.

1.4.9 Grouting (Hydraulic-Cement)

Hydraulic-cement grouting is simply the use of a grout that depends upon the hydration of Portland cement, Portland cement plus slag, or pozzolans such as fly ash for strength gain. These grouts may be sanded or unsanded (neat) as required by the particular application. Various chemical admixtures are typically included in the grout. Latex additives are sometimes used to improve bond. Hydraulic-cement grouts may be used to seal dormant cracks, to bond subsequent lifts of concrete that are being used as a repair material, or to fill voids around and under concrete structures. Hydraulic-cement grouts are generally less expensive than chemical grouts and are better suited for large volume applications. Hydraulic cement grout has a tendency to separate under pressure and thus prevent 100 percent filling of the crack. Normally the crack width at the point of introduction should be at least 3 mm. Also, if the crack cannot be confined on all sides, the repair may be only partially effective. Hydraulic-cement grouts are also used extensively for foundation sealing and treatments during new construction.

1.4.10 Jacketing

Jacketing consists of restoring or increasing the section of an existing member (principally a compression member) by encasing it in new concrete. The original member need not be concrete; steel and timber sections can be jacketed. The most frequent use of jacketing is in the repair of piling that has been damaged by impact or is disintegrating because of environmental conditions.

It is especially useful where all or a portion of the section to be repaired is underwater. When properly applied, jacketing will strengthen the repaired member as well as provide some degree of protection against further deterioration.

1.4.11 Precast Concrete

Precast concrete is concrete cast elsewhere than its final position. The use of precast concrete in repair and replacement of structures has increased significantly in recent years and the trend is expected to continue. Compared with cast-in-place concrete, precasting offers a number of advantages including ease of construction, rapid construction, high quality, durability, and economy. Typical applications of precast concrete in repair or replacement of civil works structures include navigation locks, dams, channels, floodwalls, coastal structures, marine structures, bridges, culverts, tunnels, retaining walls, and highway pavement.

1.4.12 Preplaced-Aggregate Concrete

Preplaced-aggregate concrete is produced by placing coarse aggregate in a form and then later injecting a Portland-cement-sand grout, usually with admixtures, to fill the voids. As the grout is pumped into the forms, it will fill the voids, displacing any water, and form a concrete mass. Typically, preplaced-aggregate concrete is used on large repair projects, particularly where underwater concrete placement is required or when conventional placing of concrete would be difficult. Typical applications have included underwater repair of stilling basins, bridge piers, abutments, and footings. The advantages of using preplaced-aggregate concrete include low shrinkage because of the point-to-point aggregate contact, ability to displace water from forms as the grout is being placed, and the capability to work around a large number of block outs in the placement area.

1.4.13 Rapid-Hardening Cements

Rapid-hardening cements are defined as those that can develop a minimum compressive strength of 20 MPa (3,000 psi) within 8 hr or less. The types of rapid-hardening cements and patching materials available and their properties are described in REMR Technical Note CS-MR-7.3 (USAEWES 1985g). A specification for prepackaged, dry, rapid-hardening materials is given in ASTM C 928/C928M.

1.4.14 Shotcrete

Shotcrete is mortar pneumatically projected at high velocity onto a surface. Shotcrete can contain coarse aggregate, fibers, and admixtures. Properly applied shotcrete is a structurally adequate and durable repair material that is capable of excellent bond with existing concrete or other construction materials. Shotcrete has been used to repair deteriorated concrete bridges, buildings, lock walls, dams, and other hydraulic structures. The performance of shotcrete repair has generally been good. However, there are some instances of poor performance. Major causes of poor performance include inadequate preparation of the old surface and poor application techniques by inexperienced personnel. Satisfactory shotcrete repair is contingent upon proper surface treatment of old surfaces to which the shotcrete is being applied. In a repair project where thin repair sections (less than 150 mm deep) and large surface areas with irregular contours are involved, shotcrete is generally more economical than conventional concrete because of the saving in forming costs. Most shotcrete mixtures have a high cement and therefore a greater potential for drying shrinkage cracking compared to conventional concrete. Also, the overall quality is sensitive to the quality of workmanship.

1.4.15 Stitching

This method involves drilling holes on both sides of the crack and grouting in stitching dogs (U-shaped metal units with short legs) that span the crack. Stitching may be used when tensile strength must be reestablished across major cracks. Stitching a crack tends to stiffen the structure, and the stiffening may accentuate the overall structural restraint, causing the concrete to crack elsewhere. Therefore, it may be necessary to strengthen the adjacent section with external reinforcement embedded in a suitable overlay.

1.4.16 Underwater Concrete Repair

A large part of the cost of repairing the underwater portions of concrete structures is devoted to dewatering the structure so conventional concrete-placing techniques can be used. A review of the state-of-the-art techniques for concrete surface preparation underwater and underwater repair suggested that concrete could be effectively placed underwater by pumping when newly developed anti-washout admixtures were used and, thus, the dewatering cost could be eliminated. Concrete mixtures usually developed in the laboratory using these new admixtures to minimize the reduction in concrete quality that is normally associated with the placement of concrete underwater. In addition, several repair concepts (for example, use of precast elements) and various underwater concrete placement techniques (inclined tremie, pumping, etc.) were identified.

1.4.16.1 Underwater concrete placement

Underwater concrete placement is simply placing fresh concrete underwater with a number of well recognized techniques and precautions to ensure the integrity of the concrete in place. Concrete is typically placed underwater by use of a tremie or a pump. The quality of cast-in-place concrete can be enhanced by the addition of an anti-washout admixture which increases the cohesiveness of the concrete. Flat and durable concrete surfaces with in-place strengths and densities essentially the same as those of concrete cast and consolidated above water can be obtained with proper mixture proportioning and underwater placement procedures.

1.4.16.2 Applicability and limitations.

(1) Placing concrete underwater is a suitable repair method for filling voids around and under concrete structures. Voids ranging from a few cubic yards to thousands of cubic yards have been filled with tremie concrete. Concrete pumped underwater or placed by tremie has also been used to repair abrasion-erosion damage on several structures (EM 1110-2-2002). Another specialized

use of concrete placed underwater is in the construction of a positive cutoff wall through an earthfill dam.

(2) There are two significant limitations on the use of concrete placed underwater. First, the flow of water through the placement site should be minimized while the concrete is being placed and is gaining enough strength to resist being washed out of place or segregated. One approach that may be used to protect small areas is to use top form plates under which concrete may be pumped.

The designer, contractor, and inspectors must all be thoroughly familiar with underwater placements. Placing concrete underwater is not a procedure that all contractors and inspectors are routinely familiar with since it is not done as frequently as other placement techniques. The only way to prevent problems and to ensure a successful placement is to review, in detail, all aspects of the placement (concrete proportions, placing equipment, placing procedures, and inspection plans) well before commencing the placement.

1.5 OVERVIEW ON HYDRAULIC STRUCTURES PROBLEMS IN EGYPT

Egypt has, since time immemorial, been described as the “gift of the river Nile”, and so it is not surprising that management of water resources has been central to all aspects of national strategy. Its reliance on the Nile is reflected in the fact that 90% of the population lives on 5% of the land area around the stem of the river Nile and the Delta. Along the river Nile, many concrete structures have been constructed to regulate the flow of water, control the discharges, and to adjust the water levels. Egypt had started its prescribed plan in 1902 by constructing the Aswan reservoir, followed by Assuit barrage on the same year, then old Esna barrage in 1908, and lastly the construction of the High Aswan dam in 1968 (Tawfik A.E., 2003). There are mainly twelve big regulators along the river Nile. These structures are diversified in their concrete dimensions, shape and applied forces, according to their purposes. Moreover, many of these structures have already passed over 100 years of age. Thus, the Egyptian government is paying much attention for keeping these structures in a good health and to extend their life time to a further longer time. Replacing a concrete hydraulic structure is not an easy job. Usually, it consumes long time in constructing new structures, removing the old one with a much extra costs. In addition, longer time will be taken, a lot of environmental problems due to the disposal of the old structures might also occur, huge amount of auxiliary works might also be needed, etc…

Recently and due to the insufficient amount of the existing produced electric energy; the Egyptian government is thinking to make use of the head difference between upper and down streams of the current regulators to generate more energy necessary for the agriculture purposes at each district (Tawfik A.E., 2003). This could be done by installing some turbines in the current existing hydraulic structures and this will consequently lead to a further research in the field of strengthening and repair of these structures.

1.6 OBJECTIVES OF THE STUDY

The thesis main objectives are to identify new methods and techniques used to maintain, strengthen, and rehabilitate deteriorated hydraulic structures. More concentration has been placed on the evaluation and strengthening of regulators, the most commonly used structure along the river Nile. In this study, different components of the regulator will be studied such as, the arched part connecting piers together, beams, and the portions containing grooves of the piers. Thus, the main objectives of the thesis can be summarized as follow:

1. Having a better understanding of the cause of concrete distress and deterioration.
2. Identification and evaluation of existing cracks in concrete structures.
3. Strengthening and repair of different structural components of hydraulic structures using modern techniques.

1.7 Guided Tour

The thesis consists of 8 chapters; the overall purpose is to gain further knowledge about problems of hydraulic concrete structures as well as introducing new methods for strengthening and repairing of the deteriorated parts of these structures. The following are summary for the chapters:

***Chapter 1*:** General background and brief illustration about problems and deterioration facing the concrete structures. Special focus on problems accompanied to hydraulic structures in Egypt. This chapter also, includes ways to inspect and evaluate hydraulic concrete structures, causes of deteriorations, and conventional ways for repairing of these structures.

***Chapter 2*:** Introduction of a new approach for crack detection in concrete structures using ultrasonic pulse velocity (UPV) test. The method was applied on initially cracked members with different shapes and sizes.

***Chapter 3*:** Evaluation of using engineered cementitious composites (ECC) in strengthening of flexural elements such as beams. Combinations of using both ECC and carbon fiber reinforced polymers (CFRP) were also applied on small and big size beams. Contact stresses were also evaluated for cases of pasting CFRP sheets on both concrete and ECC substrates.

***Chapter 4*:** Repairing of pre-cracked concrete members using ECC and CFRP was conducted. Contrast with conventional used methods in repairing was also shown.

***Chapter 5*:** Scaled down plain concrete arched specimens with different strengthening conditions using CFRP were destructively tested. The ductility for each combination was calculated and compared. The optimum strengthening condition was then determined experimentally.

***Chapter 6*:** Different strengthening combinations for short columns containing grooves were conducted using CFRP. The chapter also includes introduction of a new expression for estimating the strength of columns wrapped with CFRP.

Chapter 7: Summery of thesis, conclusions and recommendations for further works are given.

Chapter 8: Japanese translation of the summary of thesis is given.

CHAPTER 2

2. CRACK DETECTION IN CONCRETE USING UPV – NEW APPROACH

2.1 INTRODUCTION

Among non-destructive testing (NDT) of structure, ultrasonic pulse velocity (UPV) test is considered an effective tools used for structure health monitoring (BS 1881-part 203, 1986). The main idea of the test is to measure the traveling velocity in concrete. Actually, there is no unique relationship between the measured velocity and the strength of concrete but under specific conditions the two quantities are directly related (Neville, 1981). The determined velocity is function of many factors that identifies the homogeneity of the concrete; for example it is directly proportional to the concrete strength, and inversely proportion to the amount of voids in the specimen. The length of the specimen as well as the presence of large aggregates might affect the results.

UPV test is being used for surface crack depth determination and inspection of concrete quality for decades. Measuring crack depth as well as evaluating the condition of concrete structures – especially those of massive sections as in dams, piers, and bridges …etc. – nondestructively have become of great concern in recent years (Neville, 1981). Visual inspection requires a lot of experience and might give suggestions for the cause of cracks but might not give information about their depths. Destructive testing like coring is expensive, time consuming, increases structural defects and may only be applied in a limited locations. This consequently will not give a true representation of the real in-situ condition. Thus, using a promising NDT appears to be a suitable solution for that purpose. On the other hand, UPV test methods require qualified personnel with sufficient experience in the interpretation of survey results. It is also recommended to dry the area around crack from water as ultrasonic energy can travel through liquids causing errors in identifying the real crack depth (Malhotra and Cairno, 1991, Neville, 1981).

The current chapter shows a proposed new configuration utilizing UPV test to detect location of cracks in concrete with fine resolution. This method is not only suitable for concrete but it can also be applicable to determine defects in asphalt, and metals as well. The new approach aimed to define single ellipse corresponding to each UPV reading; the formed ellipse was then considered a locus for all points that can represent inner edge of the crack. Thus, the intersection of ellipses generated from different readings represents the other end of the crack. Four plain concrete specimens, 3 beams with different sizes in addition to an arched specimen, were prepared for examination. The specimens contained artificial cracks created by placing a separator in the moulds before casting of concrete. Encouraging results were achieved from specimens with flat and arched surfaces. However, precautions and sufficient experience are required when using the new approach with surfaces of high curvature.

The current research shows several advantages of the new method over the conventionally used methods; 1) the transducers can be placed on surfaces of different planes, 2) ability to detect inclined or embedded cracks, and 3) transducers can also be placed on arched surfaces. Conventionally used methods for crack determination such as 1) Tc-To method (Malhotra and Cairno, 1991), 2) Delta method (Ogata et al., 2006, Kewalramani, and Gupta, 2006), and 3) B.S. method (BS 1881-part 203, 1986) were also expressed and results were put into glance with their corresponding values obtained by the new method.

2.2 UPV – PRINCIPAL AND APPLICATIONS

The general principal of UPV test is that the transmission of wave takes the shortest path between the transmitter and the receiver. Thus, the receiving transducer detects the arrival of the component of the pulse that arrives earliest, which generally is the leading edge of the longitudinal vibration (Underwood and Kim, 2003). By measuring the traveling time, it is easy to determine how fast this wave travels. Although the direction in which the maximum energy propagates is at right angles to the face of the transmitting transducer, it is possible to detect pulses, which have traveled through concrete in some other directions. Moreover, when an ultrasonic pulse traveling through concrete meets a concrete-air interface there is negligible transmission of energy across this interface. Thus, any air filled void or crack lying immediately between the transducers will obstruct the ultrasonic pulse wave and the first pulse arriving at the receiving transducer will diffract around the periphery of the void and the transit time will be longer than in similar concrete with no void (Neville, 1981). Generally, the used transducers should be in the range of 20 to 150 kHz though frequencies as low as 10 kHz may be useful for very long concrete path lengths and as high as 1 MHz for mortars or for short path lengths (Underwood and Kim, 2003).

Many codes have recommended the use of UPV test as a tool for assessing deterioration in concrete, determining the crack depths, and estimating the thickness of the inferior quality layer in concrete (BS 1881-part 203, 1986, ASTM C597-83, 1991). Many researchers have also applied NDT for crack determination; Masato Abe et al. (2001) determined the location of horizontal sheet-like cracks by applying NDT on concrete specimens. Ogata et al. (2006) had applied weight factor to UPV readings for better identification of crack depth. Underwood and Kim (2003) made attempts to determine crack depth in asphalt pavements.

Furthermore, numerous attempts have been made to use the UPV as a measure to determine the compressive strength of concrete. Manish, and Rajiv (2006) had conducted UPV tests on different concrete mixes, the prediction was done using multiple regression analysis and artificial neural networks. Hisham Y.Q. (2000) had also derived formulas for better prediction of the concrete strength from UPV readings.

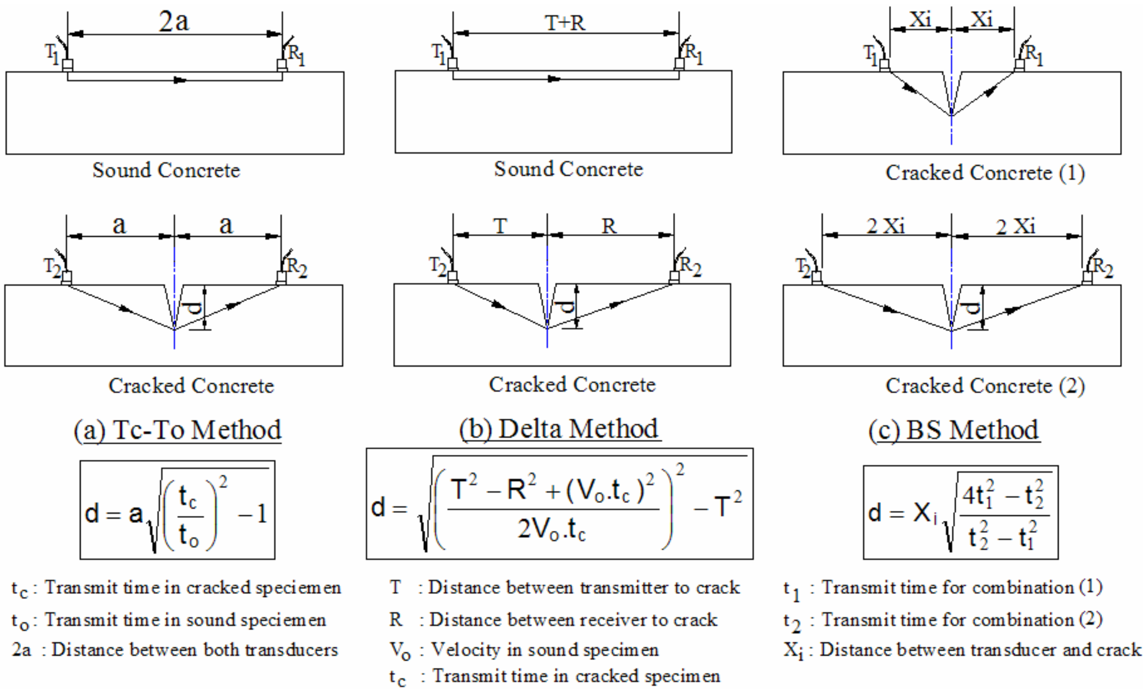

Figure 2.1: Schematic showing different conventional UPV methods used for crack detection

2.3 LITERATURE REVIEW

In the current chapter, results from the new approach were also verified with known methods such as 1) Tc-To method (L-L method), 2) Delta method, and 3) BS method. Figure1.1 shows the popular methods used for crack detection by UPV test.

2.3.1 Tc-To Method (L-L method)

In this method, both transducers are placed at equal distance (a) from the crack position. UPV test is applied twice along a distance of (2a) for both sound and cracked specimens. In both readings, the surface velocity (V_o) obtained from sound specimen and the velocity in the cracked specimens (V_c) are equalized and the crack depth can be calculated as;

$$d = a\sqrt{\left(\frac{t_c}{t_o}\right)^2 - 1} \tag{2.1}$$

Where,

d: is the crack depth, a: is the distance between any of the transducers and the crack center,

t_c: is the transmit time for signal to travel from transmitter to receiver in cracked specimen, and

t_o: is the corresponding time in a sound sample.

2.3.2 Delta Method

In this method same procedure of the T_c-T_o method is applied however, the transmitter and receiver were placed at different distances from the crack. The following equation was derived;

$$d = \sqrt{\left(\frac{T^2 - R^2 + (V_o.t_c)^2}{2V_o.t_c}\right)^2 - T^2} \qquad (2.2)$$

Where,

T: is the distance from the transmitter to the crack,

R: is the distance from crack to receiver,

V_o: is velocity in the sound specimen, and

t_c: is the transmit time in cracked specimen.

2.3.3 British Standard Method (BS Method)

In the BS method, the velocity of two successive UPV readings is equalized; where the transducers in the first reading are placed on half the distance used in the second one. For both readings, the transmitter and the receiver are placed equally from the crack. The following equation was derived;

$$d = X_i\sqrt{\frac{4t_1^2 - t_2^2}{t_2^2 - t_1^2}} \qquad (2.3)$$

Where,

X_i: is the distance between the edge of any of the transducers and the crack center, and

t_1 and t_2: are the transmit time for both combinations.

2.4 INSTRUMENTATION

UPV measuring equipment of PUNDIT type was used. The instrument consisted of a pulse generator and a pulse receiver; the pulses were generated by shock-exciting piezoelectric crystals housed in a stainless steel case transducer, with a resonant frequency of 50 kHz, and a similar transducer was used as a receiver. The transmitter was adopted to transform the electronic pulses into wave bursts of mechanical energy. The receiver changed the mechanical energy into electronic energy. The time of travel between the initial onset and the reception of the pulse was measured electronically. A thin layer of grease (couplant) was applied and the transducers were gently pressed against the concrete surface to ensure good acoustical contact. The transducers are adopted to be placed as per one of the following combinations: 1) in opposite sides (direct measure), 2) along same side (indirect measure), or 3) in two perpendicular surfaces (semi-direct), of the specimen. Photo 2.1 shows the used UPV device.

Photo 2.1: UPV meter

2.5 NEW APPROACH – THEORETICAL CONCEPT

In this section, numerical derivation of the proposed new method for crack detection is discussed. As well known, in cracked sections, UPV pulses take the shortest path between the transducers and around the crack, thus the timing device will detect the shortest traveling time (t_c). Assuming a constant pulse velocity in same concrete specimen (V_{avg}); this value can be determined by taking the average of many readings in sound parts near the crack position. The total travel distance (D) of the pulse signal can be determined by the following equation:

$$D = V_{avg} \times t_c \tag{2.4}$$

The total covered distance (D) can be expressed by two components; (i) distance from transmitter to the internal crack edge (L_1), and (ii) distance from the internal crack edge to the receiver (L_2). This can be represented as follow:

$$L_1 + L_2 = D = Constant \tag{2.5}$$

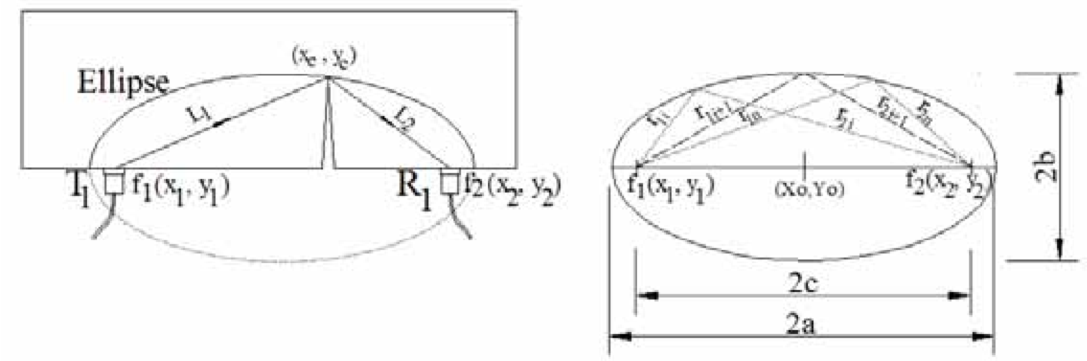

Figure 2.2: Expected UPV path in cracked section, and the corresponding formed ellipse

To solve Equation (2.5), and for only one UPV reading, infinite number of solutions can be suggested for L_1 and L_2. It was found that the locus of all points that satisfy Equation (2.5) can be represented by an ellipse. Ellipse can be defined as a curve that is the locus of all points in the plane, the sum of whose distances r_1 and r_2 from two fixed points f_1 and f_2 (the foci) separated by a distance of $2c$ is a given positive constant $2a$ (Ellipse definition - Mathworld). This results in the two-center bipolar coordinate Equation (2.6). Figure 2.2 shows a typical expected path of Ultrasonic pulse signal in cracked concrete structures and the corresponding generated ellipse.

$$\sum_{i=1}^{i=n}(r_{1i} + r_{2i}) = 2a = D \tag{2.6}$$

Where,
r_{1i} and r_{2i}: are the distances from the two foci to the ellipse surface, and
$2a$: is the longest axis of ellipse corresponding to the total distance covered by the pulse signal around the crack.

Moreover, for the generated ellipse, the distance between its foci ($2c$) will be corresponding to the distance between the two transducers and is given by:

$$2c = \sqrt{(X_1 - X_2)^2 + (Y_1 - Y_2)^2} \tag{2.7}$$

Where,
(X_1, Y_1), and (X_2, Y_2) are Cartesian coordinates of transmitter and receiver, respectively.
The shortest axis ($2b$) of the ellipse can be obtained from Equation (2.8), and the general equation of the formed ellipse can be written as shown in Equation (2.9).

$$b^2 \cong a^2 - c^2 \qquad (2.8)$$

$$\frac{(X - X_o)^2}{a^2} + \frac{(Y - Y_o)^2}{b^2} = 1 \qquad (2.9)$$

Where,

X_o, Y_o are the coordinates of the formed ellipse center, corresponding to the mid-point between the two transducers (foci).

Consequently, and as shown in Figure 2.3, if two or more readings are recorded; single ellipse can be formed for each reading and the intersection of these ellipses can represent the inner edge of the crack. Figure 2.3 shows also several configurations for the transducers where they can be placed at different planes on the same structure or even when cracks are not perpendicular to the measuring surface.

2.6 PRACTICAL EXPERIMENTS

To examine the adequacy of the new method for crack identification practically, four plain concrete specimens were prepared. The characteristic compressive strength of the used concrete was 40 N/mm^2. Two beams, B1 and B2, with dimensions of (length x depth x thickness) equal to (600 x 200 x 100 mm), one beam, B3, (400 x 100 x 100 mm), and one arched specimen, A1, having a curved soffit of radius 490 mm, were examined. Fig. 2.4 shows the geometry of all the examined specimens. Artificial cracks were produced by placing vertical separators at the bottom of the moulds before concrete casting. For A1, the crack was located at the arched soffit. The exact depths of cracks were measured by a caliber and were 62.5, 106.5, 61.0, and 63.0 mm for B1, B2, B3, and A1, respectively. For all the specimens, the cracks have a triangular shape with an opening width equal to 7.0 mm, except for B3; the opening width was measured to be 4.0 mm. After 28 days of water curing, the desired surfaces on each specimen were sufficiently smoothened and the UPV test was conducted. Ultrasonic velocity meter accompanying 50 kHz transducers was used. Thin layer of grease (couplant) was applied and the transducers were gently pressed against the concrete surface to ensure good acoustical contact.

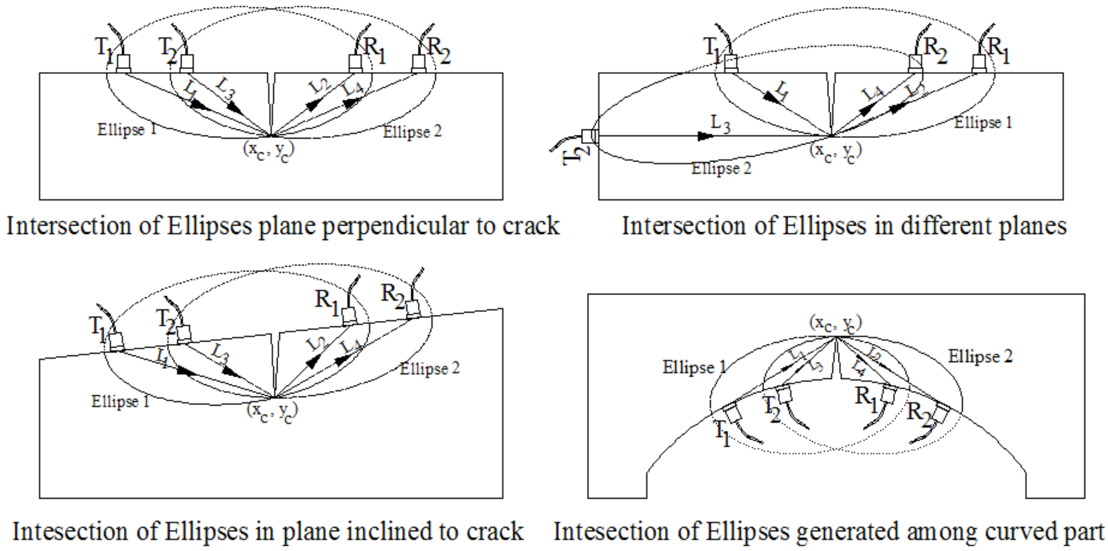

Figure 2.3: Arrangement of transducers among different shapes of structures

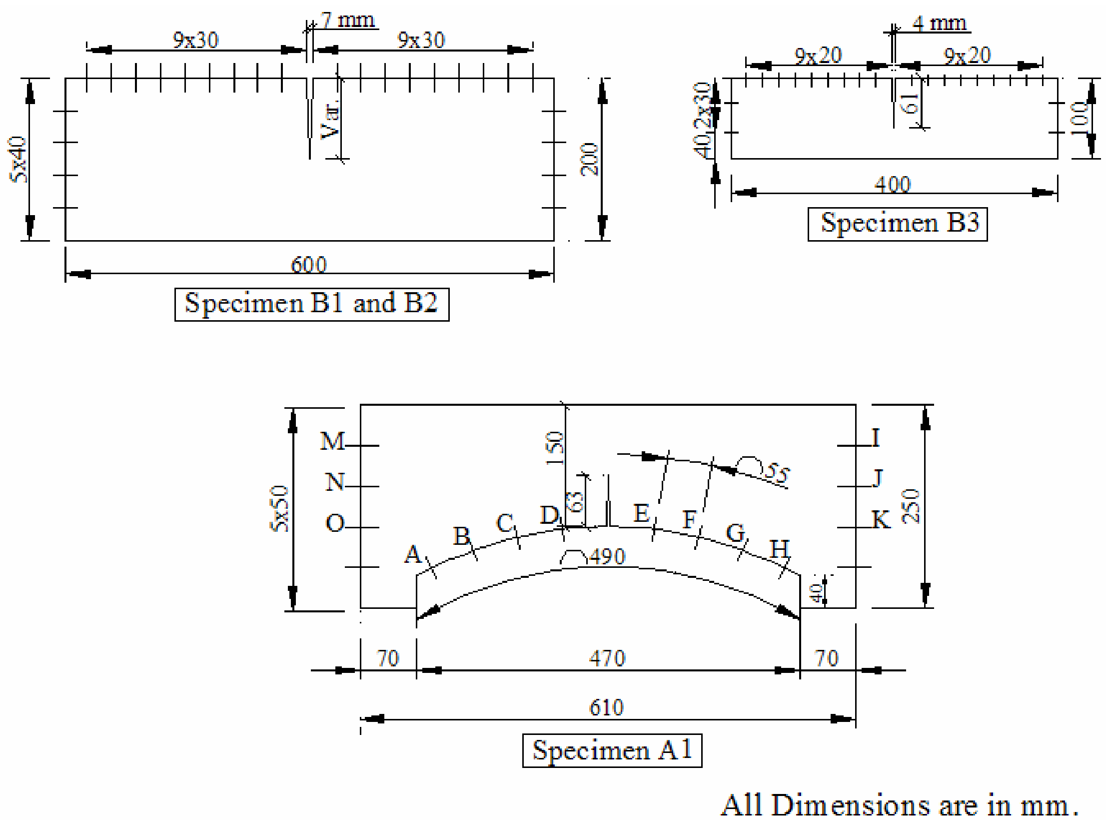

Figure 2.4: Typical detail for the used beams

Photo 2.2 a): Indirect transmission and, b): Semi-direct transmission for UPV test

For conducting UPV test, the cracked surface and sides of the specimens were marked at equal intervals – See Figure 2.4. For B1 and B2, and B3, the cracked surfaces were divided into spacing of 30, and 20 mm, respectively, on both sides from the crack edge, while the sides were divided into spacing of 40, and 30 mm, respectively. For A1, the soffit was divided into spacing of 55 mm, while the spacing along sides was adjusted to 50 mm. For B1 and B2, and B3, the marked divisions were given coordinates with respect to a virtual coordinate system placed at the mid-point of the top surface of the specimens, i.e. laid on the center of crack opening width. For A1, the desired marks were given nominations to facilitate dealing with the tested points on the arched surface (see Figure 2.4). Two combinations of UPV test readings were recorded; combination 1, corresponding to indirect transmission condition while combination 2, corresponding to semi-direct condition – see Photos 2.2a and b. More details will be given and explained later. Furthermore, for each specimen, a set of six UPV readings where transducers were placed in a direct transmission position across the thickness of the specimen were recorded and the average pulse velocity was determined. The measured average pulse velocities were 4.51, 4.51, 4.50, and 4.53 km/s for B1, B2, B3, and A1, respectively.

2.7 RESULTS AND DISCUSSION

2.7.1 Beams with Constant Cross-Section

At the beginning, general survey to approximate crack depth estimation was done by placing the transmitter and receiver at equal distances from the crack edges at the marked positions shown in Figure 2.4. For each reading, corresponding ellipse was drawn and the intersection of that ellipse with vertical line drawn from the crack center would determine the estimated depth of the crack. The obtained depths were plotted and shown in Figure 2.5; in which the vertical axis represents the estimated crack depth while the horizontal axis represents the equidistance of the transducers from crack edge. The plot shows slightly over estimation of the crack depth as transducers were placed near the crack edge, followed by a flat plateau with values very close to the actual depth.

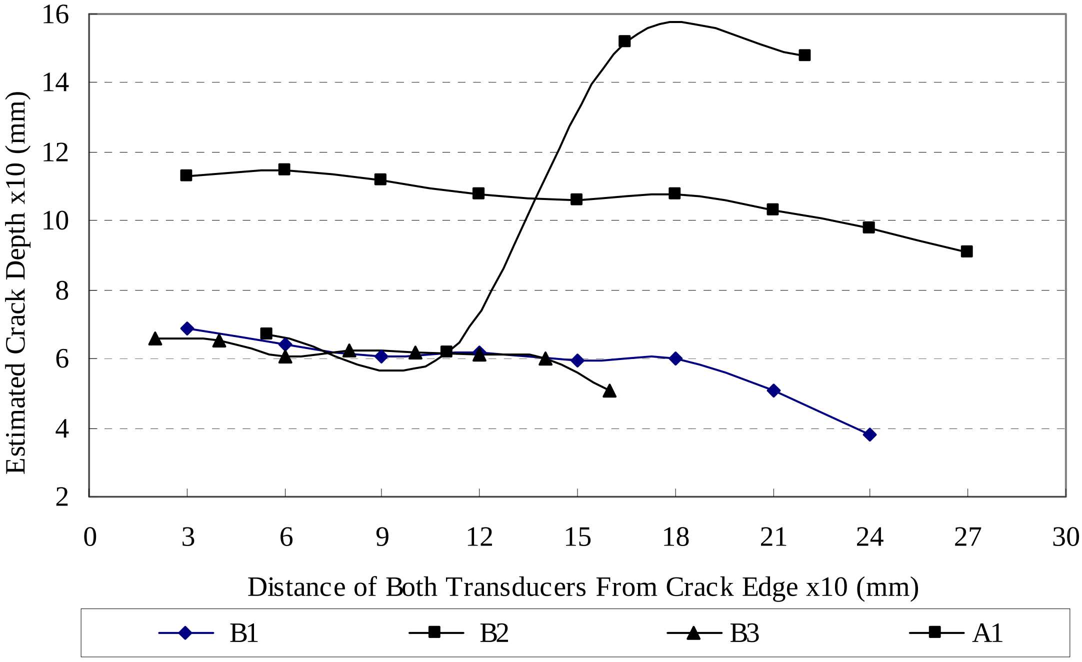

Figure 2.5: Relation between transducers equidistance from crack edge and estimated crack depth

The plot also shows a decrease in the estimated values of crack depth as transducers placed at far distances. The reason was that in the current research, a constant pulse frequency of 50 kHz with a corresponding wavelength of 90mm was used. At distances near the crack, the pulse wavelength was longer than the actual distance between the transmitter and the inner crack edge and consequently high values for the crack depth were obtained. It is known that in short distances, pulses of very high frequencies and short wavelengths with a clear defined onset are preferred to be used (Underwood and Kim, 2003). The flat plateau was considered as an optimal zone where the pulse was diffracted almost around the crack inner edge and reliable results can be obtained. The inaccuracy in estimating the crack depth at further far distances from the crack position might be because the longer the covered distance in concrete by the pulse, the more influence by the concrete mix proportions and erroneous readings might be expected.

2.7.1.1 Both transducers on upper surface (COMB1)

After determining the optimal zone for conducting UPV test, combinations of readings were recorded along this zone. The intersection of the formed ellipses from each pair of conjugate readings was determined. The transmitter and the receiver were first placed at an unequal distances from the crack followed by reversing these distances, i.e. if the transmitter and the receiver were placed at 60 and 90 mm, respectively, in different sides from the crack then in the second configuration the distances were reversed and the transmitter and the receiver were placed at 90 and 60 mm from the crack, respectively. The average was also determined so that error could be minimized. Tables 2.1 through 2.3 show the estimated crack depths based on surface readings only (COMB1) for beam B1, B2, and B3, respectively. In the first rows of these tables, results from placing the transducers at equal distances from crack were shown. The rest of the tables were results obtained from placing transducers at conjugate locations consecutively. Half the crack opening width was added to all the transducers coordinates of combination done on the flat surface beams. The tables also show a comparison with both Tc-To, and Delta methods.

Though, determining the crack depth by these methods can be obtained based on a single reading taken at the cracked specimen, it was thought that taking the average of the error of two or more readings could facilitate the comparison with results from the new method. The absolute values of errors obtained by the new method were between 0.7 – 6.8% for B1, 0.2 – 9.3% for B2, and 0.6 – 6.0% for B3. It was also noticed that the conventionally used methods were not always applicable for all the conducted combinations. Moreover, the percentage error by using B.S. method was also calculated and it was found between 1.6 – 16.8% for B1, 8.0 – 16.86% for B2, and 0.0 – 13.6% for B3.

Table 2.1: Estimated crack depth for beam B1 (COMB1)

Transducers Coordinates		New Method			Tc-To Method		Delta Method	
Transmitter	Receiver	Crack depth (mm)	Average crack depth (mm)	Error (%)	Crack depth (mm)	Error (%)	Crack depth (mm)	Error (%)
(-63.5,0)	(63.5,0)	64.1	61.4	-1.7	59.5	-3.8	N.A.*	N.A.
(-93.5,0)	(93.5,0)	60.6			56.9			
(-123.5,0)	(123.5,0)	61.6			69.7			
(-153.5,0)	(153.5,0)	59.5			54.4			
(-63.5,0)	(93.5,0)	61.8	60.5	-3.2	N.A.	N.A.	58.9	-8.5
(-93.5,0)	(63.5,0)	59.2					55.5	
(-63.5,0)	(123.5,0)	65.4	63.7	1.9			62.2	-4.9
(-123.5,0)	(63.5,0)	61.9					56.7	
(-63.5,0)	(153.5,0)	64.1	63.1	1.0			60.5	-7.65
(-153.5,0)	(63.5,0)	62.1					55.0	
(-93.5,0)	(123.5,0)	58.7	58.2	-6.8			53.9	-15.5
(-123.5,0)	(93.5,0)	57.8					51.7	
(-93.5,0)	(153.5,0)	59.1	60.4	-3.4			53.8	-14.0
(-153.5,0)	(93.5,0)	61.6					53.7	
(-123.5,0)	(153.5,0)	56.6	62.1	-0.7			49.0	-13.2
(-153.5,0)	(123.5,0)	67.6					59.5	

****N.A.: The method is not applicable***

Table 2.2: Estimated crack depth for beam B2 (COMB1)

Transducers Coordinates		New Method			Tc-To Method		Delta Method	
Transmitter	Receiver	Crack depth (mm)	Average crack depth (mm)	Error (%)	Crack depth (mm)	Error (%)	Crack depth (mm)	Error (%)
(-93.5,0)	(93.5,0)	112.0	107.3	0.8	101.6	-3.0	N.A.*	N.A.
(-123.5,0)	(123.5,0)	107.8			100.2			
(-153.5,0)	(153.5,0)	105.9			95.3			
(-183.5,0)	(183.5,0)	107.9			105.2			
(-213.5,0)	(213.5,0)	107.3			115.4			
(-63.5,0)	(93.5,0)	113.4	116.4	9.3	N.A.	N.A.	113.1	8.95
(-93.5,0)	(63.5,0)	119.4					119.0	
(-93.5,0)	(123.5,0)	110.7	109.6	2.9			110.3	2.5
(-123.5,0)	(93.5,0)	108.5					108.0	
(-93.5,0)	(153.5,0)	108.4	107.5	1.0			107.9	0.5
(-153.5,0)	(93.5,0)	106.7					106.1	
(-93.5,0)	(183.5,0)	114.7	111.0	4.3			114.3	3.7
(-183.5,0)	(93.5,0)	107.0					106.6	
(-93.5,0)	(213.5,0)	111.0	108.1	1.5			110.4	0.8
(-213.5,0)	(93.5,0)	105.0					104.4	
(-123.5,0)	(153.5,0)	108.0	106.7	0.2			107.5	-0.3
(-153.5,0)	(123.5,0)	105.4					104.8	
(-123.5,0)	(183.5,0)	110.0	109.0	2.4			109.4	1.7
(-183.5,0)	(123.5,0)	108.0					107.3	
(-123.5,0)	(213.5,0)	109.1	107.5	0.9			108.5	-0.2
(-213.5,0)	(123.5,0)	105.8					104.9	
(-183.5,0)	(213.5,0)	107.2	106.3	-0.2			106.3	-1.1
(-213.5,0)	(183.5,0)	105.3					104.3	

***N.A.: The method is not applicable**

Table 2.3: Estimated crack depth for beam B3 (COMB1)

Transducers Coordinates		New Method			Tc-To Method		Delta Method	
Transmitter	Receiver	Crack depth (mm)	Average crack depth (mm)	Error (%)	Crack depth (mm)	Error (%)	Crack depth (mm)	Error (%)
(-62.0,0)	(62.0,0)	60.6	61.6	1.0	54.5	-8.6	N.A.*	N.A.
(-82.0,0)	(82.0,0)	62.4			58.3			
(-102.0,0)	(102.0,0)	62.1			52.9			
(-122.0,0)	(122.0,0)	61.1			57.3			

Transducers Coordinates		New Method			Tc-To Method		Delta Method	
Transmitter	Receiver	Crack depth (mm)	Average crack depth (mm)	Error (%)	Crack depth (mm)	Error (%)	Crack depth (mm)	Error (%)
(-62.0,0)	(82.0,0)	61.8	63.2	3.6	N.A.	N.A.	60.5	2.4
(-82.0,0)	(62.0,0)	64.5					63.0	
(-62.0,0)	(102.0,0)	59.4	64.6	6.0			75.5	12.2
(-102.0,0)	(62.0,0)	63.5					61.5	
(-62.0,0)	(122.0,0)	61.4	63.1	3.5			59.8	0.2
(-122.0,0)	(62.0,0)	64.9					62.4	
(-82.0,0)	(102.0,0)	65.8	64.6	6.0			64.0	2.7
(-102.0,0)	(82.0,0)	63.5					61.3	
(-82.0,0)	(122.0,0)	65.4	63.3	4.0			63.5	-0.1
(-122.0,0)	(82.0,0)	61.2					58.5	
(-102.0,0)	(122.0,0)	59.9	61.4	0.6			57.4	-3.9
(-122.0,0)	(102.0,0)	62.8					59.9	

N.A.: The method is not applicable

2.7.1.2 Transmitter on upper surface and receiver on side surface (COMB2)

Further arrangement for the transducers position was also conducted; the transmitter was kept on the cracked surface while the receiver was placed on the opposite vertical side of the specimen (COMB2). Tables 2.4 through 2.6 show the estimated crack depths based on readings from the second combination for both beams B1 and B2, respectively.

Table 2.4: Estimated crack depth for beam B1 (COMB2)

Transducers Coordinates		Average Crack depth (mm)	Error (%)
Transmitter	Receiver		
(-63.5,0)	(300,-4)	64.4	3.0
(63.5,0)	(-300,-4)		
(-63.5,0)	(300,-8)	63.3	1.3
(63.5,0)	(-300,-8)		
(-153.5,0)	(300,-4)	63.0	0.8
(153.5,0)	(-300,-4)		
(-153.5,0)	(300,-8)	65.5	4.8
(153.5,0)	(-300,-8)		

Table 2.5: Estimated crack depth for beam B2 (COMB2)

Transducers Coordinates		Average Crack depth (mm)	Error (%)
Transmitter	Receiver		
(-63.5,0)	(300,-4)	103.0	-3.3
(63.5,0)	(-300,-4)		
(-63.5,0)	(300,-8)	103.7	-2.6
(63.5,0)	(-300,-8)		
(-153.5,0)	(300,-4)	99.7	-6.4
(153.5,0)	(-300,-4)		
(-153.5,0)	(300,-8)	104.4	-2.0
(153.5,0)	(-300,-8)		

Table 2.6: Estimated crack depth for beam B3 (COMB2)

Transducers Coordinates		Average Crack depth (mm)	Error (%)
Transmitter	Receiver		
(-62.0,0)	(200,-3)	60.8	-0.3
(62.0,0)	(-200,-3)		
(-62.0,0)	(200,-6)	60.9	-0.2
(62.0,0)	(-200,-6)		
(-122.0,0)	(200,-3)	56.9	-6.7
(122.0,0)	(-200,-3)		
(-122.0,0)	(200,-6)	56.8	-6.9
(122.0,0)	(-200,-6)		

The results also show the adequacy of the new method when transducers were placed in different planes. The absolute values of the error were ranging from 0.8 – 4.8% for B1, 2.0 – 6.4% for B2, and 0.2 – 6.9% for B3. It was also obvious that the conventionally methods were again not capable to define the crack depth in this combination.

2.7.2 Arched Specimens

2.7.2.1 Both transducers on soffit surface (COMB1)

The new approach was also verified on surfaces with higher curvature. Arched specimen A1 was used for that purpose. At the beginning, transducers were placed on soffit at equidistance of interval 55 mm starting from the crack edge. For A1, the positions of both transducers were given notations and shown in Figure 2.4. The results obtained when transducers were placed on the cracked soffit (COMB1) are shown in Table 2.7. The first two rows of the table show a high percentage error when transducers were at far distances from crack. The following two rows – transducers were placed closer to the crack – show reasonable estimation for the crack depth.

At a distance close to the crack, slightly over estimation of the crack depth was obtained while at a little bit far distance, the optimal zone was achieved and the result was much better. It was noted that until this portion, results were not much affected by the curvature. Thus, combinations were conducted by placing the transducers at conjugate locations as done with the beams. Encouraging results were achieved and the new method was found adequate. When placing the transducers at further far distances from the crack, i.e. downwards, near the end of the curved soffit, higher estimation values for the crack depth were predicted, in contrast with flat surfaces – see Figure 2.5. The longer time recorded by the timing device would suggest either the longitudinal pulse had covered a longer distance rather than being reflected around the inner crack edge; or the receiver might detect another component of the pulse which is slower than the desired longitudinal wave.

Table 2.7: Estimated crack depth for A1 (COMB1)

Transducers Location		Crack depth (mm)	Average depth (mm)	Error (%)
Transmitter	Receiver			
A	H	148.0	148.0	134.9
B	G	152.0	152.0	141.3
C	F	62.0	62.0	-1.6
D	E	67.0	67.0	6.4
B	E	62.0	67.6	7.2
D	G	73.1		
C	E	60.2	62.7	-0.5
D	F	65.2		

Table 2.8: Estimated crack depth for A1 (COMB2)

Transducers Location		Crack depth (mm)	Average depth (mm)	Error (%)
Transmitter	Receiver			
D	I	67.0	66.5	5.6
E	M	66.0		
D	J	60.5	60.5	-4.0
E	N	60.5		
D	K	62.4	59.6	-5.4
E	O	56.8		
C	I	64.0	62.1	-1.4
F	M	60.2		
C	J	57.3	55.5	-11.9
F	N	53.7		
C	K	59.1	58.2	-7.6
F	O	57.3		
D	S	58.7	62.5	-0.8
E	T	66.3		
D	R	69.8	67.2	6.7
E	U	64.6		

Transducers Location		Crack depth (mm)	Average depth (mm)	Error (%)
Transmitter	Receiver			
C	S	71.2	66.0	4.7
F	T	60.7		
C	R	67.0	63.6	0.9
F	U	60.1		

However, after representing the solution graphically and based on the estimated average pulse velocity value, it was clearly noted that the generated ellipse almost cut the upper surface of the specimen, i.e. the longitudinal wave was reflected from the upper surface of the specimen. The above mentioned factors might lead to inaccuracy in detecting the exact crack depth from soffit readings based on records at very far distances from the crack edge.

2.7.2.2 Transmitter on soffit surface and receiver on side surface (COMB2)

Combinations between sides and soffit (COMB2) were conducted and shown in Table 2.8. It was clearly shown that the new method was also capable to predict the crack depth on curved surfaces with fine accuracy.

Finally, it was thought that utilizing many records would give better identification for the crack depth. Figure 2.6, shows a graphical representation for B1, and A1 where many readings were analyzed and solved together.

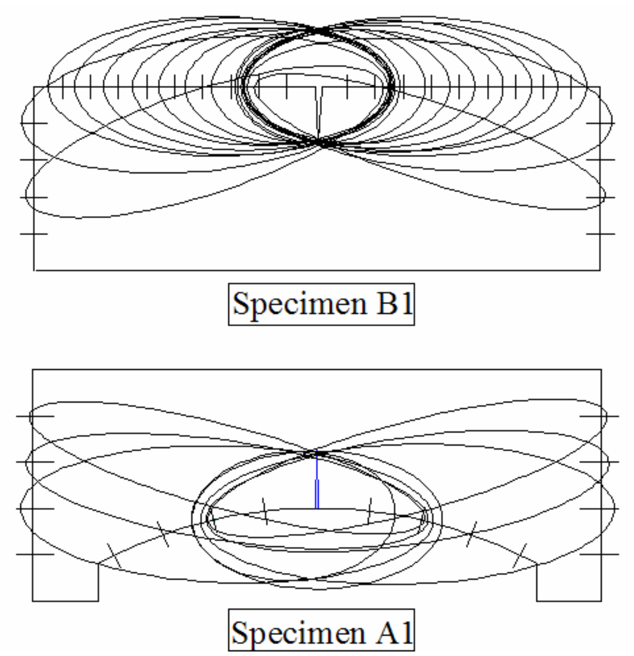

Figure 2.6: Utilizing many UPV readings

2.8 CONCLUSIONS

The current chapter explores a new method UPV based, for crack identification. The new approach was verified by utilizing the UPV readings recorded among three beams and one arched specimen made of concrete. Results were achieved with an acceptable percentage error. Moreover, results from conventional method were obtained and the contrast between them was shown. The followings findings were drawn:

(1) The new approach can be applied to determine vertical or inclined, surface or embedded cracks in concrete structures with flat or arched surfaces; however, sufficient experience is required with surfaces of high curvatures.

(2) According to current approach, crack depth can be identified from placing the transducers at different surfaces of concrete member at the same time.

(3) For rectangular prisms, the identification of crack depth was better than arched specimens. For prisms, errors based on one surface readings ranged from 0.2 to 9.3%, the corresponding values for arched specimen were between 0.5 to 141.3%.

(4) Identification of cracks based on semi-direct transmission was also effective in determining the crack depth. For prisms errors were ranged from 0.2 to 6.9%, while for arched specimens, the errors were ranged from 0.8 to 11.9%.

(5) Although the results in this paper were only based on the average of two UPV readings, it is thought that the accuracy could be enhanced if a set of more readings are processed together.

CHAPTER 3

3. COMPARATIVE STUDY ON USING CFRP AND ECC FOR STRENGTHENING OF CONCRETE BEAMS

3.1 INTRODUCTION

Carbon fiber reinforced polymers (CFRP) have been widely used to repair and strengthen concrete structures. Recently, CFRP have been found suitable both for research and practical disciplines. It was found adequate for repairing and strengthening of various structures such as concrete, steel, and wood (Shaun Hay et. al, 2006, Islam M.R. et. al, 2005, JCI TC952, 1998). It has been stated that CFRP offers several advantages over conventional materials, such as a superior strength/weight ratio, high stiffness, corrosion and chemical attack resistance, durability enhancement, saving in labor and material costs, and its high speed in installation and curing (Taehoon and Makarand, 2006, Maalej M. and Leong K.S., 2005). In the eighties of the last century, CFRP started to be implied for strengthening and repair of many concrete structures, (JCI TC952, 1998). CFRP can afford high tensile strength without adding extra weight to structure. Moreover, CFRP can be presented in the form of sheets that can be pasted externally without changing the structure geometry, (Islam et al., 2005).

The interfacial debonding of CFRP is considered the critical main failure mode, and probably governs the overall strength of the strengthened members (Gao et al. 2006). Attempts to minimize the occurrence of the debonding mode of failure were conducted; Xiong et al (2007) used U-shape fibre strips near the ends of the main CFRP sheet. Another group of researchers, Malek et al. (1998), Smith & Teng (2001) calculated the ultimate shear and normal stresses along the adhesive aiming to avoid reaching their failure limits.

The development of high performance fiber reinforced cementitious composites and particularly the engineered cementitious composites (ECC) by Li (2002), nearly two decades ago, attracted many researchers to utilize ECC for repairing and strengthening purposes. ECC is a class of high performance fiber reinforced cementitious composites (HPFRCC) and has a strain hardening behavior when exposed to tensile forces. It also exhibits a tensile strain capacity up to 200 times that of concrete (Maleej & Leong 2005). The many cracks with very small width are among its superior characteristics. ECC was recommended by many researchers as a repair material, Kanada et al (2002) used ECC in a spray form for rehabilitation of walls.

In the current chapter, CFRP sheets were simultaneously used with ECC for strengthening of concrete beams. A simple experiment was first conducted to examine the bonding efficiency of CFRP applied on the ECC substrate. The investigation showed that the bonding of CFRP on ECC was better than in the case of concrete substrates. The study expanded to evaluate the effect of ECC thickness, applied at the soffit of concrete beams, with and without strengthening by external CFRP sheets. Contrast in terms of the maximum load carrying capacity and the mode of failure for each combination was highlighted. It was noted that as the thickness of ECC increased, both the ductility and the section loading capacity increased as well. It was also shown that the change in the ECC thickness before additional strengthening with CFRP did not show a significant difference in the section loading capacity, it was, however, capable of preventing the occurrence of the undesirable interfacial mode of failure.

3.2 EXPERIMENTAL PROGRAM

3.2.1 Materials

The mix proportion for both concrete and ECC are shown in Tables 3.1 and 3.2, respectively. The concrete mix was designed as per the American Concrete Institute, ACI 211.1. ECC incorporates high modulus polyethylene fibers. The fiber length is 12.7 mm and diameter of 38 microm, tensile strength of 1,690 MPa and an elastic modulus of 40,600 MPa. A polycarboxylic-acid-based superplasticizer was used. A bio-saccharide type viscous agent was also applied to provide compatibility between fluidity and fiber dispersibility. In addition, an expansive agent and an alcohol-type shrinkage reducing agent were added. The commercially ready mixed ECC mixture was brought from Kajima Technical Research Institute in Japan (Kajima Corporation website). More details about the used ECC were reported by Kanda et al. (2006). The measured compressive and flexural strengths of concrete at 28 days were 40 MPa, and 6 MPa, respectively. The corresponding values for ECC were 27 MPa, and 9 MPa, respectively. As supplied by the manufacturer, the used unidirectional CFRP sheets were of 0.111 mm thickness, tensile strength of 3,400 MPa and modulus of elasticity of 3,400 MPa. The bonding epoxy has flexural strength of 40 MPa, tensile strength of 30 MPa and shear strength of 10 MPa. Unidirectional CFRP sheet was applied at the soffit of beams using two compounds epoxy resin. Tables 3.3 and 3.4 show the physical properties of the used CFRP sheets and the epoxy resin. The same materials were used elsewhere in the thesis unless otherwise is mentioned.

Table 3.1: Mix proportions of concrete

Maximum aggregate size (mm)	**Slump (mm)**	**Air Content (%)**	**W/C (%)**	**S/A (%)**	**Unit content (kg/m^3)**			
					Water	**Cement**	**Sand**	**Gravel**
20	100	2	54	38	200	370	650	1,056

Table 3.2: Mix proportions of ECC per unit volume

Ready mixed powder (Kg)	**Water (Kg)**	**W/C (%)**	**Fiber volume fraction (%)**	**Supper plasticizer (Kg)**	**Anti-Shrinkage agent (Kg)**	**Surface active agent* (Kg)**	**Slump Flow (mm)**	**Air Content (%)**
1,562	350	46	2	16.9	15.3	3.1	500	10$\pm$4

* Diluted with 24 times of water mass

Table 3.3: Physical properties of CFRP sheets

Product Commercial Name	FF-CR120
Thickness (mm)	0.111
Weight (g/m^2)	200
Tensile strength (N/mm^2)	3,400
Modulus of Elasticity (N/mm^2)	2.45 x 10^5

Table 3.4: Physical properties of the bonding epoxy

Product Commercial Name	D-70
Specific gravity	1.17+0.1
Flexure strength (N/mm^2)	40
Tensile strength (N/mm^2)	30
Shear strength (N/mm^2)	10
Viscosity (mPa.s)	20,000
Mix proportion	2:1
color	Blue

N.B.: CFRP and epoxy properties were given as supplied by manufacturer.

3.2.2 Procedure

In the current research, four phases of experiments were conducted to evaluate; 1) the enhancement of concrete beams after repairing with the conventional CFRP sheets and ECC, 2) the adequacy of pasting CFRP directly on ECC substrates, 3) the induced contact shear stresses between CFRP and ECC substrates, and 4) the effect of applying ECC with different thicknesses at the beam soffit before strengthening with CFRP.

To achieve the previous objectives, different sets of experiments were conducted. This section describes general overview of the test procedure. More details about each experiment will be given further at the corresponding sections.

Mainly, beams made of concrete and ECC of dimensions equal to 400 x 100 x 100 mm were prepared and tested destructively in a four point loading algorithm with a bending span of 300 mm, (Photo 3.1). For all the examined beams, deflections and tensile strains at the soffit mid-span were measured. For all the conducted combinations, two sets of beams were kept as reference; beam (C100) represents prisms completely made of concrete, while beam (E100) represents beams made completely of ECC. Table 3.5 shows further details about the nominations given to each group of beams.

The first phase of the experiment includes conducting concrete beams strengthened either with i) external CFRP sheets, namely (C100-1CFRP) and (C100-2CFRP) for beams strengthened with one and two layers of CFRP, respectively, and ii) ECC layers, namely (C90E10), (C70E30), and (C50E50) for beams with partial concrete replacement from the soffit side with 10%, 30%, 50% of the beam depth by ECC.

Photo 3.1: Typical loading configuration

Table 3.5: Details of the tested beams

Beam name	Strengthening condition
C100	100 mm depth /Concrete beam without strengthening
E100	100 mm depth/ECC beam without strengthening
C200	200 mm depth /Concrete beam without strengthening
C90E10	100 mm depth /Concrete beam with 10 mm ECC layer at its soffit
C70E30	100 mm depth /Concrete beam with 30 mm ECC layer at its soffit
C50E50	100 mm depth /Concrete beam with 50 mm ECC layer at its soffit
C100-1CFRP	100 mm depth /Concrete beam with one CFRP sheet at its soffit
C100-2CFRP	100 mm depth /Concrete beam with two CFRP sheets at its soffit
C200-1CFRP	200 mm depth /Concrete beam with one CFRP sheet at its soffit
E100-1CFRP	100 mm depth /ECC beam with one CFRP sheet applied at its soffit
E100-2CFRP	100 mm depth /ECC beam with two CFRP layers applied at its soffit
C90E10-CFRP	100 mm depth /Concrete beam with 10 mm ECC layer at its soffit + 1CFRP sheet
C70E30-CFRP	100 mm depth /Concrete beam with 30 mm ECC layer at its soffit + 1CFRP sheet
C50E50-CFRP	100 mm depth /Concrete beam with 50 mm ECC layer at its soffit + 1CFRP sheet
C1800E20-CFRP	200 mm depth /Concrete beam with 20 mm ECC layer at its soffit + 1CFRP sheet
C140E60-CFRP	200 mm depth /Concrete beam with 60 mm ECC layer at its soffit + 1CFRP sheet
C100E100-CFRP	200 mm depth /Concrete beam with 100 mm ECC layer at its soffit + 1CFRP sheet

The second phase includes examining the bonding strength between ECC and CFRP as well as comparing the failure behavior with similar cases of CFRP pasted on concrete substrates. The experiment involved indirect pull-out test. The detailed description is given later.

In the third phase, two sets of beams (E100-1CFRP) and (C100-1CFRP), corresponding to ECC and concrete beams strengthened with one layer of CFRP sheet, respectively. Strain gauges were mounted along the bottom fiber of the beams. Comparisons between the induced shear stresses for both cases were conducted.

In the last stage of the experiment in this chapter, the effect of ECC thickness before applying the external CFRP strengthening was examined. Same beam size as well as larger reinforced concrete beams of dimensions 700 x 200 x 100 mm was used. For the large size beams, the following conditions were prepared; (C200), (C200-CFRP), (C180E20-CFRP), (C140E60-CFRP), and (C100E100-CFRP) corresponding to the following cases respectively, control beam, concrete beam with CFRP strengthening, followed by concrete beams with 10%, 30%, and 50% partial replacements by ECC layer with additional strengthening with external CFRP sheets. For the small prisms, the same combinations were conducted and were named (C90E10-CFRP), (C70E30-CFRP), and (C50E50-CFRP) for the same replacement ratios, respectively.

3.2.3 CFRP Application

After 28 days of water curing, the specimens were taken out from water; the required surface was polished and refined using sand stone. The surface was then cleaned using compressed air and water to remove the unwanted dust and the remaining loose particles. The specimens were then left in open for 1 day at room temperature for complete drying (Guoqiang and Amanuel, 2006), and then a primary coat was painted. After then, a manual procedure was followed for pasting the CFRP sheets. As per manufacturer’s recommendations, a layer of epoxy, 400 g/m^2, was applied first followed by pasting the CFRP sheet. Specific type of metallic roller was used over the pasted sheet to remove the entrapped air and to squeeze out extra resin. Another epoxy layer of 200 g/m^2 was applied on the top surface of the CFRP sheet, and then a brush was used to get a smooth surface finishing. The CFRP strengthened specimens were left to cure for 5 days at normal room temperature (Houssam and William, 1997).

3.3 STRENGTHENING OF BEAMS WITH ECC

The overall flexural performance of concrete beams with different ECC thickness partially replacing thin layers of concrete was evaluated. Five groups with a total of twelve specimens of dimensions (400 x 100 x 100 mm) were prepared. Two groups were kept as control and cast to the full beam depth with either concrete or ECC and named C100, and E100, respectively. Three groups were prepared with a partial replacement of concrete by ECC from the bottom; the replacement depths were 10, 30, and 50% of the total specimen depth and named C90E10, C70E30, and C50E50, respectively. In all combinations, ECC was cast and poured directly over the fresh concrete. All the beams were subjected to four points loading flexure test. Small size prisms were used for simplicity and for reducing the expensive costs necessary to prepare large size ECC beams.

At the beginning, a comparison between the used strengthening materials was conducted; Figure 3.1 shows that ECC has a more ductile trend than the used concrete. After the initial cracking of ECC, the beam was still able to carry more loads with sufficient increase in its mid-span

deflection. Figure 3.1 also shows that ECC has a lower elastic modulus comparing to concrete. This behavior was found attractive to enhance the concrete beams with small layers of ECC applied to the beam soffit. Figure 3.2 shows the enhancement of the flexural strength as well as the improvement of the ductility of the strengthened beams. It was noted that the increase in the ultimate load carrying capacity over the control beam, C100, were 11%, 30%, and 74% for beams C90E10, C30E70, and C50E50, respectively. The ductility can be noted by measuring the maximum deflection achieved by each specimen. It was also observed that the ultimate mid-span deflection of C90E10, C30E70, and C50E50 was 0.33 mm, 0.66 mm, and 2.21 mm, in contrast with C100 which was only 0.042 mm.
For all the examined specimens, flexure failure with no spalling of the ECC layer was achieved. This reveals to the strong bonding and compatibility between ECC and the basic concrete substrate where the two materials deform and interact together as one material. Photo 3.2 shows a typical failure mode for the examined specimens. The crack directly started at the middle third portion of the beam and continued directly until complete failure.

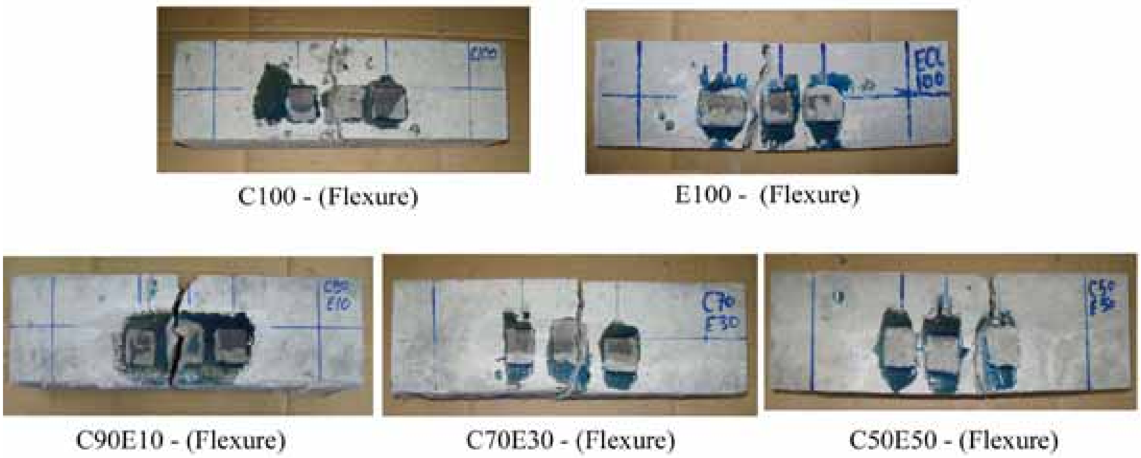

Photo 3.2: Flexure mode of failure for specimens with ECC strengthening

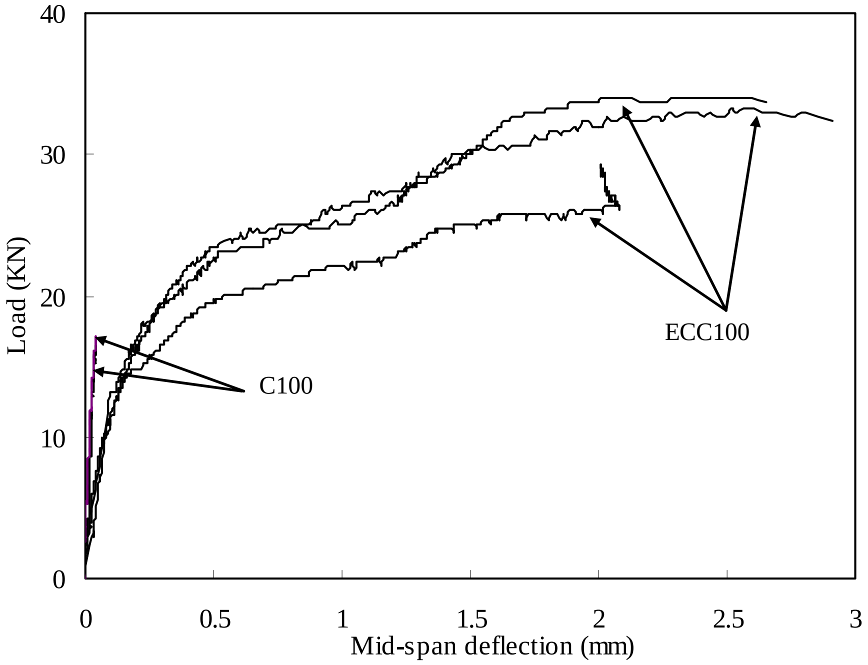

Figure 3.1: Load deflection curves for C100 and E100

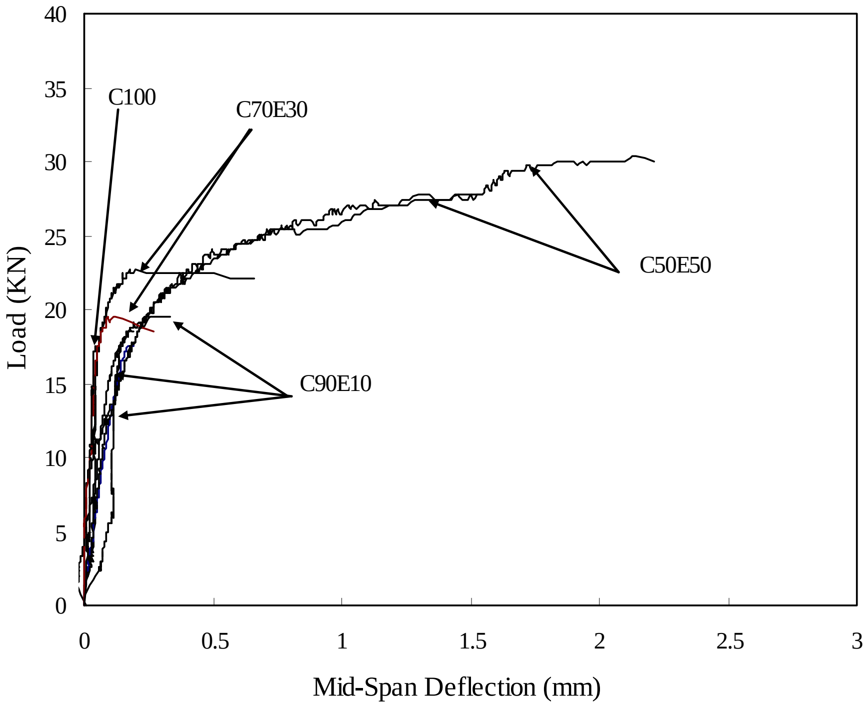

Figure 3.2: Load deflection curves for beams strengthened with ECC

3.4 STRENGTHENING OF BEAMS WITH CFRP

In the following experiment, two groups of small size beams 400 x 100 x 100 mm were again examined. The first group was made of concrete beams externally strengthened with one layer of CFRP, denoted as C100-1CFRP, while the second group corresponds to beams strengthened with two layers of CFRP and denoted as C100-2CFRP.

The results showed significant enhancement in the section loading capacity while the ductility of the beams was slightly enhanced compared to cases strengthened with ECC layers. The average enhancement in the gained strength for C100-1CFRP, and C100-2CFRP was 129% and 159% respectively over the control beam C100.

It was also observed that the interfacial debonding was the governed mode of failure (Photo 3.3). Flexure cracks were started approximately at the mid-span portion, almost under one of the loading points, causing a concentration on stresses around the vicinity of cracks. The debonding started to flow towards the cut-off position until complete failure occurred.

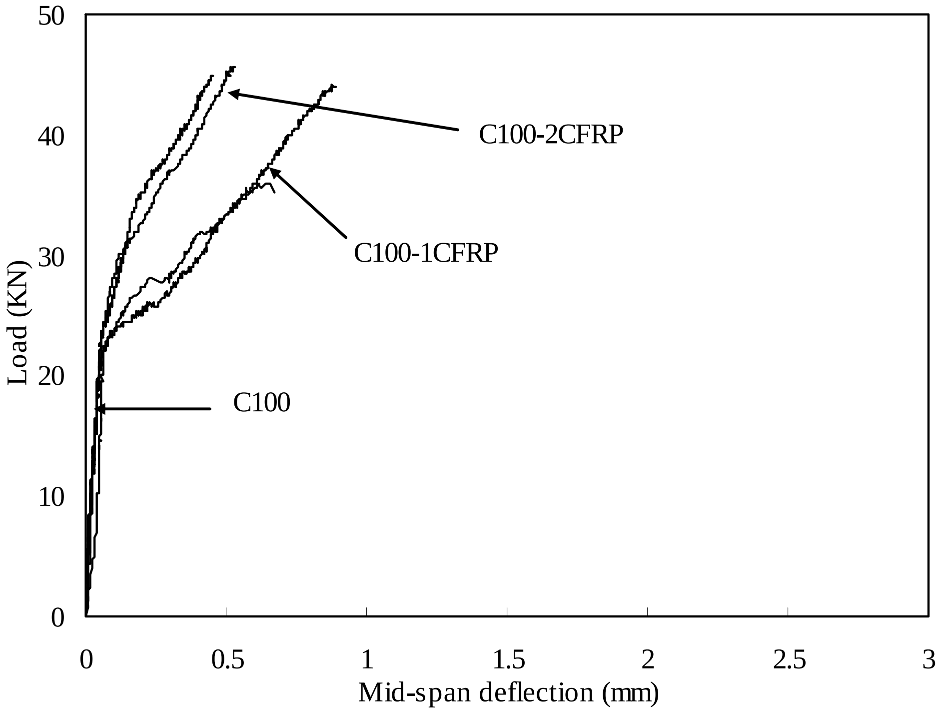

Figure 3.3: Load-Deflection curves for beams strengthened with CFRP

C100-1CFRP (Debonding) C100-2CFRP (Debonding)

Photo 3.3: Interfacial mode of failure for beams strengthened with CFRP

It was therefore thought of utilizing both ECC and CFRP for better beam strengthening. The CFRP would work towards achieving high strength while ECC could help in increasing the ductility of the strengthened beam. It was however, thought to conduct a preliminary test to check the compatibility between ECC and CFRP.

3.5 APPLICATION OF CFRP ON ECC AND CONCRETE SUBSTRATES

Before proceeding further in the study, it was necessary to check the adequacy of pasting CFRP on ECC substrate. Thus, a preliminary experiment with a configuration similar to that shown in Photo 3.4 was conducted. The assembly consisted of two blocks, each of dimensions (100 x 100 x 200 mm) and joined together using one layer of CFRP sheet (280 x 90 mm) attached to the base of the blocks leaving approximately 2 mm gap between the two blocks. This assembly was repeated twice, one for ECC while the other for concrete. The assemblies were subjected to a four point loading bending test of a bending span equal to 300 mm. The modes of failure for both the concrete and ECC assemblies are shown in Photos 3.5 and 3.6, respectively. The interfacial debonding failure mode was observed in case of concrete while shear failure with no interfacial debonding was observed in case of ECC. This might be attributed to the ductile behavior of ECC, where the absorbed energy during loading was released through a ductile shear failure; i.e. the ductility of ECC worked on redistributing the flow of forces shifting them from the high stressed bottom zone to less stressed portions.

The observed diagonal tension failure occurred in case of ECC revealed that the bonding strength between CFRP and ECC substrate was even higher that the tensile strength of ECC. The brittleness of concrete did not allow compatibility in the deformation between the CFRP sheet and the concrete substrate; this consequently led the lower corner edge of one of the concrete blocks to be broken followed by interfacial debonding failure. The longitudinal strains at the mid-span and at cut-off were measured and shown in Figure 3.4. It was also noted that the ECC assembly failed in a load value higher than that of concrete (38% more than concrete).

Photo 3.4: Typical indirect tension test configuration

Photo 3.5: Interfacial debonding in case of concrete substrate

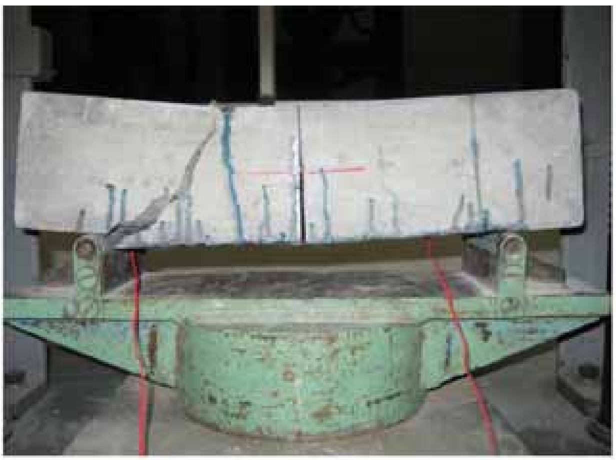

Photo 3.6: Shear failure in case of ECC substrate

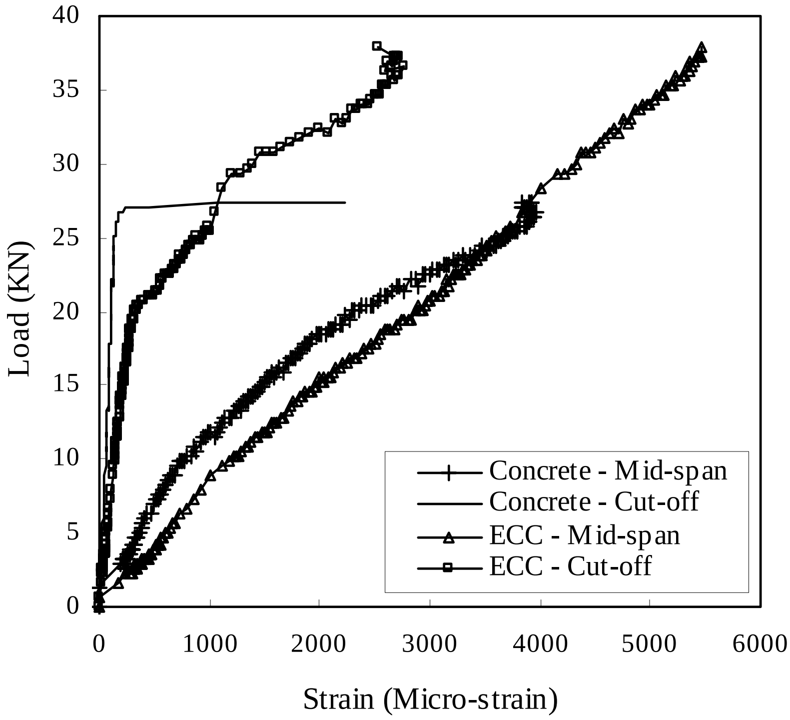

Figure 3.4: Measured strains for both concrete and ECC

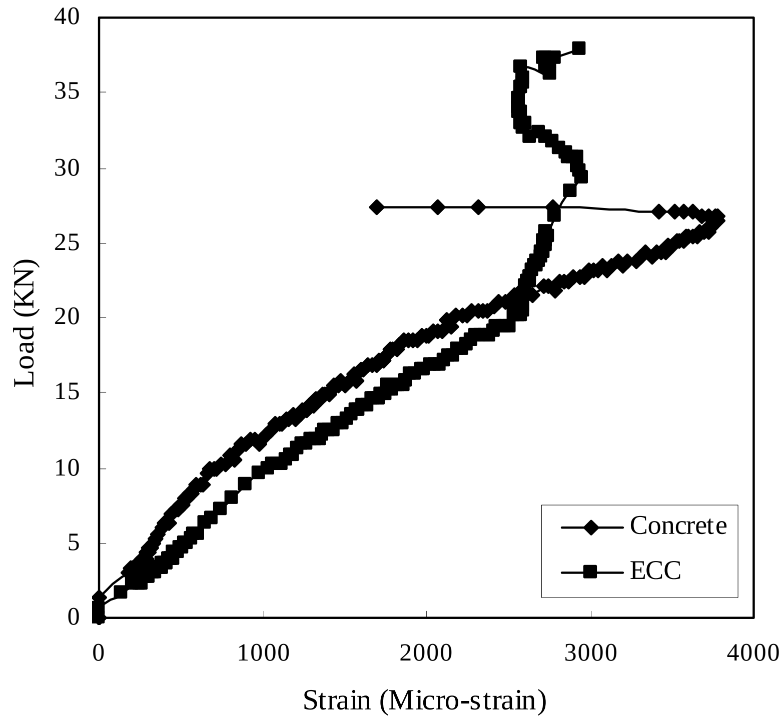

Figure 3.5: Difference in stain values between mid-span and cut-off for concrete and ECC

To check the flow of stresses along the CFRP sheet in both assemblies, the difference in the strain values were plotted for each assembly and shown in Figure 3.5. Both ECC and concrete showed nearly the same shear flow until a load level around 20 KN. Shear failure was then started in case of ECC with a sudden release to the strains along the CFRP sheet. For concrete, a constant increase in the shear flow among the adhesive was observed until sudden interfacial mode of failure occurred.

3.6 STRENGTHENING OF BEAMS USING BOTH CFRP AND ECC

3.6.1 Interfacial Shear Stresses

In this part, strengthening of ECC beams with CFRP as well as comparing the induced shear stresses with corresponding cases with concrete substrates. Four Prisms of dimensions 400 x 100 x 100 mm, made of ECC were strengthened with one and two layers of CFRP, denoted as ECC-1CFRP, and ECC-2CFRP, respectively. External CFRP sheets were pasted after polishing and preparing the required surfaces. The beams were tested in typical flexure test, as above mentioned. The deformations of the beams were observed and compared with similar cases made of concrete that were shown in Section 3.4. The results show that the creation of small size cracks in ECC prevented the concentration of stresses along the attached CFRP sheet; consequently, the interfacial debonding failure mode was prevented. In contrary, all the examined concrete beams strengthened with CFRP ended-up with the undesirable interfacial debonding failure mode. On the other hand, the strengthening efficiency was found higher in case of normal concrete beams than that of the ECC beams. Furthermore, investigation to study the induced interfacial stresses was conducted for concrete and ECC beams strengthened with only one CFRP sheet.

The load-deflection curve of the strengthened ECC is shown in Figure 3.6. For concrete cases, the corresponding curves were already shown in Figure 3.3. Generally, it can be seen that the ultimate loading capacity was significantly enhanced by adding CFRP sheets in case of concrete beams while slight enhancement was achieved in case of ECC beams. The strengthening of ECC and concrete beams with one sheet of CFRP increased the overall loading capacity over the control beams with 21% and 132%, respectively, whereas two sheets of CFRP caused enhancement of 25% and 158% respectively. For concrete beams, the load-deflection curves started with a linear elastic trend until exceeding the elastic limits. After then, all the tensile stresses were only carried by the CFRP sheets and that was the reason why the more the CFRP thickness continued the loading with higher curve slope and gave higher loading capacity. For the ductile ECC beams with no CFRP, the loading started with a semi-linear trend followed by strain hardening behavior. After applying CFRP, the trend shows enhancement in the overall rigidity of the members, shown in higher initial curves slopes, with a little increase in the total section loading capacity. In general, the external CFRP sheet in case of the strengthened ECC beams minimized the creation of the cracks at the mid-span and consequently avoided the high stress concentration at the vicinity of the cracks as in case of concrete substrates. It was observed that the CFRP sheet/s and the ECC beams deformed compatible to each other without the occurrence of the debonding failure for both cases (ECC-1CFRP) and (ECC-2CFRP). The change in the

CFRP thickness did not show a significant difference in the section loading capacity in case of ECC beams, it might be attributed to the occurrence of shear failure mode and consequently prevents the beams from reaching their ultimate flexural capacity limits. It was also observed that the strengthened concrete beams with one CFRP layer exhibited a larger strain values than all the other specimens. It was noted that for both ECC and concrete beams, the increase in CFRP thickness led to minimize the overall deflection and strain values. Figures 3.7 and 3.8 show bar graphs for load carrying capacity and deflection with respect to their control beams, respectively.

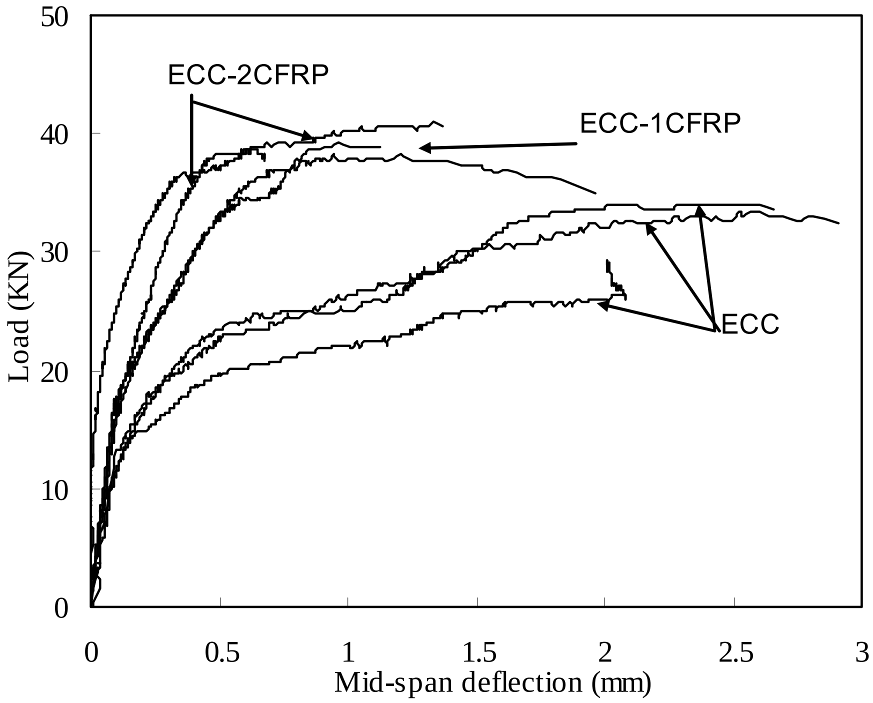

Figure 3.6: Load deflection curves for ECC beams strengthened with CFRP

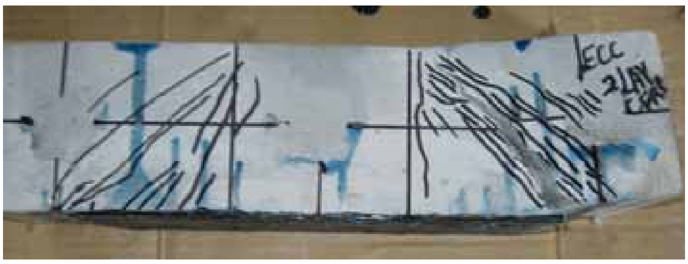

Photo 3.7: Shear failure mode for ECC beam strengthened with CFRP

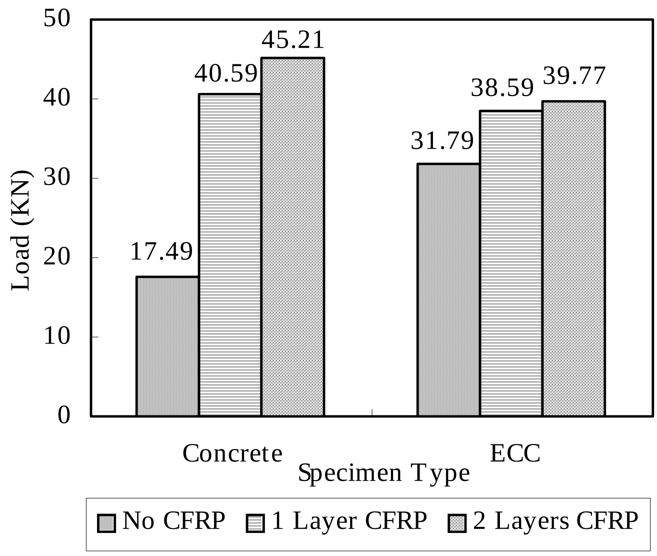

Figure 3.7: Contrast between concrete and ECC beams strengthened with CFRF in terms of the load carrying capacity

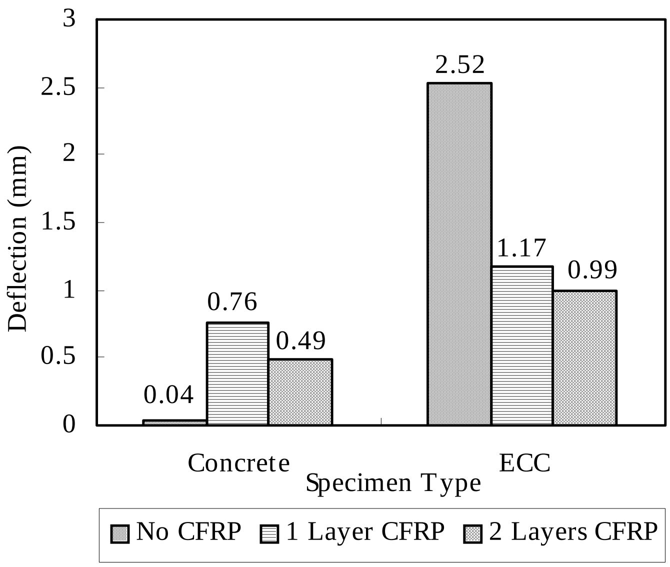

Figure 3.8: Contrast between concrete and ECC beams strengthened with CFRF in terms of the maximum displacement

The modes of failure of the examined beams would have a great influence on the final judgment. For ECC with one and two CFRP layers, pure shear failure, accompanied with many diagonal fine cracks, was observed with no signs of interfacial debonding failure along the CFRP sheet (see Photo 3.7). This conclusion was found very important, useful and should be utilized for further applications. This suggested the use of a combination of ECC simultaneously with CFRP sheets to strengthen and repair the deteriorated concrete beams by replacing the inferior layer of concrete with ECC. Thus, ECC could act as a transition material with an expected good contact between both the base concrete and the external CFRP.

Furthermore, another investigation was carried out to monitor the induced interfacial stresses between ECC beams and CFRP sheets as well as comparing with normal concrete beams. To deeply monitor the difference between the responses of both ECC and concrete beams with the attached CFRP sheet, four strain gauges were mounted along half the length of the CFRP sheet; this was only applied for cases with only one layer of CFRP. The strain gauges were located at distances 5, 25, 55, 140 mm from the CFRP sheet cut-off. Figures 3.8 and 3.9 show the measured strains for ECC and concrete beams, respectively.

The strain values were first compared at a load value nearly equal to the elastic limits of the concrete beams, it was noted that the developed stains on the ECC beam were more than that in case of concrete. This might be attributed to the high ductility of the ECC which allows compatible deformations with CFRP sheet while the CFRP elongation was resisted in case of concrete substrate. After exceeding the elastic limits of concrete, localized crack was developed nearly at the mid-span, this allowed the strain value to develop significantly in case of concrete substrate. It was noted that at the failure load value of the ECC beam, the value of the strain of the CFRP sheet attached to concrete was almost 40% higher than that attached to ECC beam. It was also shown that the strain value at the cut-off was higher in case of ECC substrate than in case of concrete allover the loading time. ECC dissipated the gained energy through excessive deformations among the whole member, while the rigid concrete only dissipated the absorbed energy at locations of very high stresses. It was also noted that the change in the slope of the strain value curves in case of ECC dramatically increased before collapse. This was due to the generation of shear crack, associated with the generation of many fine cracks, and preventing the member from achieving its flexural strength. In this particular case, ECC released the absorbed energy by means of shear cracks with no interfacial debonding.

For better understanding, the difference between the strain values at both the cut-off and the mid-span was calculated for both cases and shown in Figure 3.10. It was noted that at an early stage of loading the strain difference was slightly larger in case of ECC, after then, the strain difference in case of concrete was extremely increased, which revealed to the generation of a local crack. The figure could be used as a double check and confirmation for the reason why the interfacial debonding happened in case of concrete substrate while no debonding occurred in case of ECC beam. Generally, the higher the strain differences along the laminar, the higher the interfacial shear stress, and the ease the occurrence of the interfacial debonding failure.
Figures 3.11 and 3.12 show the measured strain at selected loading values for both the ECC and the concrete beam. The figures show the relatively high strain gradient near the cut-off in case of ECC at low level loading which increased slightly without sudden change.

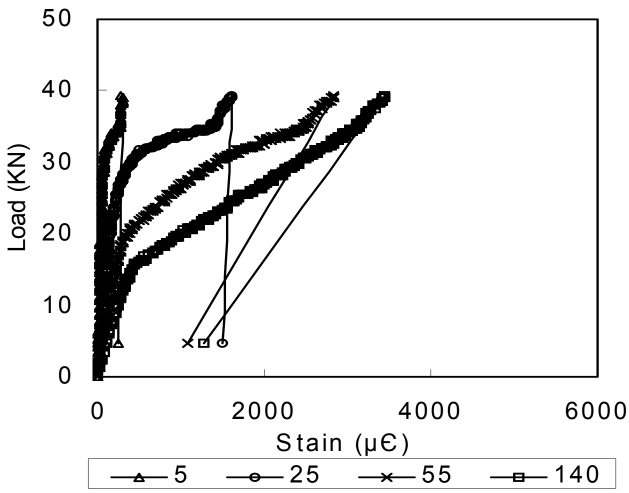

Figure 3.8: Measured strain along the CFRP sheet for the ECC beam

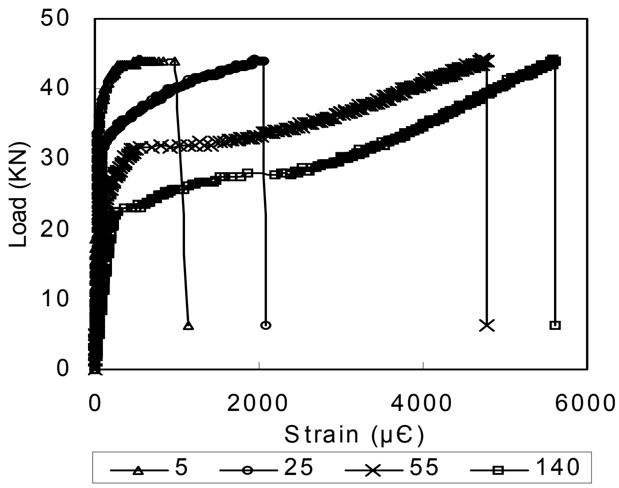

Figure 3.9: Measured strain along the CFRP sheet for the concrete beam

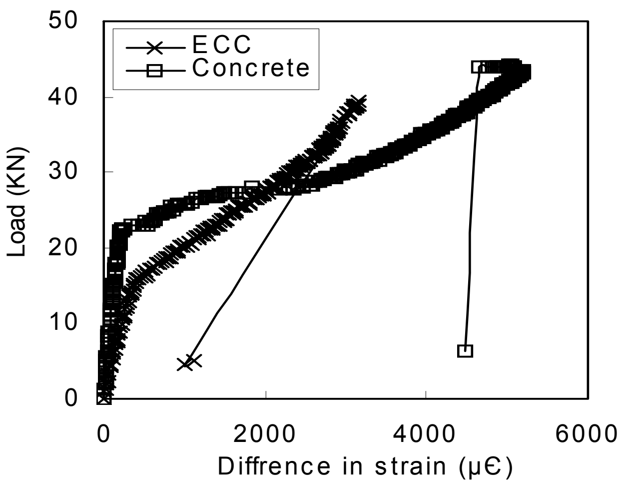

Figure 3.10: Difference in the strain values at the cut-off and the mid-span position

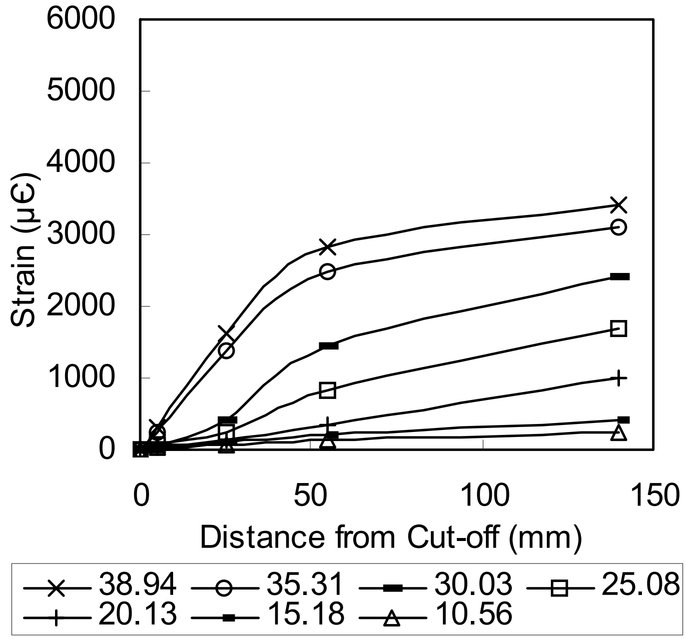

Figure 3.11: Strain along the CFRP sheet attached to the ECC beam at different loading stages

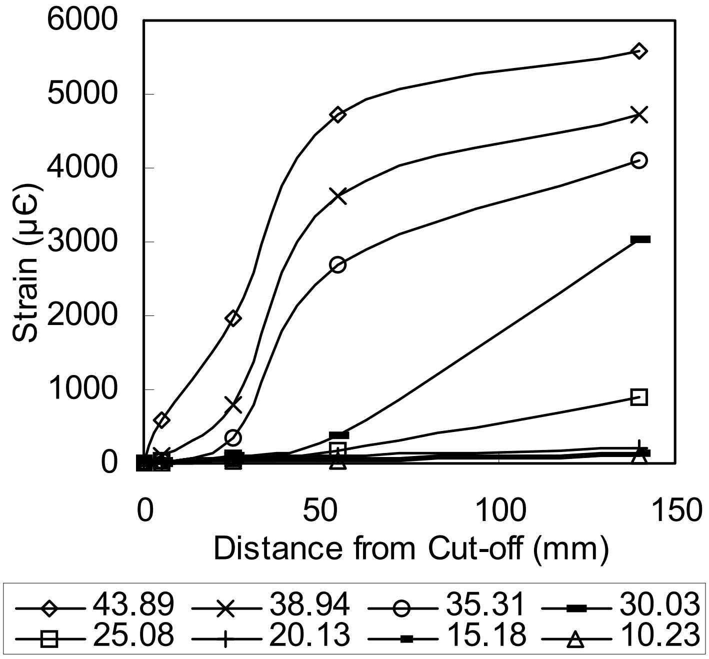

Figure 3.12: Strain along the CFRP sheet attached to the concrete beam at different loading stages

In contrary, the concrete beam exhibited low strain gradient near the cut-off and exhibited a sudden variation in the strain values after exceeding the elastic limits. This might also end-up with the same reason for the interfacial debonding that occurred in case of concrete and was avoided in case of ECC.

3.6.2 Effect of ECC Thickness before CFRP Application

The next step was therefore, evaluating the performance of concrete beams strengthened with combinations of both ECC and CFRP. In this section, two sets of beams were tested destructively. The first was replication of the beams given in Section 3.3 after application of one layer of CFRP to their soffit, and were denoted as C90E10-CFRP, C70E30-CFRP, and C50E50-CFRP. The second set of beams were prepared by applying CFRP sheets to large scale reinforced concrete beams with dimensions 700 x 200 x 100 mm (Figure 3.13 and Photo 3.8). The reinforced concrete beams were prepared by overlaying ECC layer on fresh concrete and finally strengthened with CFRP sheets. The large size beams were denoted as C180E20-CFRP, C140E60-CFRP, and C100E100-CFRP for beams with partial replacement of concrete by ECC layer with 10%, 30%, and 50% of the beam total depth, respectively.

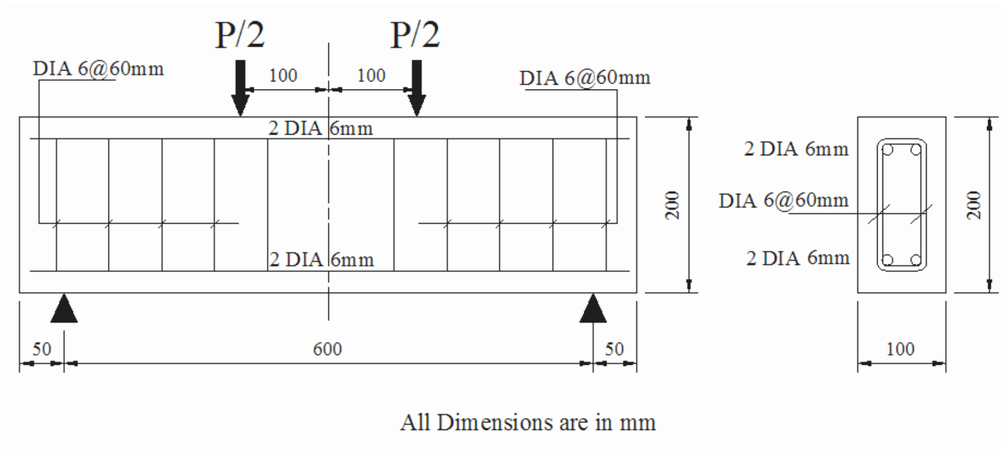

Figure 3.13: General layout for reinforced concrete beam

Photo 3.8: Moulds containing the reinforcement of concrete beams

Figure 3.14 shows the load deflection curves for the layered specimens for the small specimens. For layered specimens with external strengthening with CFRP sheets, the load deflection curves do not show significant variation in the peak load value in case of the small specimens comparing to strengthening directly with CFRP (C100-CFRP). It was however observed that the application of ECC layer before pasting the CFRP sheet was significant in delaying the interfacial debonding or even preventing this failure mode. The existence of the ECC layer acted as a transition zone between the brittle concrete, with high probability to form local cracks, and the high tensile strength CFRP sheets. The very good contact between the ductile ECC and the CFRP sheet led to dissipate the absorbed energy during loading through weaker planes in the specimens. In this study, the shear failure was dominant and replaced the common interfacial debonding failure for the small size beams. For C100-CFRP, the undesirable interfacial mode of failure was the govern mode, the crack started at the location of one of the applied point loads followed by complete debonding of the CFRP sheet.

It was suggested to re-examine the beams after confining the shear zones. Thus, large scale beams with sufficient amount of shear reinforcement were examined. Figure 3.15 shows the load deflection curves for the large scale beams. The traditional interfacial debonding of CFRP, resulted from flexure cracks, was not observed when ECC was used with different thicknesses. Beams C100E100-CFRP and C140E60-CFRP were found the best in achieving the highest section capacity. They were however ending up with a diagonal shear failure followed by interfacial debonding mode of failure. The shear and longitudinal reinforcement worked on decelerating the shear failure; however it was observed that the shear failure started a little before debonding of CFRP. In fact the debonding started due to non-linearity in the beam geometry which was created due to the high beam curvature beside the crack. This suggested that the there was much compatibility in the behavior between the small and large scale beams. Beam C180E20-CFRP showed flexure crack in a position slightly under the load position followed by debonding of the ECC layer itself. This could be attributed to 1) the very week stiffness of the ECC layer compared to that of the beam, and 2) ECC layer was lying under the main reinforcement bars and therefore missed the additional confinement of them. For C200-CFRP, the conventional debonding of CFRP was achieved in a position under one point of the applying loads. The enhancement in the section capacity was 70%, 130%, 134%, and 10% for C100E100-CFRP, C140E60-CFRP, C180E20-CFRP, C200-CFRP, respectively over the control beam C200.

Finally, it can be said that ECC worked as a transition layer between the concrete beam and the external CFRP sheet. The high ductility of ECC allowed compatibility in the deformation of the brittle concrete and the elastic CFRP. ECC deformed with CFRP smoothly and minimize the probability of the interfacial debonding failure or even prevented it. It was noted that for effective strengthening, ECC should extend beyond the main reinforcement to approximately a distance at least equal to double the main reinforcement cover depth. The modes of failure for all the examined beams are shown in Photos 3.9 and 3.10 for small and big beams, respectively.

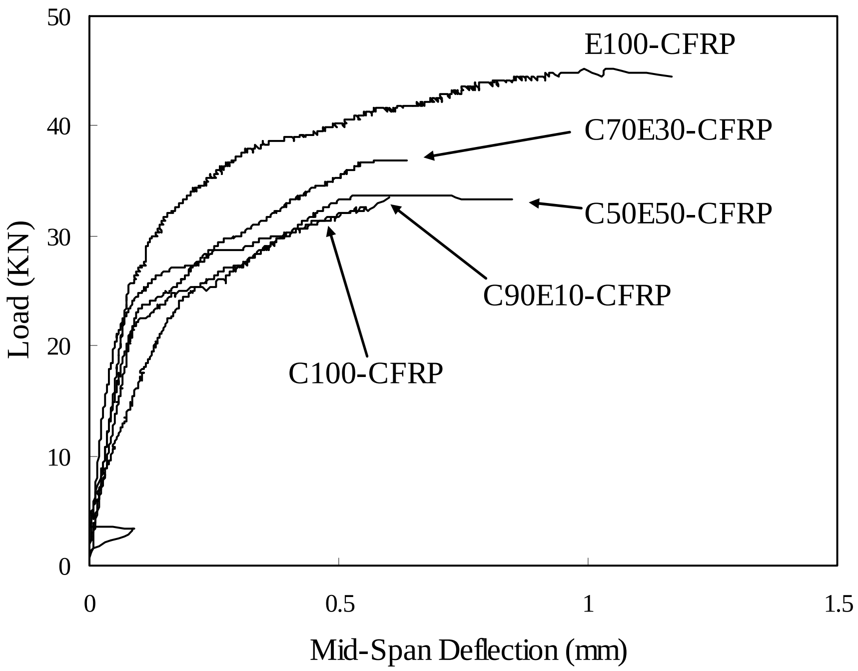

Figure 3.14: Load-deflection curves for layered small beams

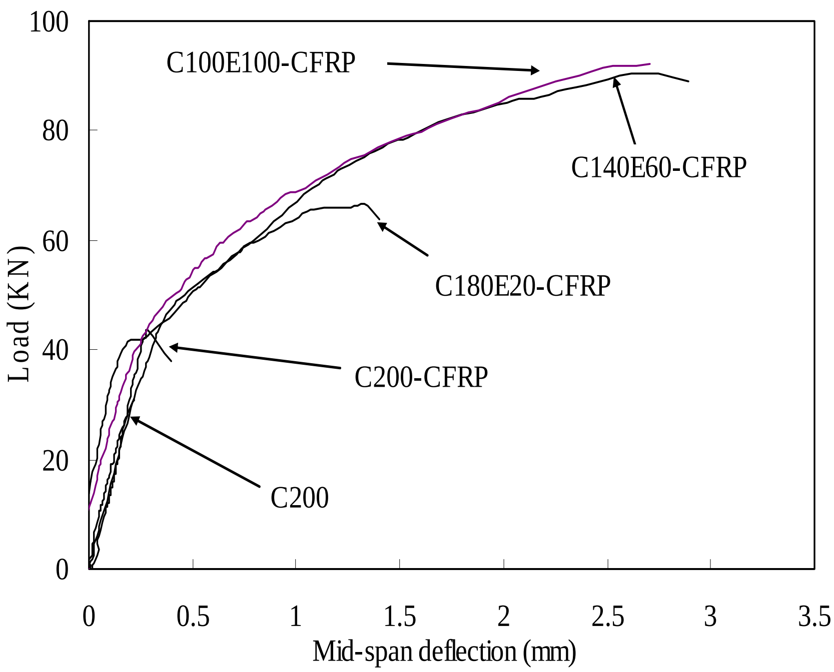

Figure 3.15: Load-deflection curves for layered big beams

C90E10/CFRP - (Shear) C70E30/CFRP - (Shear) C50E50/CFRP- (Shear)

Photo 3.9: Modes of failure for small specimens

Photo 3.10: Modes of failure for big specimens

3.7 REASONS FOR THE GOOD BONDING BETWEEN ECC AND CFRP

The reasons for the strong bonding between ECC and CFRP were due to: 1) the micromechanical behavior of ECC contaminated with the strain hardening trend when subjected to tensile forces, where the ECC can develop a 200 times tensile strain more than that of the concrete (Gao et al. 2006, Li 2002). This behavior led the ECC and CFRP not to create large differential strains and consequently decreased the interfacial shear stresses in the adhesive and decelerated the debonding failure mode. 2) ECC creates many but micro-size cracks in the most stressed portions which consequently decreases the shear stress gradient between the CFRP sheet and the ECC substrate near the vicinity of cracks, 3) ECC is relatively of high porosity with high voids ratio (nearly around 12%, while normal concrete is only around 2%). This led a large amount of the adhesive epoxy resin to penetrate through and develop a better contact strength, and 4) the remaining small amount of fiber on the polished surface of ECC along with the high amount of fibers just underneath the prepared surface can create a strong reinforced adhesive compound which helped in decelerating the debonding failure. The previous explanation might not be applicable in case of concrete where one or few localized cracks appeared followed by the concentration of stresses in the vicinity of cracks and subsequently inducing sudden interfacial debonding failure. Photo 3.11 shows the concrete and ECC surfaces before pasting the CFRP sheet and after peeling of the CFRP. It is observed that a very fine layer was spalled out with the CFRP sheet in case of concrete beams, while for ECC beams, relatively thicker layer of ECC was spalled out, traces of the epoxy was observed along with the large amount of fibers.

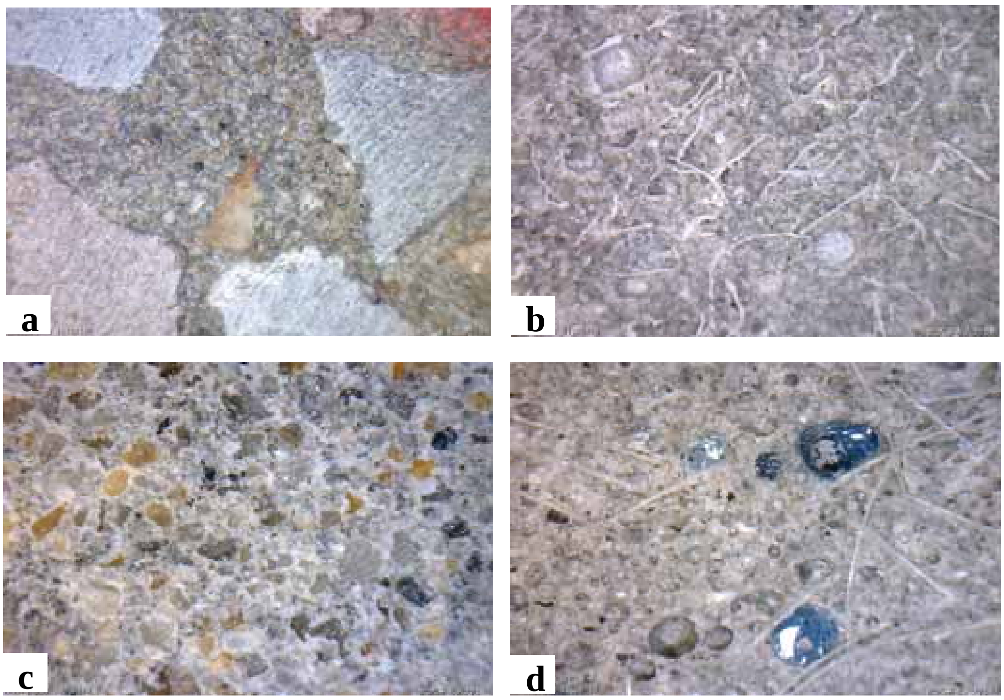

Photo 3.11: a)Concrete surface after polishing, b) ECC surface after polishing, c) Concrete surface after peeling the CFRP sheet, and d) ECC Surface after peeling the CFRP sheet

3.8 CONCLUSIONS

In the current chapter, large and small size concrete beams were prepared to evaluate the effectiveness of using ECC as a strengthening material. The study showed that using ECC in combinations with external CFRP sheets could lead to better sectional loading capacity with reasonable enhancement in the ductility of beams. Examination of the induced interfacial shear stresses between ECC and CFRP were also conducted and compared with corresponding case of concrete. The following are among the main findings of this chapter:

(1) In all the examined ECC beams, the bonding between CFRP and ECC was found strong enough and even better than that of the concrete due to material ductility.

(2) For systems with no external CFRP, as the depth of ECC increased, the section loading capacity and ductility was enhanced proportionally.

(3) The concrete beams exhibited high strength efficiency when strengthened with CFRP; however, it did not have the same significance when strengthened alone with ECC. Combination between CFRP and ECC showed promising results. ECC acted as a transition material between concrete and CFRP and consequently decelerate or even prevent the occurrence of the undesirable debonding mode of failure of CFRP that usually occurs in case of concrete.

(4) The interfacial shear stress gradient at the cut-off in case of ECC was lesser than in case of concrete beams at same loading values.

(5) It was recommended to use ECC before pasting the external CFRP with a depth equal to double the covering depth of the reinforced concrete beam.

(6) The shear confinement by means of the additional stirrups in case of reinforced concrete beams did not affect the mode of failure, but it only allows the beam to achieve higher load carrying capacity.

CHAPTER 4

4. REPAIR OF INITIALLY CRACKED CONCRETE BEAMS USING COMBINATIONS OF ECC AND CFRP

4.1 INTRODUCTION

Deterioration of concrete structures can be expressed in the form of extra strains, excessive deformations, and consequently the appearance and generation of many surface cracks. Degradation of concrete structures could be due to natural degradation of the structure materials or due to the combined effect of both external loads and environmental factors. The compatibility of the repairing material with the original substrate has a great influence on the overall performance of the repaired structural elements. Many factors affect the selection of the repair materials such as; the ease of use in a wide variety of situations, simplicity, speed of application, and the total required cost. Repair of concrete structures requires sufficient experience to the various ranges of the existing repair materials with their different physical and chemical properties as well as the optimum method for their application.

Many researches have studied the repair and retrofitting of concrete members containing cracks. Thanoon et al. (2005) have used cement grout, epoxy injection, ferrocement layer, carbon fiber strip and section enlargement to repair cracked concrete slabs. The introduction of a high performance fiber reinforced cementitious composites (HPFRCC) called engineered cementitious composites (ECC) by Li (2002), nearly two decades ago, attracted many researchers to utilize this material for repairing and strengthening purposes. ECC has strain hardening behavior when exposed to tensile forces. It also exhibits a strain level two orders of magnitude higher than that of concrete (Maleej and Leong, 2005a). The many cracks with very small width are considered one of its superior characteristics. The fibers inserted in ECC help in bridging the applied forces through the generated cracks. Cost wise, ECC is very expensive to be used on a big scale and should only be applied at particular places of the damaged structures. Li et al. (1995), and Lim and Li (1997) have overlaid the concrete substrate by layers of ECC, It was shown that the delamination and spalling modes did not occur; micro size cracks were found instead. Kamada and Li (2000) have found that smooth surface preparation of the substrate concrete achieved good structure performance than the corresponding cases with rough surface. Zhang et al. (2006) conducted theoretical and experimental studies to check the suitability of using ECC as a strengthening material for beams, the results showed enhancement in the flexure behavior of beams with increasing ECC thickness. On the other hand, Maalej and Leong (2005b) have conducted a primary study to strengthen reinforced concrete beams, containing ECC layer located at its base, with CFRP. However, the study was preliminary and required further investigations.

The current chapter addresses ECC as a new alternative for retrofitting initially cracked concrete beams. Twenty-one plain concrete beams with pre-defined artificial cracks were prepared and repaired using different combinations of ECC alone or together with CFRP. The study showed that replacement of the inferior layer from the bottom of the deteriorated beams with a thin layer of ECC could be able to restore the beam to a condition better than its original state. Moreover, the repair with ECC was found effective in enhancing the member ductility as well. ECC was able to bridge the internal forces along the crack edges. It was also shown that pasting CFRP directly over ECC substrate resulted in shear failure rather than the undesirable interfacial debonding mode of failure that typically occurs in case of concrete structures – the results are coinciding with those obtained in the previous chapter. The experimental investigations also showed conventional repair methods for the initially cracked beams either by direct injection with epoxy or combined with pasting of external CFRP sheets at the soffit of the beam.

4.2 EXPERIMENTAL WORK

Twenty-one scaled down plain concrete beams with dimensions (length x width x depth) equal to (400 x 100 x 100 mm) were prepared. Small size beams were selected to minimize the cost of the used ECC. The specimens contained artificial cracks, 50 mm depth and 2 mm width, located at their mid-spans.

Table 4.1: Description of the examined specimens

Group	**Type of specimen**	**Replication**	**Description**
1A*	C100	1	Beam with no cracks (Original state)
2A	C100-cr	1	Beam with pre-defined cracks (Damaged state)
3A	C100-cr/epoxy	1	Repaired only by epoxy injection
3B**	C100-cr/CFRP	2	Repaired by epoxy injection followed by pasting a CFRP sheet along the beam soffit
4A	C100-EL	2	Local repair with ECC extended to the crack depth
4B	C100-EL/CFRP	2	Local repair with ECC followed by pasting a CFRP sheet along the soffit.
5A	C90E10-cr	2	ECC is applied along the beam soffit with a depth of 10 mm + epoxy injection for the crack
5B	C90E10-cr/CFRP	2	ECC is applied along the beam soffit with a depth of 10 mm followed by pasting a CFRP sheet along the soffit.+ epoxy injection for the crack
6A	C70E30-cr	2	ECC is applied along the beam soffit with a depth of 30 mm + epoxy injection for the crack
6B	C70E30-cr/CFRP	2	ECC is applied along the beam soffit with a depth of 30 mm followed by pasting a CFRP sheet along the soffit.+ epoxy injection for the crack
7A	C50E50-cr	2	ECC is applied along the beam soffit with a depth of 50 mm + epoxy injection for the crack
7B	C50E50-cr/CFRP	2	ECC is applied along the beam soffit with a depth of 50 mm followed by pasting a CFRP sheet along the soffit.+ epoxy injection for the crack

* A: denotes to specimens without CFRP
** B: denotes to specimens with CFRP pasted at the beam soffit

Photo 4.1: Specimens before repair

The cracked beams were designed so that their load carrying capacity should not exceed 20% of the sound specimens. The above condition was confirmed by conducting many side experimental tests. The cracks were conducted by placing separators in the moulds before casting the concrete. The combined concrete/ECC beams were prepared through two stages; first, the concrete was cast leaving a free space in the moulds as shown in Photo 4.1, second, after 28 days of water curing to the concrete beams, ECC with different thicknesses was added to fill the remaining free spaces in the moulds. ECC was placed in different configurations; either locally around the crack, or with thicknesses of 10, 30 and 50mm from the bottom of the beam. For more details about the notation of specimens as well as the number of replications for each case, refer to Table 4.1. After casting ECC, the final repaired specimens were again kept for curing in water for another 28 days.

The specimens were mainly divided into seven groups. Group 1A, represents the original state of the beams before deterioration, and was kept as a target condition to all the deteriorated specimens. Group 2A, represents the deteriorated severe cracked case with no repair. The current research aimed to retrofit the beams from condition similar to Group 2A to reach its original state (i.e. Group 1A). Group 3A and 3B represent conventional repairing condition using either epoxy injection only or along with pasting CFRP sheet at the soffit surface. The other four groups represent beams with new repairing combinations incorporating ECC.

To distinguish the groups, either a letter “A” or “B” was added to the group number. The letter “A” refers to group where the repair was done only using ECC. The letter “B” denotes groups where CFRP sheets were applied simultaneously with ECC.
The specimens were subjected to four points loading bending test with a bending span of 300 mm. Load deflection curves were measured at the mid spans of the beams. In the current study, the repair length of ECC was 280 mm, i.e. 20 mm lesser than the bending span and divided equally from supports at both sides. The difference in age of both concrete and ECC might also coincide with real conditions as the base material is usually of very old age compared to the new repairing

materials. It was thought that these configurations could help in studying the spalling of ECC from concrete substrate, if any, and could end-up with a better understanding of the flexural performance of the repaired composite beams. Same materials described in Chapter 3 with same physical and mechanical properties were used again in this chapter. It was however found a little enhancement in the properties of concrete at 56 days. At the test day, the concrete compressive and tensile strength values were 42 N/mm^2, and 4.5 N/mm^2, respectively.

4.3 RESULTS AND DISCUSSION

4.3.1 Recovering the Beam Strength

The load–mid-span deflection curves for the conventionally used methods are shown in Figure 4.1; while the corresponding curves for the current repairing methods are shown in Figures 4.2 and 4.3 for Groups A and B, respectively. Generally, notable enhancement in the section capacity over the control specimen (C100-cr) was observed for all specimens. Specimen repaired only with traditional epoxy injection (C100-cr-epoxy) showed 130% enhancement in the section capacity over the cracked specimen (C100-cr). It, however, failed to reach the section capacity of the original state of beam (C100). It was also noted that the traditionally used repair technique (C100-cr/CFRP) exhibited a section capacity 133% higher than the target beam (C100). In the current research, the repair with ECC alone was found effective in enhancing both the loading capacity and the ductility of the repaired beams. For (C100-El), ECC was only applied locally for a distance around 100 mm at the beam base and extended to the full crack depth. The enhancement in the section capacity was 220% more than the damaged state (C100-cr). Although this combination was still not able to reach the initial original state of the beam; it was found better than the traditional case (C100-cr/epoxy). The low loading capacity might be attributed to the relatively small contact area between ECC and the base concrete at a zone of extremely high normal stresses. The application of ECC layers, with different thicknesses with a longer distance among the beam soffit, improved the flexure performance a lot. It was observed that ECC acted as a bridge to convey the internal forces between both sides of the crack. Retrofitting of the damaged beams with ECC showed that the original integrity was not only restored but enhanced as well. The section capacity for (C90E10-cr), (C70E30-cr), and (C50E50-cr) was found 12%, 42%, and 75%, respectively, more than the target specimen (C100) and 505%, 640%, and 790%, respectively higher than the damaged specimen (C100-cr). Generally, the increase in ECC thickness led to an increase in the section load carrying capacity. For better understanding of the effectiveness of each of the repaired combination, the results were again re-plotted in bar form as shown in Figures 4.4a, and 4.5a. The figures show the significant effect of ECC when applied alone to bridge the gap between cracks in beams as well as to enhance the ductility of beams by achieving higher deflection values at the beams' ultimate load.

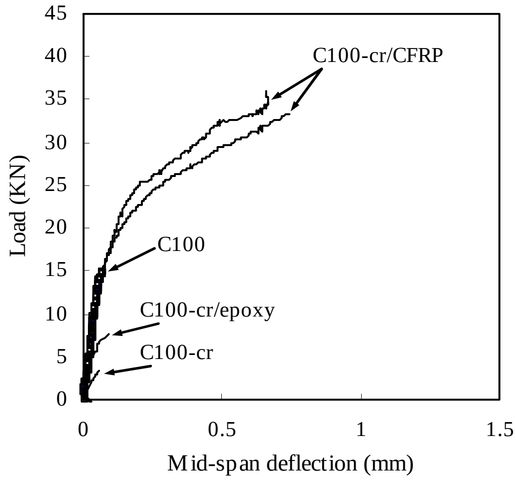

Figure 4.1: Load-deflection curves for traditional repairing methods

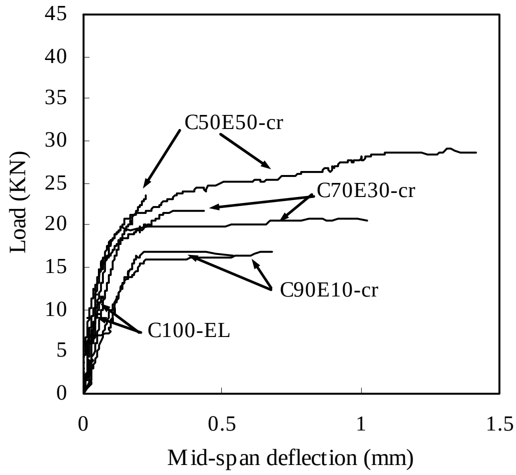

Figure 4.2: Load-deflection curves for repair using ECC only

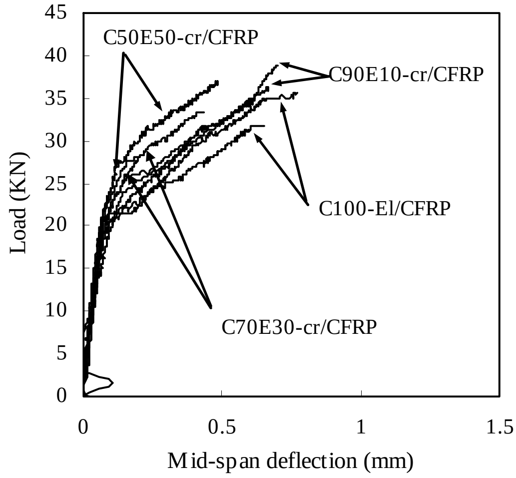

Figure 4.3: Load-deflections curves for repair using combinations between ECC and CFRP

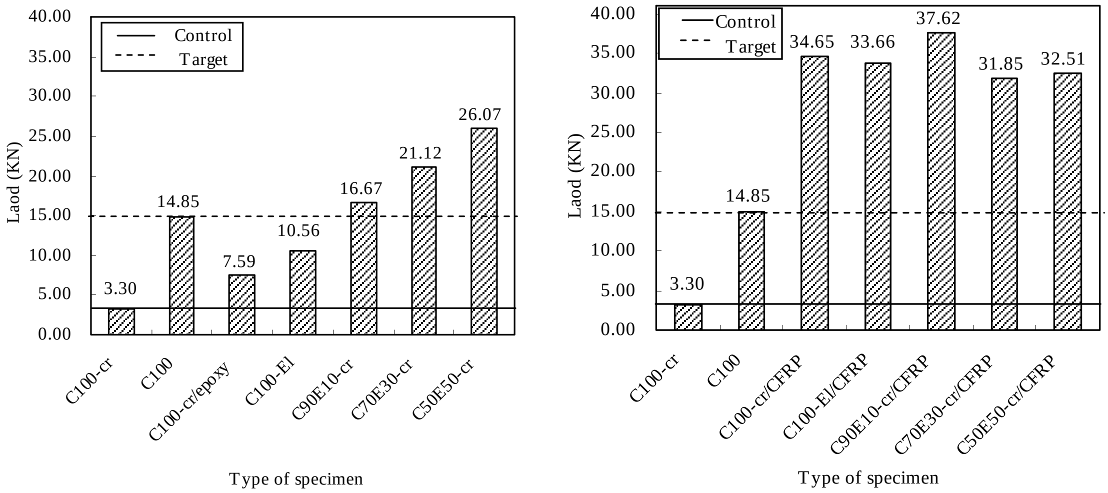

Figure 4.4: Load carrying capacity for the examined specimens a): without adding CFRP, and b): after adding CFRP

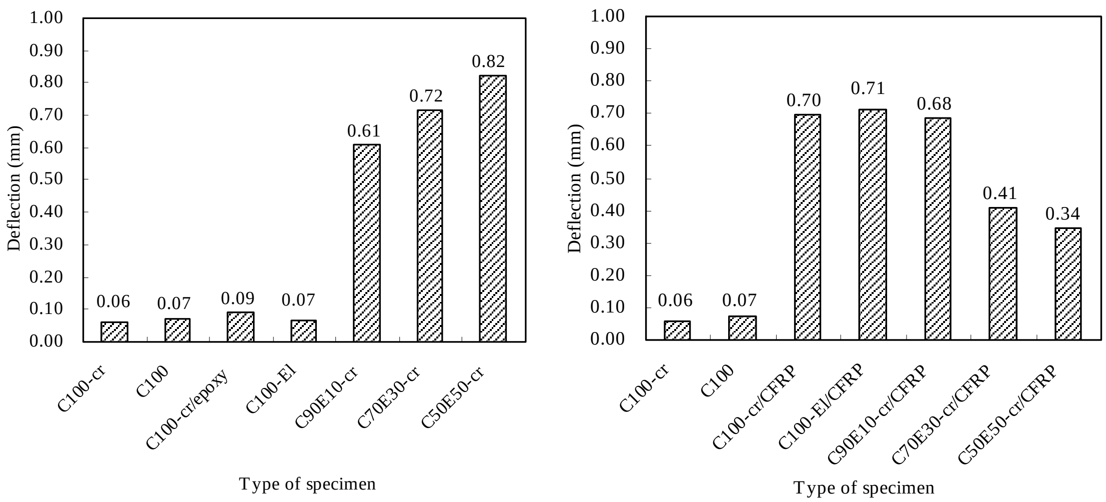

Figure 4.5: Mid-span deflection curves for the examined specimens a): without adding CFRP, and b): after adding CFRP

The same combinations were again repeated after applying CFRP sheets at the beam soffit. The results showed that the mitigation in the section capacity for (C100EL/CFRP), (C90E10-cr/CFRP), (C70E30-cr/CFRP) and (C50E50-cr/CFRP) over the target beam (C100) were 127%, 153%, 115%, and 119%, respectively. The previous values did not show substantial variation in the achieved strength and a little bit lesser than that of (C100-cr/CFRP) except for the case where ECC was of minimum thickness.

Table 4.2: Flexure test results for all the examined specimens

Specimen ID	Flexural test load			Mid-span deflection		
	Ultimate Load capacity (KN)	Percentage increase compared to control beam (%)	Percentage increase compared to target beam (%)	Ultimate Deflection (mm)	Percentage increase compared to control beam (%)	Percentage increase compared to target beam (%)
C100-cr	3.30	-	-77.78	0.06	-	-14.29
C100	14.85	350.00	-	0.07	16.67	-
C100-cr/epoxy	7.59	130.00	-48.89	0.09	50.00	28.57
C100-EL	10.56	220.00	-28.89	0.07	16.67	0.00
C90E10	16.67	405.16	12.26	0.61	916.67	771.43
C70E30	21.12	540.00	42.22	0.72	1,100.00	928.57
C50E50	26.07	690.00	75.56	0.82	1,266.67	1,071.43
C100-cr/CFRP	34.65	950.00	133.33	0.70	1,066.67	0.00
C100-EL/CFRP	33.66	920.00	126.67	0.71	1,083.33	914.29
C90E10/CFRP	37.62	1040.00	153.33	0.68	1,033.33	871.43
C70E30/CFRP	31.85	865.16	114.48	0.41	583.33	485.71
C50E50/CFRP	32.51	885.16	118.92	0.34	466.67	385.71

This could be attributed to the geometry of the beam itself, when applying CFRP, and in case of concrete substrate, single flexure crack combined with stress concentration at the vicinity of crack followed by debonding of CFRP sheet. In case of ECC substrates, the ductility of ECC allowed extra deformations in the beams without localized flexure cracks, and therefore the govern mode of failure in this case is the shear failure with no debonding of CFRP sheet or spalling of ECC layer. It was however, noticed that as the thickness of ECC layer increased, its rigidity increased as well and the probability to spall from the base concrete became higher at large deformations. This could also contribute in decreasing the shear resisting area near the supports and make the shear failure faster to occur than the flexure failure. This could help illustrating why (C90E10-cr/CFRP) achieved higher strength than both (C70E30-cr/CFRP) and (C50E50-cr/CFRP). The previous explanation might be verified by comparing (C100EL/CFRP) and (C100-cr/CFRP) as both specimens have same shear resistance capacity higher than their flexure capacity; thus both specimens failed on flexure followed by debonding of CFRP with almost same loading capacity (see Figures 4.4b and 4.5b).

In general, the application of CFRP led to increase the absorbed energy by the beam until failure. This energy was in the form of high loading capacity accomplished with small deflection. That was the reason for having small variation in the load carrying capacity for all the specimens incorporated CFRP. That could also be the explanation of why beams repaired only with ECC

exhibited higher ductility and deflection at ultimate loads with lower load carrying capacity than those containing CFRP. Table 4.2 shows the flexure test results for all the examined specimens.
For instance, it can be suggested that the use of ECC with CFRP did not influence the section loading capacity so much; on the contrary, ECC was found significant to act as a transient material between concrete of low tensile strain capacity and CFRP of relatively high stain capacity. ECC was also able to change the mode of failure of the beams and will be shown in details in the following section. Simply, it can be said that when adding CFRP, the flexural strength of all the beams was almost of the same range regardless to the ECC thickness. This value was higher than the shear capacity in case of composite layered beams (concrete/ECC) so the shear failure governed the failure mode. It was noticed that this value was lesser than the shear strength for pure concrete beams, so the flexure failure followed by debonding of CFRP was achieved.

4.3.2 Modes of Failure

In general, the mode of failure changes by changing the repair method. Photo 4.2 shows the modes of failure for the examined specimens. It was observed that both the control (C100-cr) and target (C100) specimens exhibited pure flexure mode of failure. For the traditional used repair method, (C100-cr-epoxy), flexure failure had also occurred; the crack started exactly from the same place of the pre-existing fault after peeling of the epoxy from one of the crack sides. For (C100-EL), flexure crack with spalling of the local ECC was noticed. This revealed that the contact between the concrete layer and the ECC was not capable to withstand the induced tensile stresses. For (C90E10-cr) and (C70E30-cr), flexure mode of failure started exactly at the crack position and continued through the whole ECC thickness. It was noted that the contact length was sufficient and spalling of the ECC layer was not observed. The effect of the repairing material stiffness was significantly noticed when ECC thickness reached 50 mm. For (C50E50-cr), the failure of one of the specimens was observed early after debonding and spalling of the ECC layer, nearly at a position just under the applied load point. The relatively high flexural rigidity of the ECC layer prevented the ECC from following the same deformation of the concrete beam, thus spalling occurred. The second specimen failed almost by the same mode but the separation was only limited to one side surface of the ECC layer, the crack started at one side of ECC and followed vertically causing separation of ECC from concrete; the crack was then preceded directly to the support. It was shown that in the repairing process, the thickness along with the length of the applied ECC should be precisely selected and more investigations are still required.

After applying CFRP sheets at the beam soffit, the mode of failure was changed. It was however noted by many researchers that applying CFRP sheets directly to concrete surface could end up with undesirable interfacial debonding mode of failure. The concentration of the interfacial shear stresses near the vicinity of the crack was the main cause of the delamination of the CFRP sheet (Maalej and Leong, 2005b). For (C100-cr/CFRP), flexural crack induced interfacial debonding mode of failure was observed, the debonding location started just underneath the load position, this fact was also noted by Aprile et al. (2001). For (C100-El/CFRP), flexure crack in which the crack passed around the repaired ECC followed by interfacial debonding of CFRP.

In contrast with concrete, for all the other specimens where CFRP was applied over the ECC layer with different thicknesses, the common interfacial debonding of CFRP was changed to shear failure. Flexure shear crack was observed in case of (C90E10-cr/CFRP) while (C70E30-cr/CFRP) and (C50E50-cr/CFRP) underwent a pure shear mode of failure and the crack was found extending from the support directly to the loading point. The shear crack split the concrete near the support leaving a small portion attached to the ECC layer. Moreover, it was noted that 30 - 50% reduction in the effective shear resisting cross-section for both (C70E30/CFRP) and (C50E50/CFRP), respectively, was behind the observed pure shear failure. This emphasizes the great influence of ECC on delaying the interfacial debonding failure or even preventing its occurrence. It was thought that if the beams were well confined in shear, the previous trends might have little changes. Moreover, it might be expected that the interfacial debonding would have happened but after achieving higher loading value. The reasons for the strong bonding between ECC and CFRP was mentioned in details in the previous chapter and was attributed to the ability of ECC to develop very high strain comparing to concrete; along with the small size cracks that were created in case of ECC. The previous reasons might lead to minimize the induced shear stress in the adhesive layer and decelerated the debonding failure.

Photo 4.2: Typical Modes of failure for the examined specimens

The presence of large amount of fibers on the prepared surface and just underneath this surface created also strong bonding between CFRP and the ECC substrate, it effectively helped in resisting both the induced shear and normal stresses generated along the intermediate adhesive.
Finally, it can be concluded that the dissipation of the consumed energy during loading for system repaired with CFRP might follow either, i) developing of a sudden localized crack at the most stressed bottom surface followed by the debonding failure mode when pasting the CFRP directly over concrete surface, ii) developing of another crack failure mode – here it was shear crack – rather that the interfacial debonding failure mode when pasting CFRP directly on the transition material ECC. Ductility is the ability of the repaired beams to carry deformation under peak load without full collapse. Figure 4.2 shows also the enhancement in the member ductility with the increase of ECC thickness. The maximum deflection was also noted and shown in Table 4.2. It was clear that the undergone deflection was directly proportional with the ECC thickness. The application of CFRP showed only minor changes in the maximum deflection achieved by the specimens.

4.4 CONCLUSIONS

In the current research, twenty-one plain concrete specimens were prepared to examine the effectiveness of using ECC as a repair material for cracked concrete beams combined with/without pasting of CFRP sheets. The following were concluded:

(1) ECC had the ability to bridge the internal forces between the crack sides due to its high ductility and perfect contact with the original substrate concrete without the use of any adhesives.

(2) Local placing of ECC at the crack position had no great significance in restoring the integrity of the damaged structures but it was found better than only injection with epoxy.

(3) As the thickness of ECC increased, both the section capacity and the ductility of the damaged beam were enhanced.

(4) The repair incorporating CFRP sheets showed almost similar flexure strength achievements. However, when ECC was used as a substrate to the CFRP, the mode of failure was changed from the undesirable interfacial debonding to shear failure.

(5) The minimum thickness of ECC followed by CFRP was found optimum in enhancing both section capacity and ductility with low probability of interfacial debonding.

(6) The change in the curing ages between the ECC and the concrete beam did not show any weakness in their contact.

CHAPTER 5

5. STRENGTHENING OF ARCHED HYDRAULIC STRUCTURES BY CFRP

5.1 INTRODUCTION

Recently, Carbon Fiber Reinforced Polymers (CFRP) have proven adequacy in rehabilitation of variety of structures on both practical and experimental fields. However, their performance with arched structures is still under consideration. Arched structures play an important role in serving the civil environment especially those with long spans like bridges or even with relatively short spans like a vent in a multi-vent regulator. Due to their presence in severe conditions across water streams and big rivers; many problems can occur due to: 1) Degradation because of aging problem coupled with insufficient care and maintenance, 2) Severe surrounding environment exposure accelerates the deterioration process, 3) Difficulty of repairing with the traditional materials that are neither costly nor time consuming but might sometimes affect the hydraulic geometry of these structures, 4) Many problems, such as cost, time, and change in the path of the water stream, that could happen if the decision of constructing of a new structure is taken, and 5) Increasing the applied service loads more than the originally designed loads. The above mentioned problems have led to more investigations and explorations of new ways for repairing, strengthening and retrofitting the structure to its original state. This chapter focuses mainly on using CFRP in strengthening, and rehabilitation of a prototype models of arched hydraulic structures typically used in regulator vents in Egypt. In the current study, ten plain concrete specimens were externally strengthened by CFRP sheets with variable length, thickness, and position of application. The evaluation criteria were based on the enhancement of sectional capacity, ductility, and the behavior of the specimens at failure.

Results showed effectiveness in using CFRP both in enhancing the sectional capacity and the ductility of theses structures. The study also showed that with soffit strengthening, complete brittle mode of failure was achieved while with both sides strengthening, and with combination of sides and soffit strengthening, ductile mode of failure was achieved.

CFRP have been used for many research and practical disciplines. It was found adequate for repairing and strengthening of various concrete, steel, and wood members (Shaun Hay et. al, 2006, Islam M.R. et. al, 2005, JCI TC952, 1998). It has been stated that CFRP offers several advantages over conventional materials, such as a superior strength/weight ratio, high stiffness, corrosion and chemical attack resistance, durability enhancement, saving in labor and material costs, and its high speed in installation and curing (TaeHoon and Makarand, 2006, Maalej M. and Leong K.S., 2005). The aim of the current research was to check the adequacy of strengthening prototype concrete specimens, simulating a typical single vent widely used in regulators, using CFRP sheets for further practical implementations.

Table 5.1: Nomination of specimens showing the strengthening condition

Sample ID	Group	Position of CFRP sheet
S1	Control	No repair
S2	Group A	Along middle third of soffit with single layer of CFRP
S3		Along middle third of soffit with double layer of CFRP
S4		Along middle half of soffit with single layer of CFRP
S5		Along whole soffit length with single layer of CFRP
S6	Group B	CFRP is represented in the form of 5 cm strips on both sides along the whole section
S7		CFRP covering web above the soffit place on both sides
S8		CFRP covering web along the whole section
S9	Group C	Combination of cases S3 and S7
S10		Combination of cases S3 and S8

5.2 EXPERIMENTAL PROGRAM

In order to investigate the capability of CFRP to strengthen old or deteriorated arched structures; ten scaled down arched specimens, 100 mm thickness, made of plain concrete were prepared. Schematic diagram representing the typical dimensions of the specimens is shown in Figure 5.1. For the arched specimens, one remained without strengthening and was kept as a control specimen, S1, while the rest were divided into three groups according to the strengthening location as follow; Group (A) represents specimens with soffit strengthening, Group (B) represents specimens with sides strengthening; and Group (C) represents specimens confined using combination of soffit and sides strengthening. Table 5.1 and Figure 5.2 show the nomenclature, location and dimensions of strengthening of each group. Photos 5.1 a) and b) show the arch specimens in the self-made moulds just after casting and after pasting the CFRP sheets, respectively. After 28-days, compression and flexure tests were conducted on standard size specimens following ASTM C39/C39M, and ASTM C78, respectively. The measured compressive strength, flexure strength and Young’s modulus of elasticity for concrete were 40 N/mm^2, 6 N/mm^2 and 350 GPa, respectively. While the compressive and flexure strength of specimens confined with CFRP were 75 N/mm^2 and 10 N/mm^2, respectively.

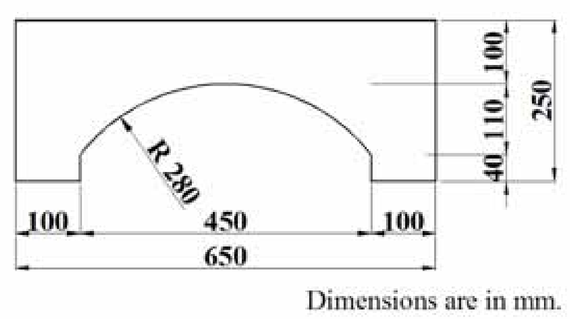

Figure 5.1: Typical concrete dimensions of the arched specimens

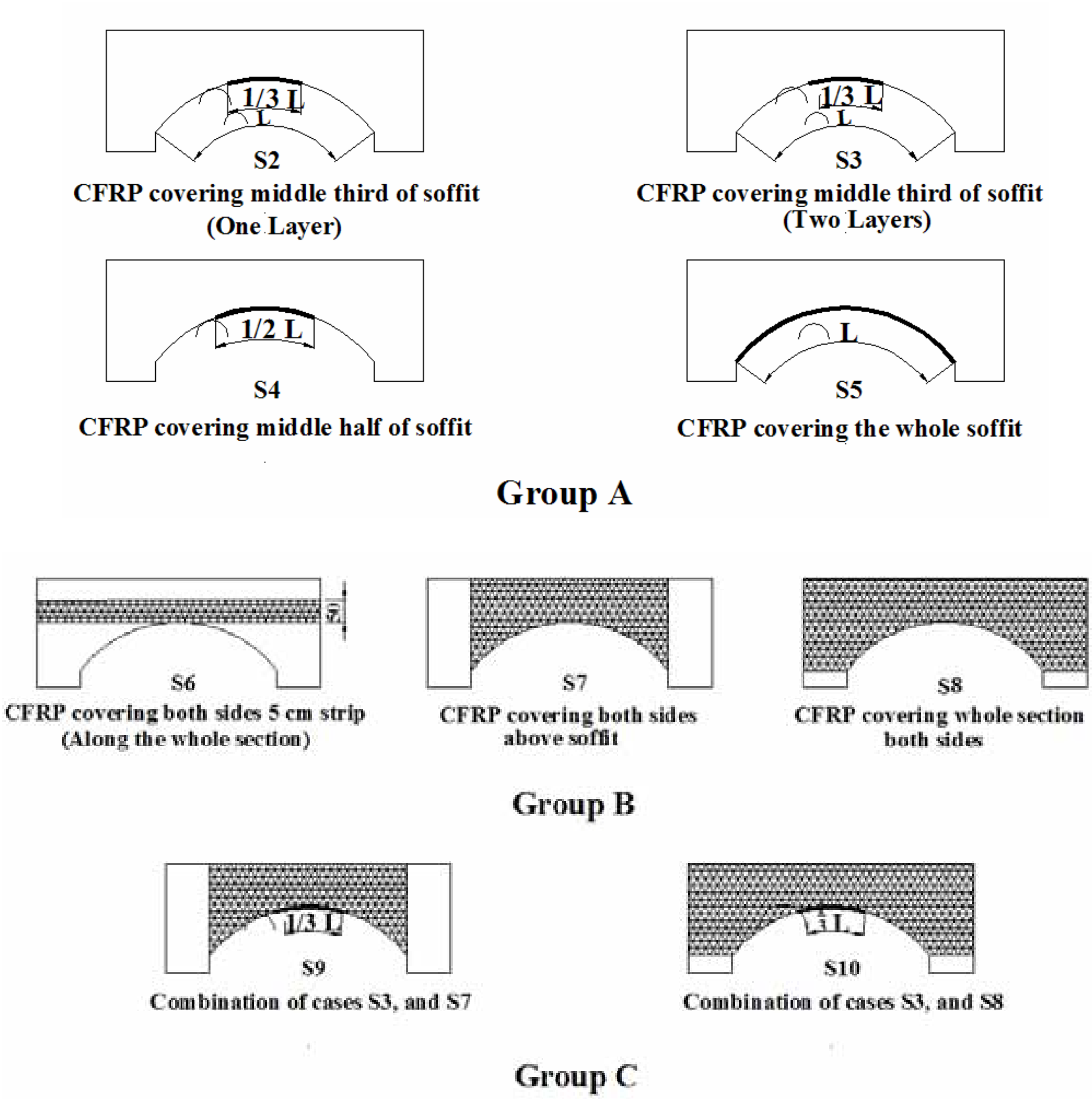

Figure 5.2: Combinations of strengthening conditions

Photo 5.1a): Moulds after casting, and b): after pasting CFRP sheets

Photo 5.2: Typical test setup

5.3 DESTRUCTIVE TESTING

Flexure test was conducted to compare the behavior of the arch specimens with and without CFRP strengthening. All arched specimens were subjected to a mid span line load across the arch thickness. The typical loading configuration is shown in Photo 5.2. Strain gauges were mounted at the mid span of the arch soffit. Load cell of capacity of 100 KN was also used for recording of the applied mid-span loads. Both strain and the applied load were recorded with a frequency of 10 readings per seconds.

5.4 BOUNDARY CONDITIONS

In order to simulate the real boundary conditions of the actual structure, where both horizontal and vertical movements of the supports are prevented, a prototype arch specimens were supported on two (100 x 100mm) leg bases and placed in full contact with a rough steel plate where the coefficient of friction between concrete and the steel base plate was assumed sufficient enough to resist the resulting sliding force. This assumption can be verified suggesting a simple strut and tie model to simulate the expected flow of internal forces in the arch specimen. First, the moment capacity of a plain concrete beam of cross-sectional area (100 x 100mm) was calculated. It was also assumed that the flexure strength of the prism should be equivalent to that of the arched specimen with similar mid-span cross-section. Consequently, and within the elastic limits, the maximum generated tensile force resulted from flexure test in case of the prism will be the same as that generated in the arch. Figure 5.3a shows the assumed strut and tie model to simulate the flow of forces in the beam. Thus, the obtained maximum tensile force in prism (14.8 KN) will again be assumed in case of the arch specimen S1 as shown in Figure 5.3b.

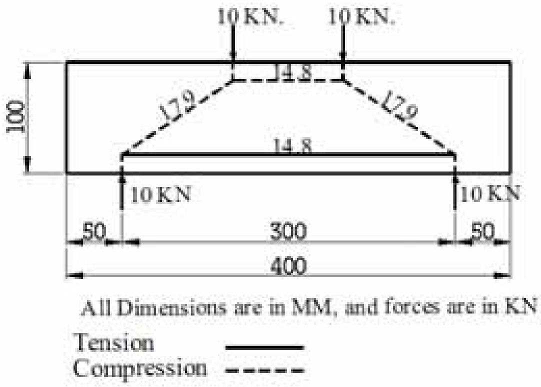

Figure 5.3 a): Strut and Tie model for small prism within elastic limits

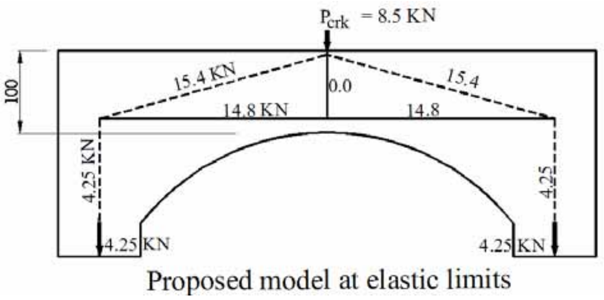

Figure 5.3 b): Strut and Tie model for S1 within elastic limits

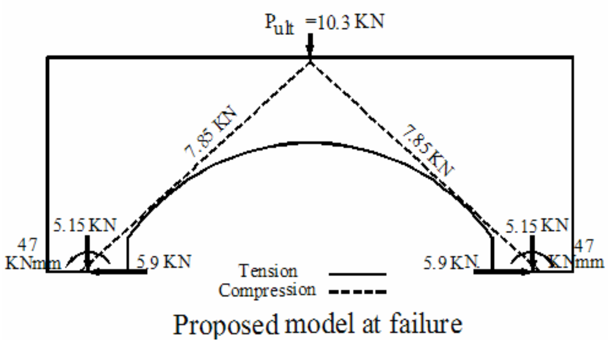

Figure 5.3 c): Strut and Tie model for S1 after exceeding elastic limits

The other compression forces among the assumed struts were determined in a backward analysis. The expected external load to initiate the crack in the soffit of the arch was determined (8.5 KN). It was found that this load was far behind the actual load obtained experimentally (10.3 KN). This again suggested that from the start of elastic limits till complete failure, the specimen did not fail due to sliding. It was however observed further extension of the crack at the mid-span until complete failure. Further check was done by simulating another truss model at the observed failure load. In the second model (Figure 5.3c); loads were assumed to flow directly to the supports where the friction force between the base plate and the concrete base is the only force to prevent the sliding of the specimen. The extreme strut slope was found equal to 1.15 and can be obtained by dividing the vertical component of the reaction over the horizontal one. This value was found big enough to ensure no movement of the supports and that the flexure failure was the cause of failure not the sliding.

5.5 RESULTS AND DISCUSSION

5.5.1 Section Capacity

It was generally noted that soffit strengthening represented by Group (A) achieved higher section capacity than those of Group (B) with only sides' strengthening. The significance of having CFRP lumped at the bottom most fiber of the specimen or having CFRP distributed along the tension zone was explored. It was found that for almost same area of CFRP placed in tension zone, i.e. below the neutral axis, when the total area was lumped at position of maximum tensile stress as in Group (A); the corresponding strains at bottom fiber was decreased and shear stress in the adhesive was also decreased that led to the delay in the interfacial debonding of CFRP. Moreover, lump the whole area of CFRP together led to the creation of longer moment arm and consequently higher section capacity. On the other hand, distribution of CFRP among the sides of the specimens as in Group (B) led the CFRP to be subjected to variable tensile strains just after starting the loading, accelerated the interfacial debonding, and decreased the section load carrying capacity.

For Group (A), it was noted that after loading the arched specimens and due to its structural nature, lateral deformations in soffit has the tendency to deform laterally outwards stretching the CFRP sheet downwards at mid-span position. This behavior accelerated the debonding failure and decreased the specimens load capacity as strengthening sheet got longer. It was observed that the loading capacity of S2, S4, and S5 was 90, 45, and 19% more than the control specimen, respectively.

Doubling the thickness of the pasted CFRP, as in specimen S3, led to a further decrease in the strains, lowered the shear stress in the adhesive and consequently increased the loading capacity (Maalej M., and Leong K.S., 2005). S3 achieved 113% enhancement in the section capacity above the control.

For Group (B), the test showed a medium enhancement in the section capacity as compared to the control specimen. For S6, S7, and S8 the enhancement in the sectional capacity was 9, 42 and

74% respectively. It was also noted that when the width of CFRP increased as in S7, the tensile forces were redistributed among the whole CFRP sheet leading to reduction of stresses in the bottom fiber and consequently, delaying the interfacial debonding of CFRP and increasing the section capacity. For S8, in addition to the same reasons of S7, it was found that increasing the CFRP bonding length led to higher section capacity. The observations also showed that Group (B) strengthening was not optimum in achieving higher section capacity but it was able to prevent the full collapse of the specimens at failure.

The best strengthening condition was achieved when using both soffit and sides' strengthening at the same time as in Group (C). For S9 and S10 the increase in section capacity was 178, and 186%, more than the control, respectively. This combination showed an optimum section behavior; the side strengthening worked towards preserving the specimens from complete collapse and postponed the initiation of cracks while the soffit strengthening targeted a high section capacity. Figures 5.4 through 5.6 show the load-strain curves for the tested specimens.

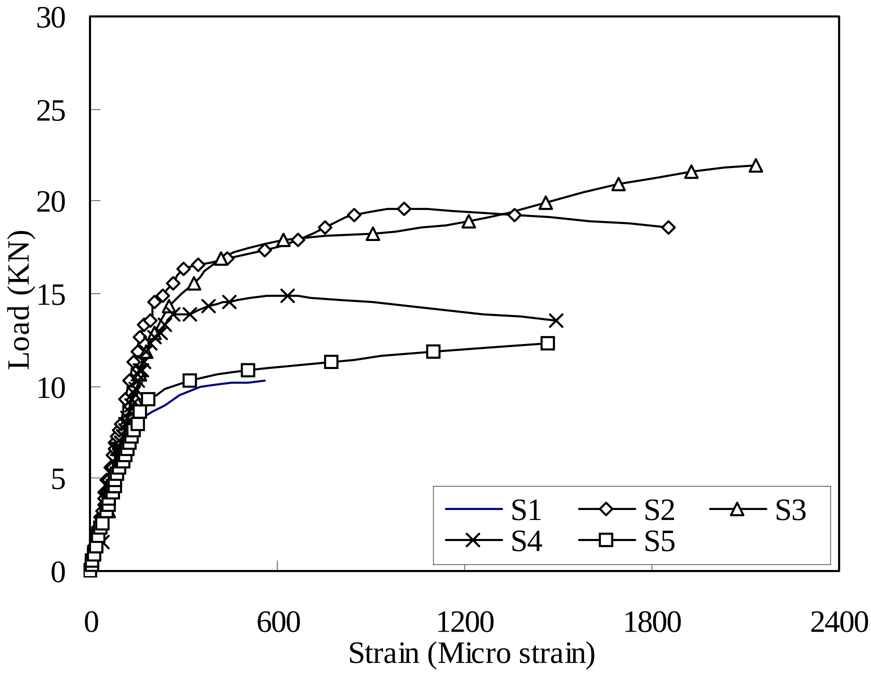

Figure 5.4: Load-strain curves for Group (A)

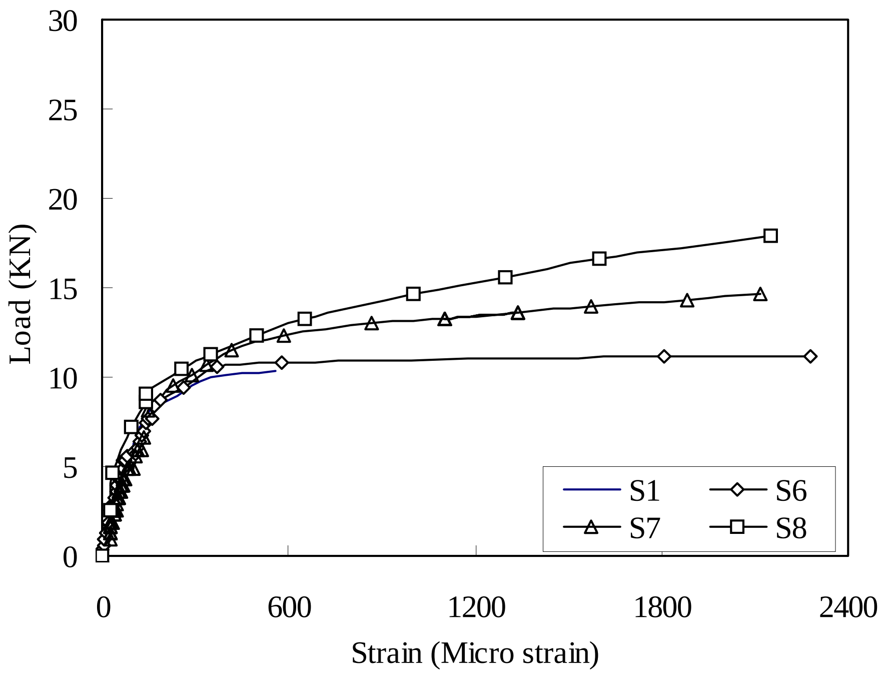

Figure 5.5: Load-strain curves for Group (B)

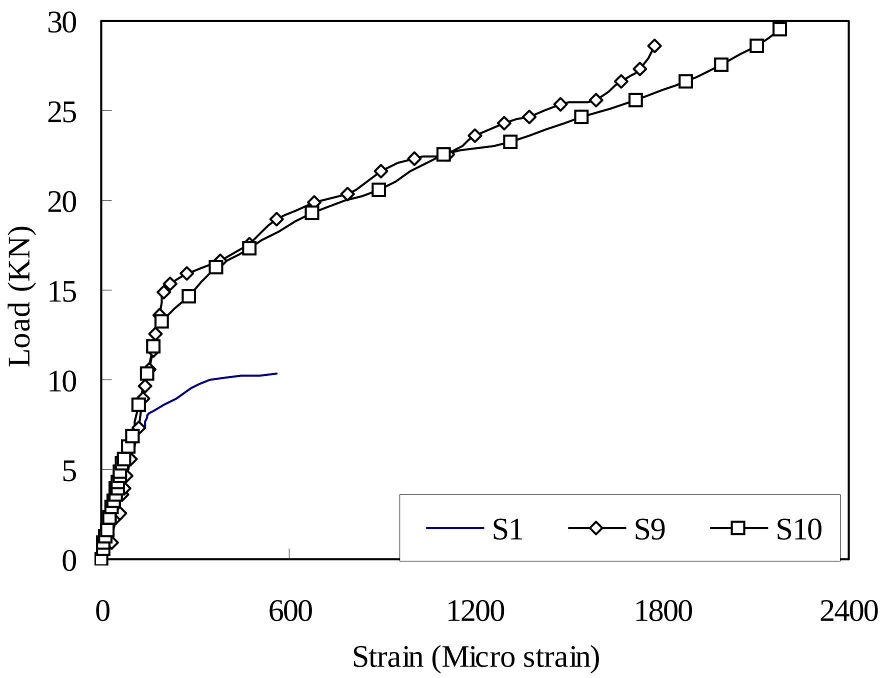

Figure 5.6: Load-strain curves for Group (C)

5.5.2 Modes of Failure

As reported earlier, the full strength of the CFRP composites can not be reached due to their debonding type of failure (JCI TC952, 1998, Bo Gao et. al, 2006). Therefore, using an effective limiting strain value for the CFRP material is the way to incorporate the effect of the bonded reinforcement in any suitable strength prediction method for the structure (Islam M.R. et. al, 2005). In general, most of the failure modes of beams with CFRP strengthening occur in a brittle manner with little or no given signs for failure (Maalej M., and Leong K.S., 2005), however, the current study showed the possibility of transforming the brittle failure mode to almost ductile failure. In the current study, in all the arched specimens, the failure occurs starting with flexure cracks at mid-span followed by interfacial debonding failure of the CFRP system while no concrete crushing at ultimate load was noticed. Photo 5.3 show different failure modes of specimens strengthened with CFRP.

Group (A) appeared to have complete brittle failure behavior; the failure mode was triggered by the formation of flexure cracks in the mid-span that yielded extremely high stresses in the vicinity of the crack. The stress concentration along CFRP helped in delaminating of the CFRP sheet starting at the crack location and propagating in a very brittle manner towards the edges of the sheet. Moreover, it might be expected that the debonding in both S4 and S5 occurred faster, with lesser ultimate load, due to the tendency of the supports to deform laterally outside, and consequently stretching the CFRP sheet and pulling it downwards at the mid span.

Photo 5.3: Modes of failure for the examined arch specimens

Although specimens of Group (B) did not show high gain in strength as compared to Group (A), but their mode of failure was almost ductile with noticeable gain in strain before failure occurred (Shamim A. et. al, 2002); that might be due to increasing in the contact surface area of CFRP which led to delay the interfacial debonding. The integrity of the specimens of this group was preserved at the maximum load without full collapse. The failure started with flexure cracks at the mid span followed by interfacial debonding of the CFRP. It was also noted that this type of strengthening minimized the lateral movement of supports and acted as a tie, satisfying the section stability, and safely conveying the applied load to the supports.

For Group (C), the failure showed an excellent behavior for specimens S9, and S10. The system remained in a good condition with no collapse even after the failure occurred. Similarly, failure started with tension cracks at the mid span followed by interfacial debonding of the attached CFRP sheets. It was also noted that after exceeding the elastic limits, strain hardening behavior was observed. This combination proved to be the optimum solution as a repair or strengthening for arched structures.

5.5.3 Ductility

To examine the ductility of the strengthened beams, the following ductility criteria were used, namely the energy ductility (Naaman and Jeong, 1995), which can be defined as follow:

$$\mu_e = (1+E_{tot}/E_{elastic})/2 \qquad (5.1)$$

Where, E_{tot} and $E_{elastic}$ are the total energy up to ultimate load (area under the load-strain curve) and elastic energy, respectively.

Table 5.2 shows a summary of the calculated energy ductility for specimens with higher section capacity and reasonable mode of failure. It is shown that both Group (B), and Group (C) were more ductile than Group (A), specimen S3 showed higher ductility that specimen S2, this was attributed to the effect of doubling the CFRP area at the arch soffit. It was also noted that in Group (C) the ductility index was slightly decreased than Group (B); this might be due to the presence of combined strengthening; the section became stiffer with high residual of elastic energy at failure and consequently lowering the ductility.

Table 5.2: Energy ductility index

Group	**Specimen ID**	**Yield load (KN)**	**Ultimate load (KN)**	**Energy ductility index (μ_e)**
Group A	S2	13.6	19.6	4.86
	S3	14.3	21.9	8.88
Group B	S7	8.1	14.6	17.91
	S8	8.6	17.9	18.41
Group C	S9	13.6	28.6	14.73
	S10	13.3	29.5	15.14

5.4 CONCLUSIONS

The current chapter concludes the following:

(1) Soffit CFRP strengthening was good in improving the section capacity, but the failure mode was sudden due to complete interfacial debonding. Combinations had showed that best location for soffit repair was in the middle third of the arch, i.e. the zone in which maximum tensile strains were developed.

(2) Doubling the area of CFRP in the soffit strengthening had led to decrease the shear stresses in the bonding adhesion and therefore increased the section capacity.

(3) Using only sides strengthening were good in enhancing section ductility, with no sudden failure. However, no significant improvement in section capacity was noticed.

(4) An optimum way for strengthening of arched sections was achieved by using soffit and sides strengthening together. The section capacity was enhanced significantly; 186% for S10 more than control specimen and at the same time a ductile mode of failure was occurred.

CHAPTER 6

6. STRENGTHENING OF GROOVED CONCRETE COLUMNS USING CFRP

6.1 INTRODUCTION

Columns are considered one of the main components of any structural system. Columns can take different shapes according to different architectural and structural reasons. Circular and square columns are the most common used shapes. Many researches have been concentrated on ways of strengthening and repairing of these columns. It is however found that almost limited number of researches has dealt with columns containing grooves. The current study is considered important to strengthen columns, abutments or piers with discontinuities in their outer surfaces. The use of externally bonded FRP composites for repair can be a cost-effective alternative for restoring or upgrading the performance of the existing concrete columns. In the current chapter, eighteen plain concrete prisms with different geometry were destructively examined under different strengthening conditions using CFRP. Additional four cylinders were tested to confirm compatibility with previous researches as well as to grantee the confinement efficiency. The study also established new expression for predicting the expecting ultimate strength for grooved columns wrapped with CFRP. The results showed that the efficiency of CFRP strengthening decreased with the presence of grooves or discontinuities external surface of columns. Moreover, the ductility of concrete prisms was significantly increased after wrapping with CFRP.

6.2 GENERAL BACKGROUND

Many researches have been dealing with deterioration problems associated with concrete columns as well as studying their behavior when repaired and confined with external fiber composites. Mirmiran and Shahawy (1997) showed a design method to estimate the expected column capacity after wrapping with fibers. Their study also showed a unique characteristic for confinement with fiber composites which is unlike steel, FRP curtails the dilation tendency of concrete as it reverses the direction of the volumetric strains. G. Wu et al. (2006) developed three new models for estimating the compressive strength of concrete cylinders confined with 1) common modulus FRP sheets, 2) high modulus FRP sheets, and 3) encased with FRP tubes. It was suggested that the confinement efficiency can be decreased with the increase in the confinement ratio (confined stress / unconfined compressive strength) for the same type of FRP.

J.F. Berthet et al. (2005) showed that the ultimate capacity of confined concrete, in term of compressive strength and axial strain, is directly connected to the confinement pressure generated by the composite jacket. Indeed, the strength gain at failure linearly increases with the confinement ratio, so it was noted that the confinement efficiency does not depend on the confinement level of the concrete.

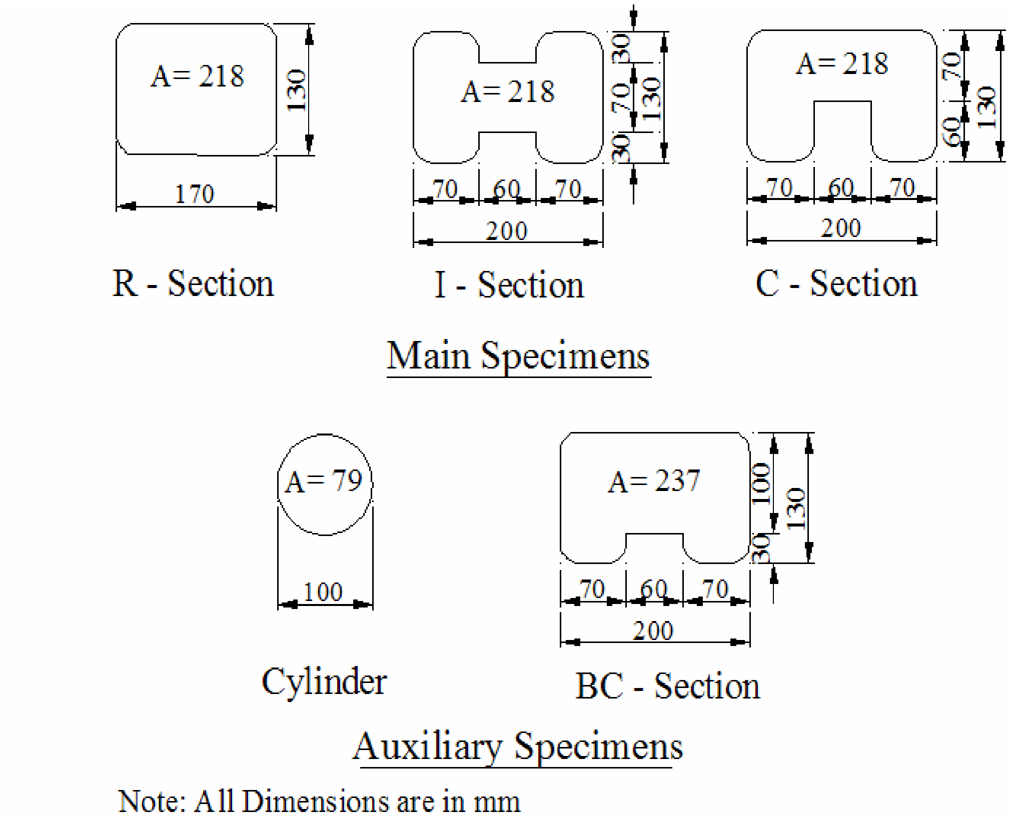

Figure 6.1: Layout of concrete specimens

Moreover, the test results by J.F. Berthet et al. (2005) showed that the cylinders confined by equal stiffness envelopes, constituted by glass or carbon fibers, presented identical behaviors. Cylinders confined respectively by one layer of carbon and three layers of E-glass (equivalents jackets in term of stiffness) present stress-strain curves confused up to an advanced stage of the pseudo-plastic zone.

Few researchers worked with concrete columns with square or rectangular shape. G. Campione (2006) showed that using local longitudinal CFRP strips at the corners before application of the continuous main layers avoids possible fiber cutting at the corners; moreover, the increase in the number of reinforcing layers produced an increase in the compressive strength and significantly increases the maximum strain capacities. However, the effect is not directly proportional to the number of layers; finally, the increase in the height of the specimens produced reduction in the achieved maximum strength.

O. chaallal et al. (2003) showed that the stiffness of the applied CFRP jacket is the key factor in the design of the external jacket retrofits. The jacket must be sufficiently stiff to develop appropriate confining forces at relatively low column axial strain levels. In addition, a stiff jacket will better control the dilation of the cross section, resulting in larger axial strain capacities. Finally, the gain in the compressive strength of concrete columns confined by CFRP depends on the ratio of the stiffness of FRP jacket in the lateral direction to the axial stiffness of the column.

Photo 6.1: Self-prepared moulds

Photo 6.2: Concrete prisms after casting

Photo 6.3: Typical test setup

B. Doran (2008) and B. Doran et al. (2008) suggested a new numerical nonlinear modeling of rectangular/square concrete columns. In their models, the cylinder compressive strength, the cohesion and the internal friction parameters of Drucker-Prager criterion have been adjusted through a parametric study. Four different relations of cohesion corresponding to various levels of lateral confinement were adopted and compared with experimental data which showed a great compatibility. Drucker-Prager type plasticity models are generally preferred for modeling the constitutive behaviors of frictional materials, like concrete, soil, rock and even masonry (Koksal et al., 2007, Koksal et al., 2004).

6.3 EXPERIMENTAL PROGRAM

6.3.1 Test Setup

In this chapter, five sets of concrete short columns with/without grooves were prepared; three sets of identical area, 218 cm^2, another set with larger cross-sectional area, 237 cm^2, and the last set was standard cylinders of cross-sectional area of 79 cm^2 (Figure 6.1). The first set was of a rectangular section with dimensions (130 x 170 mm) and composed of three specimens corresponding to different strengthening conditions. The remaining three sets are those containing grooves; every set composed of five specimens each. Different strengthening conditions for all the groups are shown in Table 6.1, and Figure 6.2. The height of the specimens was adopted to 260 mm for two reasons; the first was to be in accordance with many international standards for short columns where the ratio of the minimum side dimension to its height should be less than 10 to overcome the buckling effect, while the second was due to the compression machine dimensions limits. Additional four typical cylinders of diameter 100 mm and height 200 mm (Area = 79cm^2) were also prepared so that comparison with other works from the literature can be conducted as well as to confirm the confinement efficiency. For all rectangular specimens, the corners were rounded to a radius of 20 – 40 mm as per the recommendation of many researchers (G. Campione, 2006, O. Chaallal et al., 2003). The concrete surface was polished and smoothen using sand stone. CFRP was then applied. For all the examined specimens, the centroid was first determined then the specimens were placed concentrically with the machine axis. The applied load against measured strains and displacement readings were noted, plotted and analyzed. For each combination, a sum of eight readings, four strain gauges plus four linear variable differential transducers (LVDTs), were recorded. Each side contained both vertical strain gauge and horizontal LVDT while the opposite side contained horizontal stain gauge and vertical LVDT. The horizontal readings were taken as the average for measures obtained from each two opposite sides for both the long directions. The vertical readings were taken the average of all the measured vertical readings of all sides. The specimens were cast in non-standard self-prepared moulds as shown in Photo 6.1. Specimens were cast and left for 24 hours until de-molding then water cured for 28 days. Photo 6.2 shows group of specimens after hardening. Photo 6.3 shows typical test loading set up.

6.3.2 Materials

The concrete mix was designed as per American Concrete Institute, ACI 211.1 and the used mix proportion is shown in Table 6.2.

Table 6.1: Concrete specimens description

ID	External Dimensions A (mm)	External Dimensions B (mm)	Net Area x 100 (mm^2)	Total Area of grooves x 100 (mm^2)	Area ratio* (%)	Description
R1	130	170	218	N.A.	N.A.	No confinement
R2						Full wrapping with CFRP
R3						5cm CFRP Strips confinement, spacing 5cm
I1	130	200	218	36	14	No confinement
I2						Full wrapping with CFRP sheet
I3						5cm CFRP strips wrapping, spacing 5cm, plus separate groove strengthening
I4						Full length wrapping to the flanges. Web has no strengthening
I5						Full length wrapping to flanges ending with staggered closing at the web
C1	130	200	218	36	14	No confinement
C2						Full wrapping with CFRP sheet
C3						5cm CFRP strips wrapping, spacing 5cm, plus separate groove strengthening
C4						Full length wrapping to flanges ending with staggered closing at the web
C5						Full length wrapping to the flanges. Web has no strengthening
BC1	130	200	237	18	7	No confinement
BC2						Full wrapping with CFRP sheet
BC3						5cm CFRP strips wrapping, spacing 5cm, plus separate groove strengthening
BC4						Full length wrapping to flanges ending with staggered closing at the web
BC5						Full length wrapping to the flanges. Web has no strengthening

* Ratio between the area of grooves to the total area of an imaginary confined area based on the external dimensions

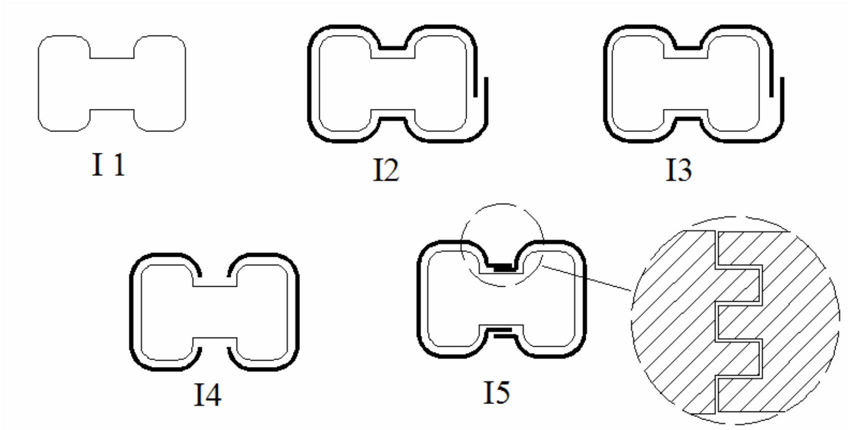

Figure 6.2: Example for the strengthening condition of I-section

Table 6.2: Mix proportions of concrete

Aggregate size (mm)	Slump (mm)	Air content (%)	W/C (%)	s/a (%)	Unit weight (kg/m^3)			
					W	C	S	G
20	100	2.5	62	42	185	300	750	1,056

After 28 days, the measured characteristic compressive strength with compliance of ASTM C39/C39M, and was equal to 25 N/mm^2. Normal strength concrete was used to be easy to simulate a condition close to the deteriorated condition in nature as well as to facilitate capturing the effectiveness of the strengthening. Unidirectional CFRP with compatible two-part epoxy similar to those presented in chapter 3 were used. The properties of CFRP and the adhesive were noted early and shown in Tables 3.3 and 3.4, respectively.

6.4 RESULTS AND DISCUSSION

Figures 6.3 through 6.11, present the load-strain curves for all the examined specimens. The right portion of the curves correspond to plots of the axial load verses transverse strains; while those in the left portion correspond to curves of axial load verses axial strains. Generally, it can be observed that the confinement of short rectangular grooved prisms with CFRP wrapping improved the compressive strength and enhanced significantly the ductility of the columns.

6.4.1 Loading Capacity

6.4.1.1 Cylinders

For cylinders, the results shows that the confined compressive strength was significantly increased, 144% more than the unconfined strength. This could be attributed to: 1) for circular cross-sections, the effective loading area is the full area of the specimen which is subjected to uniform normal stresses without any local concentration of stresses at corners like in the case of square/rectangular sections, and 2) the circular cross-sections allow continuity in the flow of forces through the CFRP sheets and consequently allowed the fibers to reach their ultimate tensile strength. It was also observed that the confined cylinder exhibited strain hardening behavior. After the fracture of the concrete core, the behavior of the load-strain curve was a straight line directed upwards, this also coincides with Berthet et al. (2005). This was due to the high efficiency of the CFRP wrapping, the linear relationship was due to the elastic linear behavior of CFRP.

6.4.1.2 Rectangular section

For the rectangular sections, the loading capacities for R2, and R3 were 23% and 14% more than the control prism, R1, with no strengthening. This could be attributed to reasons opposite to those of the cylinder case; the effective loading area was only a portion of the section and not the whole section. Moreover, the change in the phase angle, 90^o in case of rectangular or square sections, of the wrapped CFRP along the sides of the column made it difficult to achieve smooth flow of the tensile forces along CFRP among different planes. This consequently led to improper utilization of CFRP sheets and to a slight increase of the overall compressive strength of the wrapped specimens. In the current study, the corners were rounded to a fillet radius of 20 mm; the effect of this rounding could significantly enhance the overall performance of the short columns. When comparing the transverse strains in both short and long sides of the specimens (Figures 6.4 and 6.5, respectively); it could be seen that almost same level of strains were achieved. This revealed to the adequacy of the strengthening system and the rounded portions in the transmission of the tensile forces smoothly along the CFRP sheet in perpendicular planes.

The full strengthening specimens, R2, was found better than strengthening using only strips confinement, R3, that was due to the initiation of fine cracks in the unconfined spaces between the CFRP strips. This, therefore, led to a release in the absorbed energy during loading in an early stage and consequently achieved lower section loading capacity. It was also noticed that the ratio between the loads bearing area/specimens cross-sectional area had a great influence in decreasing the load carrying capacity of the columns.

6.4.1.3 I-section

The examined I-section was selected with the same cross-sectional area of the rectangular section, i.e. 218 cm^2. Two identical grooves of relatively small area, 18 cm^2 each, were symmetrically adjusted to the mid span of the long sides. It was generally observed that confinement of the I-sections with different CFRP wrapping conditions did not have significant enhancement in the section loading capacity. It was however, noted a slight reduction in the observed fracture load. The geometry of the selected I-section was behind the reduction in the achieved strength. The examined I-section mainly composed of two stiff flanges, where most of the section area is concentrated, connected with a weak web. When loading started, the whole section subjected to a uniform pressure until exceeding the section elastic limits, after then, the two stiff flanges took the load alone with considerable out of plane deformations. This led to initiation of cracks in the weak connecting web followed by splitting of the column into two pieces. In another way, the presence of stiffeners in the long direction of the column allow limited out of plane deformation along the longest side. Whereas the short direction underwent larger out of plane deformations that finally, tended to pull the weak web and accelerate the initiation of the splitting cracks.

The noted reduction in the section capacity was ranged between 5% - 9% lesser than the control. The passive wrapping effect of CFRP was another reason behind obtaining lower loading capacity. This was due to the tendency of the short sides to deform out of plane and consequently pull the CFRP from the groove position. This led also to weaken the intermediate connected web part and accelerated the failure. The best section capacity was observed for both full wrapping case and confinement with strips. The depth of the groove also played an important role in accelerating the debonding, in the current configuration; the 30 mm groove depth was also found not sufficient to provide a strong anchorage and therefore helped in accelerating the debonding failure along the sides of the grooves.

6.4.1.4 C-section

For the C-sections, the same concrete area was used but a groove of area 36 cm^2 was lumped in the mid-span of the long side of the column. The results show acceptable enhancement in the section capacity for all combinations. It was noticed that the enhancement in the overall section capacity was 28.06%, 30.83%, 28.46%, and 22.37% for C2, C3, C4, and C5, respectively over the control specimens C1. The general attitude of C-section specimens after loading was to elongate relatively higher in the side of the groove relatively more than the opposite side with no groove. This consequently led the two wings adjacent to the groove to move outwards causing initiation of cracks at the inner corner of the groove. When wrapping the C-sections with CFRP sheets, the fibers of CFRP after subjected to tension started pulling the sides of the grooves to outside and therefore accelerated the failure. For section C2, and after exceeding the elastic limits, debonding failure along the inner side of the groove was observed.

It was also, found that C5 exhibited the lowest section loading capacity and that was due to the absence of CFRP sheets along the inner side of the groove. C3 achieved the highest section capacity due to the presence of separated CFRP sheet on the inner side of the groove and extended to the groove sides in between the main CFRP strips. This led to 1) carry the longitudinal tensile forces along the groove without being affected by the pulling out forces of the main strips, and 2) the small hands connected the inner groove sides to the outer ones played an important role in decreasing the opening size and thus enhanced the overall loading capacity.

For Section C4, full wrapping was conducted with a staggered closing at the inner side of the groove. This combination was also good in achieving good section capacity and minimized the movement of the grooves sides. The failure in this combination was however different from that of C2; rotation of one side of the specimen followed by debonding of CFRP sheet at the groove inner side was observed.

6.4.1.5 BC-section

In this combination, the effect of groove size was checked. The same external dimensions for I-sections and C-sections were selected with a decrease in the groove area and increase in the concrete area equal to 18 cm^2. The new section was then named as BC- section.

It was observed a slight increase in the section loading capacity of the BC-section prisms than the other prisms, which was attributed to the slight increase in their cross-sectional area. It was however; found that the efficiency of wrapping in case of BC-section was lesser than in case of C-section. The enhancement percentage in the section loading capacity for BC-section columns was ranged from slightly higher than the control specimen to a value 8.44% more than the control. It might be attributed to the produced low confinement pressure created in this case, which was due to: 1) the depth of groove was small and consequently did not create full bonding between CFRP and concrete, thus, weak confinement was achieved, and 2) the increase in the ratio of the area of concrete/load bearing area. It was noted by B. Doran et al. (2009) that the increase in the specimens' area might affect negatively on the ultimate loading capacity of the section due to the decrease in the effective loading area.

This suggested the big influence of the groove size and depth to the overall section area. The anchorage length was found effective in increasing the section capacity. The longer the groove depth, the more the bonding length of CFRP sheet, the higher ability to decay the tensile forces in the wrapped CFRP sheet, and consequently the less probability for debonding to occur. On the other hand, the strong bonding for deep grooves might lead to facilitate the rotation of the groove side and accelerate the occurrence of cracks at the groove inner corners.

For BC2, BC3, and BC5 the increase in the section loading capacity over the control specimen BC1 was 8.44%, 4.05%, and 3.32% respectively. For BC4, the loading capacity was slightly decreased to 0.86% less than the control specimen.

Finally, it can be concluded that the groove dimensions have a big influence on the achieved compressive strength. It can be said that the ratio of the length of groove/total length of the side containing the groove as well as the ratio of the depth of groove/total specimen width at the location of the groove. In this study, it was observed that as the groove depth increase, the enhancement in the section loading capacity increased. It should be also noticed that for all the above conditions, the wrapped CFRP should have a sufficient anchorage length to prevent the debonding due to shortage in bonding strength.

6.4.2 Ductility

Many researchers have reported that wrapping columns with CFRP sheets increases the column ductility and enhances its ability to resist shear forces. In this study, the same conclusion was almost obtained. The wrapped specimens, in spite of their wrapping configurations, exhibited high transversal strain level after exceeding their elastic limits. Additionally, the longitudinal strain reached higher strain values compared to their reference specimens.

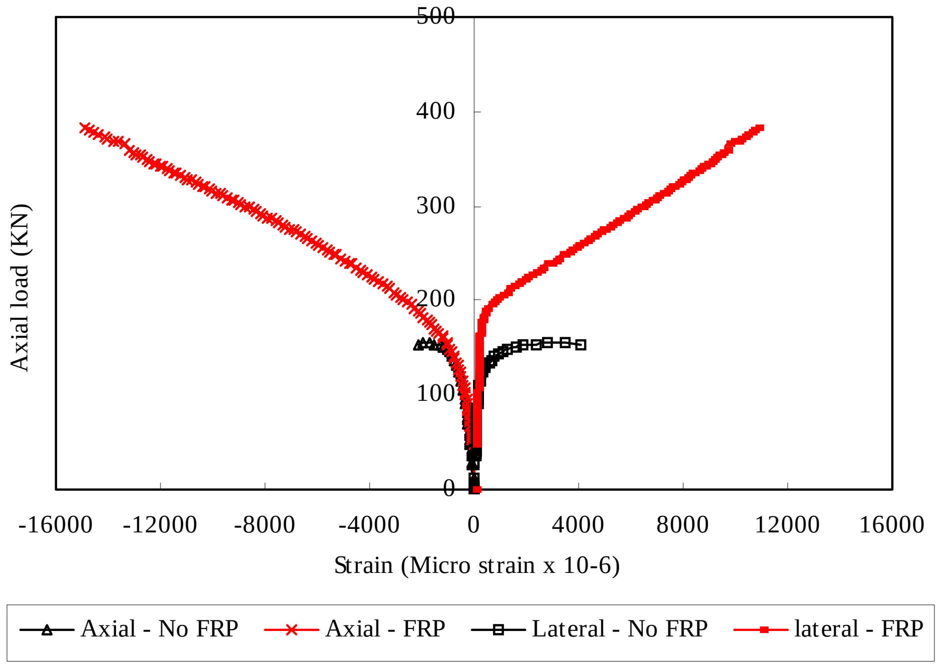

Figure 6.3: Load - strain curves for confined and unconfined cylinder specimens

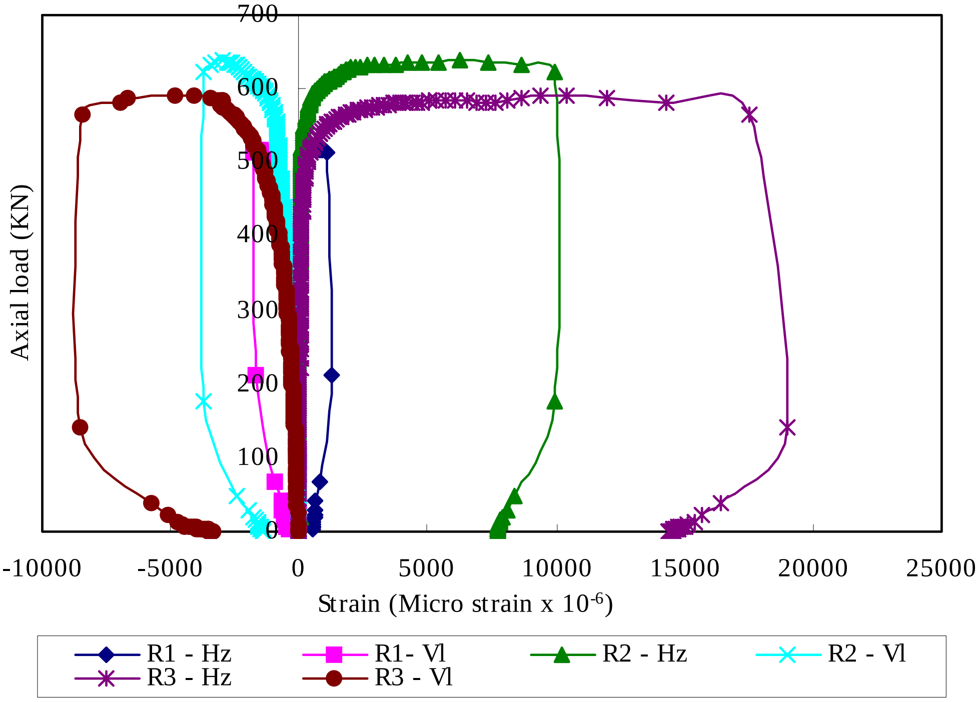

Figure 6.4: Load - strain curves for examined rectangular section – Long direction

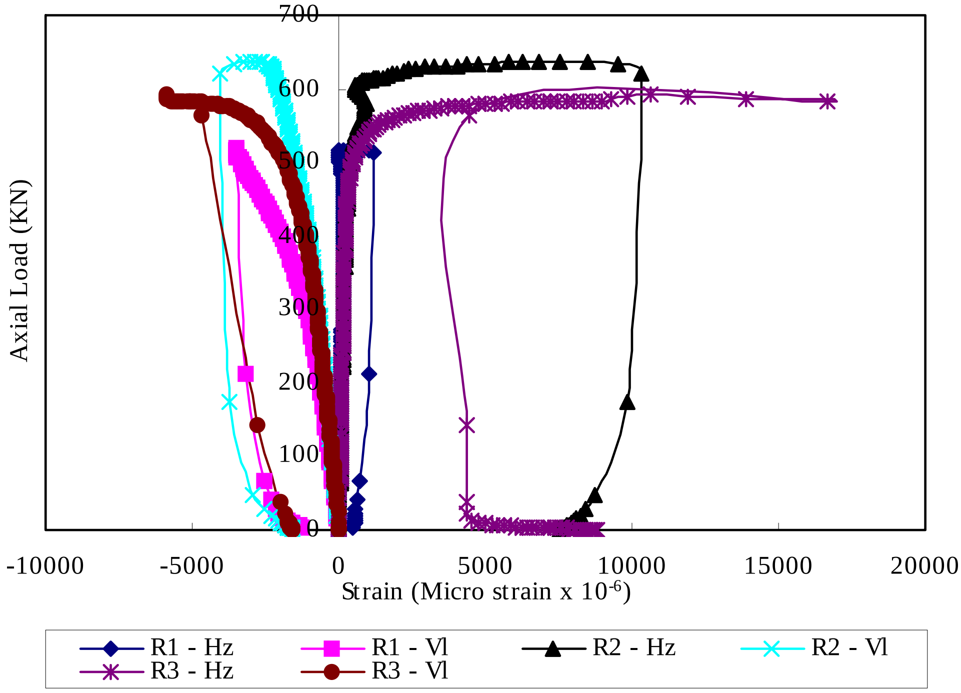

Figure 6.5: Load - strain curves for examined rectangular section – Short direction

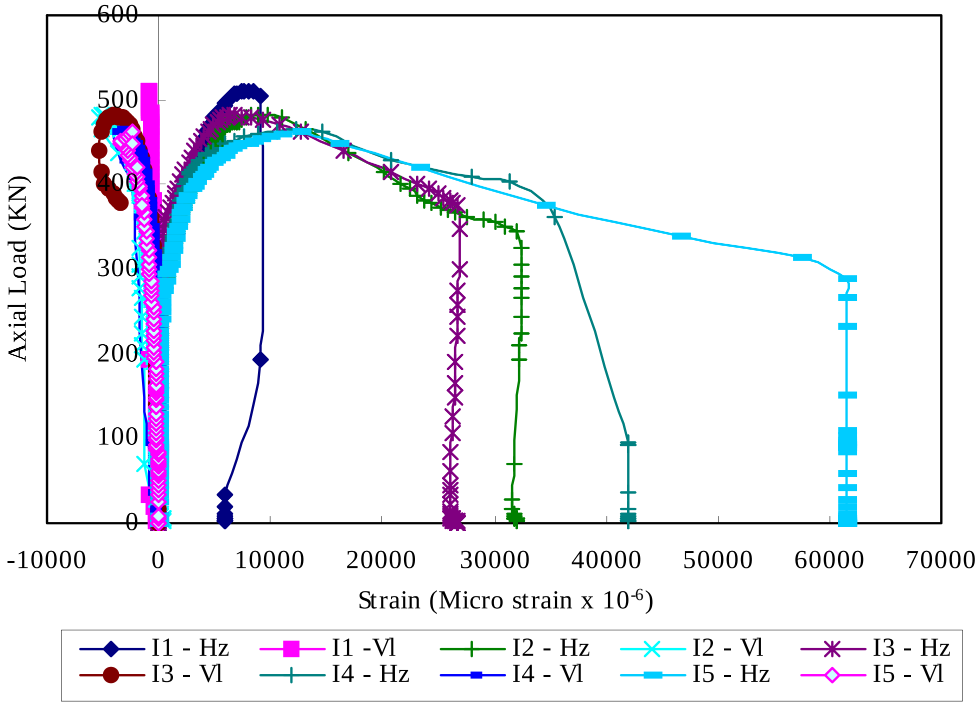

Figure 6.6: Load - strain curves for examined I- section – Long direction

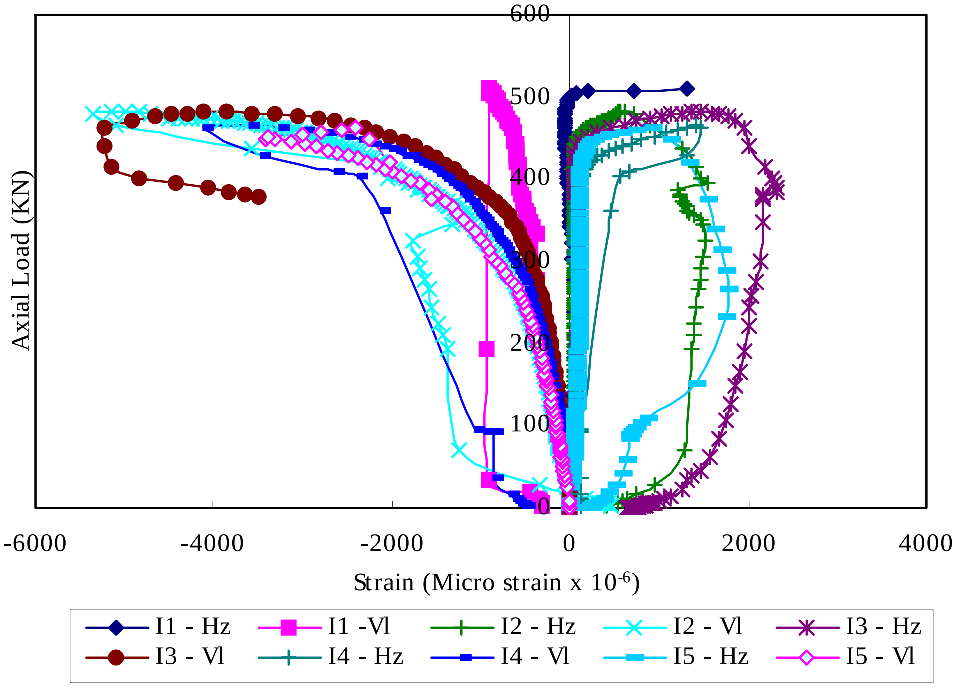

Figure 6.7: Load - strain curves for examined I- section – Short direction

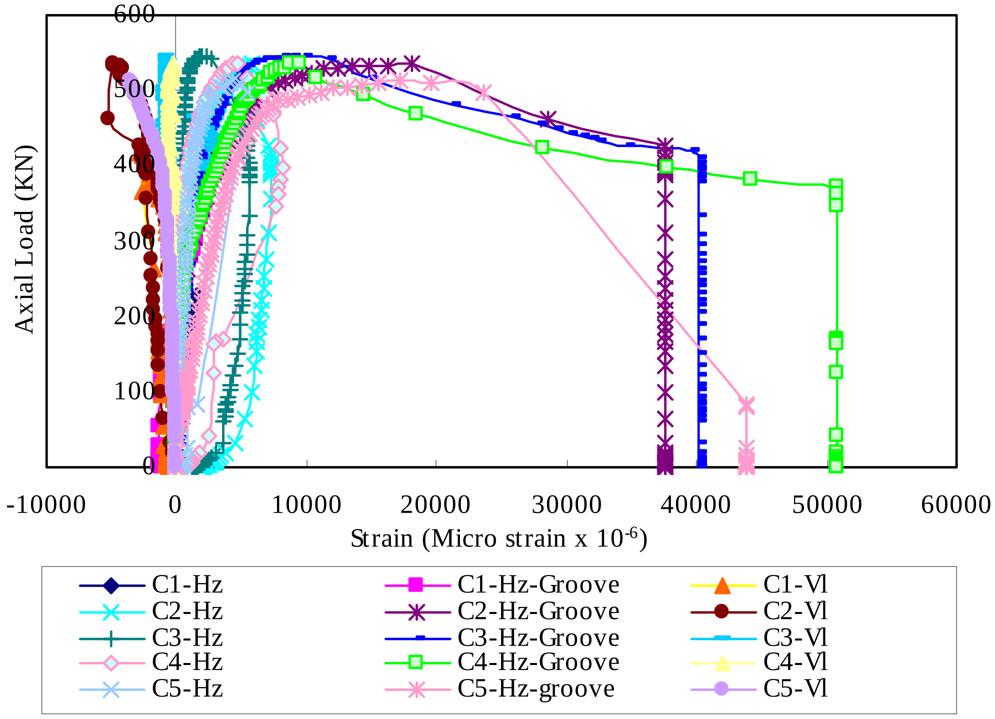

Figure 6.8: Load - strain curves for examined C- section – Long direction

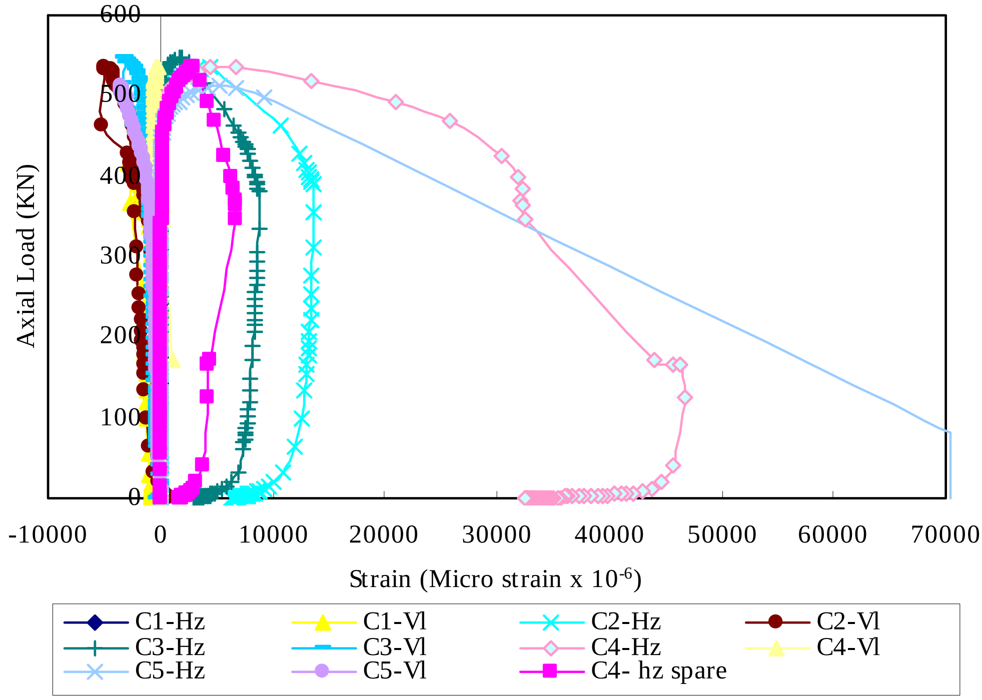

Figure 6.9: Load - strain curves for examined C- section – Short direction

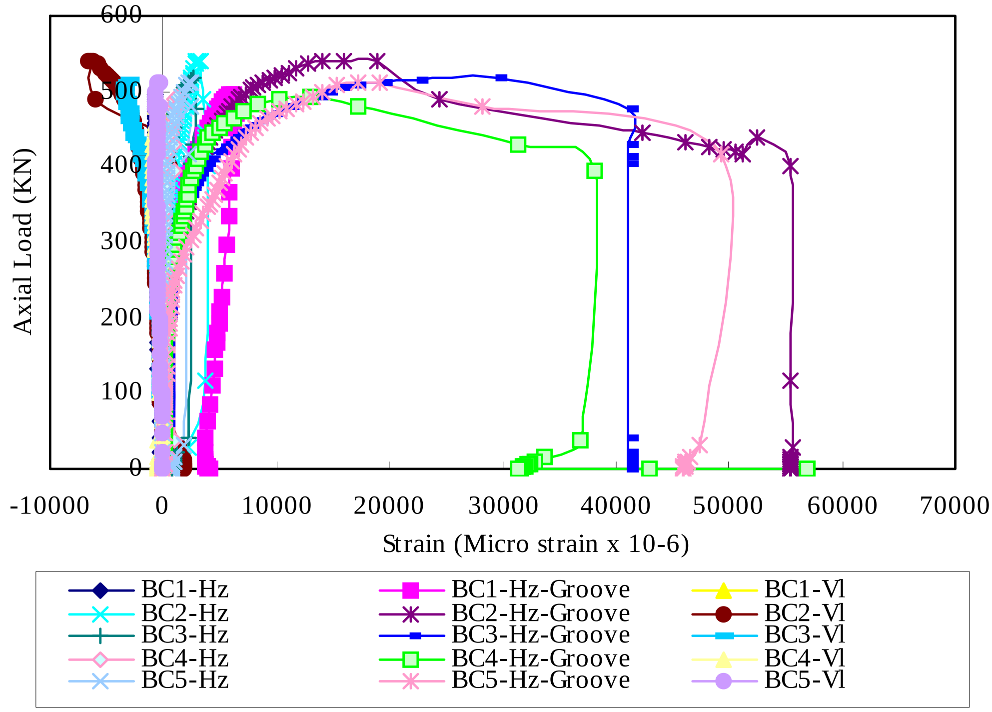

Figure 6.10: Load - strain curves for examined BC- section – Long direction

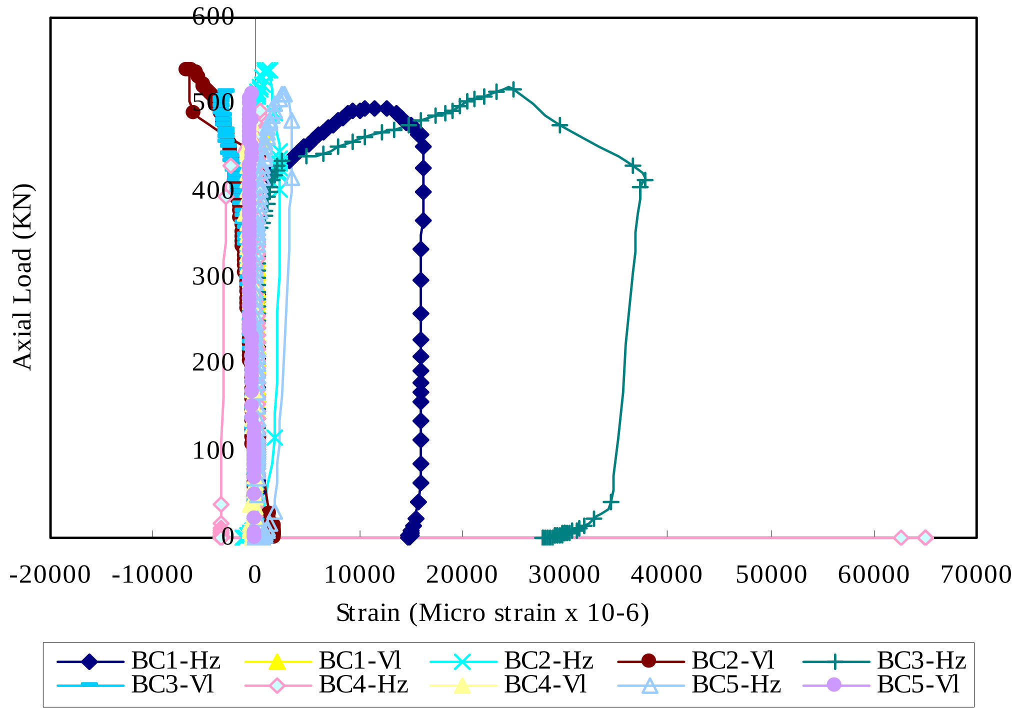

Figure 6.11: Load - strain curves for examined BC- section – Short direction

6.5 ESTIMATION OF ULTIMATE LOADING CAPACITY

Many researchers suggested different methods to predict the strength of fiber-confined concrete cylinders with reference to the well known equation proposed by Richart et al. (1928) as shown in Equation (6.1). The full wrapping condition will only be examined and analyzed for all the destructively examined specimens.

$$f_c' = f_{cu} + K.f_r \qquad (6.1)$$

Where,

f_c' = Strength of confined concrete

f_{cu} = Strength of unconfined concrete

f_r = confinement pressure

K = effectiveness coefficient, usually set between 2.0 to 4.1, according to the geometry and the experience of the designer, and can take one of the following formulas:

i- Fardis and Khalil (1982);

$$K = 3.7(f_r / f_{cu})^{-0.14} \qquad (6.2)$$

ii- Richart et al. (1928)

$$K = 6.7 f_r^{-0.17} \qquad (6.3)$$

iii- Toutanji (1999)

$$K = 3.5(f_r / f_{cu})^{-0.15} \qquad (6.4)$$

iv- Saafi et al. (1999)

$$K = 2.2(f_r / f_{cu})^{-0.16} \qquad (6.5)$$

While it was directly suggested by Miyauchi et al. (1999) to set "*K*" constant and equal to 3.5, Lam and Teng (2001) suggested "*K*" equal to 2.0 and again by Miyauchi et al. (2001) equal to 2.98.

6.5.1 Modeling of Circular Section

The mechanics of confinement is therefore dependent on two factors, the tendency of concrete to dilate and the radial stiffness of the confining member to restrain the dilation. Consequently, two conditions must be satisfied: 1) geometric (strain) compatibility between the core and the shell; and 2) equilibrium of forces in the free-body diagram for any sector of the confined section (Figure 6.12). The second condition leads to the following relationship between the confining pressure f_r, and the hoop stress f_j:

$$f_r = \frac{2 f_j t_j}{D} \tag{6.6}$$

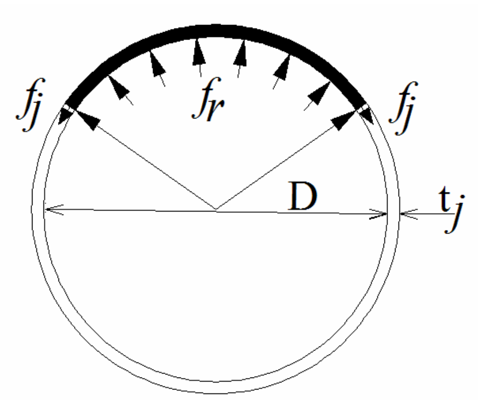

Figure 6.12: Confining model for circular section

$$f_j = E_{FRP} x \varepsilon_{FRP} \tag{6.7}$$

Where,

ε_{FRP} = Measured lateral strain during the experiment

E_{FRP} = Elastic modulus of CFRP sheet = 2.45 x 10^5 N/mm^2

By applying in Equation (6.7);

f_j = 10771 x 10^{-6} x 2.45 x 10^5 = 2638.9 N/mm^2

Thus,

f_r = 2 x 2638.9 x 0.111 / 100 = 5.86 N/mm^2

By applying in Equation (6.1);

Therefore,

$K = (f'_c - f_{cu}) / f_r$ = (49.25 – 20.13) / 5.86 = **4.97**

The effective coefficient (K) was found coinciding with values by other researchers;
By Fardis and Khalil (1982) → K = **4.40**
By Richart et al. (1928) → K = **4.96**
By Toutanji (1999) → K = **4.22**

Therefore, the applied model coincides with the experimental results as well as with models suggested by other researchers. It was then though that the same procedure will be applied for the rest of the specimens and a new expression for the value "K" will be suggested. It would therefore, be easy to predict the compressive strength of confined sections containing grooves.

6.5.2 Modeling of Rectangular Section

With the same procedure and as done with the circular section, a cross-section was taken on the mid-height of the rectangular section as shown in Figure 6.13. For simplicity of analysis, the confined pressure (f_r) will be taken constant along each side of the rectangular section. This assumption was found acceptable because the corners of the columns were sufficiently rounded with a fillet radius of 20 mm. Moreover, and from the experimental data, the measured strains in both sides were almost of same range which revealed to the smooth flow of forces along the CFRP sheet among the four sides of the tested prism.

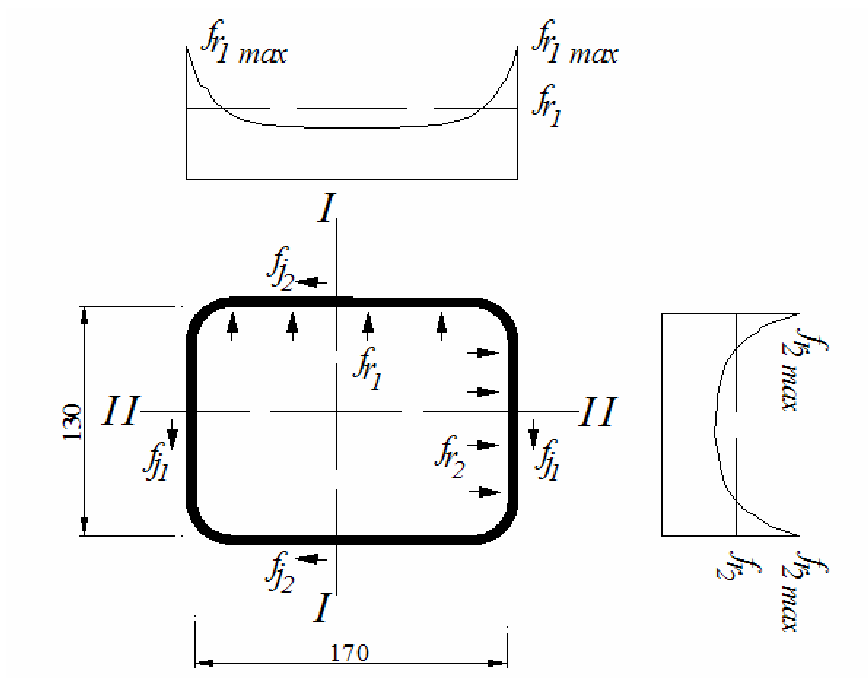

Figure 6.13: Confining model for rectangular section

The following are the specimen characterizations at peak load;
$\varepsilon_{FRP\ @\ ultimate\ load}$ (long side) = 6220 micro strain,
$\varepsilon_{FRP\ @\ ultimate\ load}$ (short side) = 7544 micro strain
$P_{ult.}$ = 516.00 KN,
$P_{confined}$ = 636.57 KN
f'_c = 29.20 N/mm^2 , and f_{cu} = 23.67 N/mm^2

Solving the free body diagram along the short side (Section I-I), the confinement pressure f_{r2} can be determined by the following equation;

$$f_{r2} = 2 \times f_{j2} \text{ / length of short side} \tag{6.8}$$

Therefore,
f_{r2} = 2 x 2.45 x 10^5 x 6220 x 10^{-6} x 0.111 / 130 = 2.60 N/mm/mm'

Applying in Equation (6.1);

K_2 = (29.20 - 23.67) / 2.60 = **2.13**

By applying the same procedure along the long side (Section II-II);

f_{r1} = 2 x 2.45 x 10^5 x 7544 x 10^{-6} x 0.111 / 170 = 2.41 N/mm/mm'

K_1 = (29.20 - 23.67) / 2.41 = **2.29**

This suggested the use of the model of Lam and Teng (2001) and Saafi et al. (1999) for rectangular section with aspect ratio equal to 0.76.

6.5.3 Modeling of I-section

The following are the specimen characterizations at peak load;
$\varepsilon_{FRP\ @\ ultimate\ load}$ (equal to the average strain along the grooved sides) = 9652.17 micro strain,
$\varepsilon_{FRP\ @\ ultimate\ load}$ (short side) = 620 micro strain
$P_{ult.}$ = 509.85 KN,
$P_{confined}$ = 482.79 KN
f'_c = 22.15 N/mm^2 , and f_{cu} = 23.39 N/mm^2

Solving the free body diagram along the short side (Section I-I), the confinement pressure f_{r2} can be given by the following equation;

$$f_{r2} = 2 \times f_{j2} \text{ / length of short side}$$

Therefore,

f_{r2} = 2 x 2.45 x 10^5 x 9652.17 x 10^{-6} x 0.111 / 130 = 4.04 N/mm/mm'

Applying in Equation (6.1);

K_2 = (22.15-23.39) / 4.04 = **- 0.31**

By applying the same procedure along the long side (Section II-II);

f_{r1} = 2 x 2.45 x 10^5 x 620 x 10^{-6} x 0.111 / 200 = 0.168 N/mm/mm'

K_1 = (22.15-23.39) / 0.168 = **- 7.38**

The obtained negative meaning has no meaning, which revealed to that the achieved load after strengthening is lesser than that with no confinement. The previous might be due to improper loading condition or error in the loading test. It was however suggested a minimal of 5% enhancement value and recalculate the confinement coefficient based on the new value based on the same strain values as an approximation.

Therefore,

f'_c = 24.56 N/mm^2

K_2= **0.29**, and K_1 = **6.96**

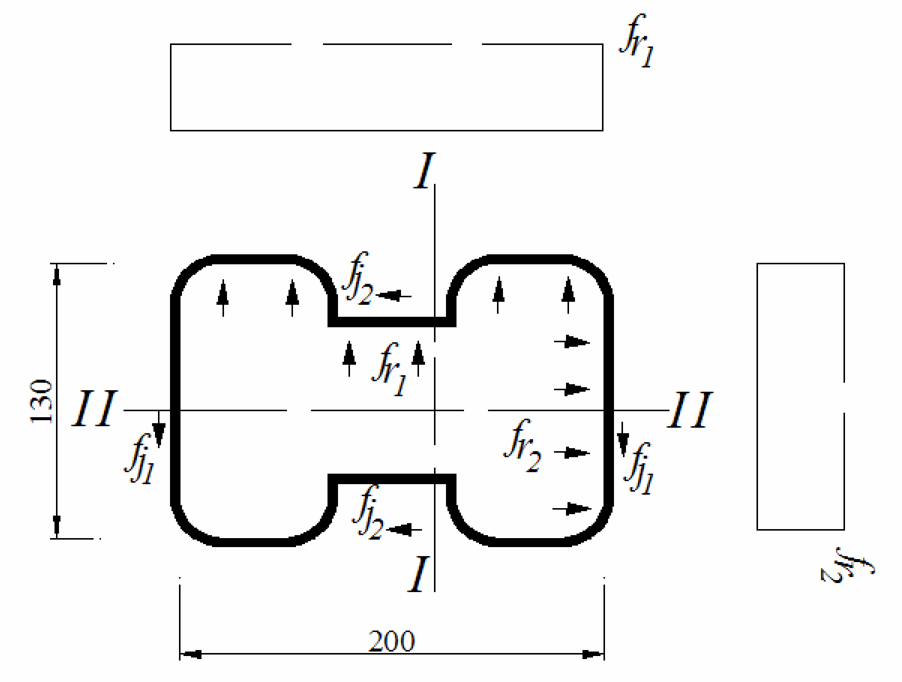

Figure 6.14: Confining model for I- section

6.5.4 Modeling of C-section

The following are the specimen characterizations at peak load;

$\varepsilon_{FRP\ @\ ultimate\ load}$ (average of both the grooved and the flat sides) = 11996.16 micro strain,

$\varepsilon_{FRP\ @\ ultimate\ load}$ (short side) = 4461.54 micro strain

$P_{ult.}$ = 417.45 KN,

$P_{confined}$ = 534.6 KN

$f'_c = 24.52\ N/mm^2$, and $f_{cu} = 19.15\ N/mm^2$

Solving the free body diagram along the short side (Section I-I), the confinement pressure f_{r2} can be given by the following equation;

$$f_{r2} = 2 \text{ x } f_{j2} \text{ / length of short side}$$

Therefore,

$f_{r2} = 2 \text{ x } 2.45 \text{ x } 10^5 \text{ x } 11996.16 \text{ x } 10^{-6} \text{ x } 0.111 / 130 = 5.02$ N/mm/mm'

Applying in Equation (6.1);

K_2 = (24.52-19.15) / 5.02 = **1.07**

By applying the same procedure along the long side (Section II-II);

$f_{r1} = 2 \text{ x } 2.45 \text{ x } 10^5 \text{ x } 4461.54 \text{ x } 10^{-6} \text{ x } 0.111 / 200 = 1.22$ N/mm/mm'

K_1 = (24.52-19.15) / 1.22 = **4.40**

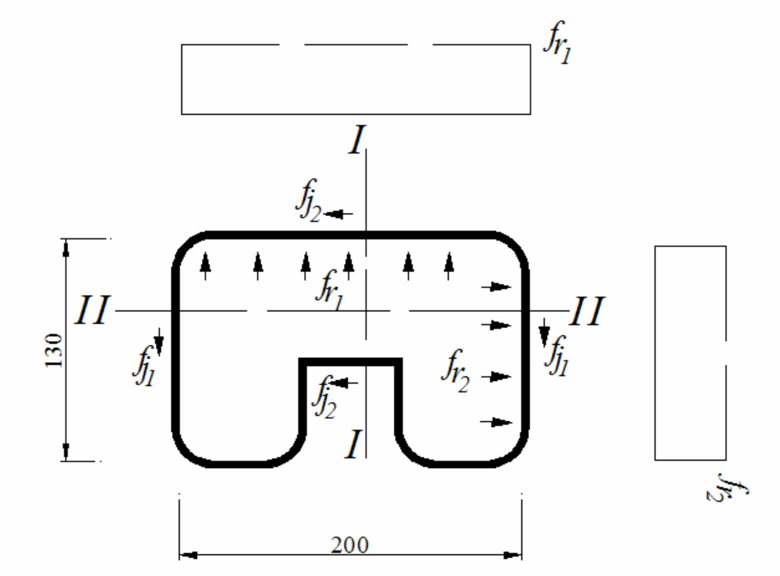

Figure 6.15: Confining model for C- section

6.5.5 Modeling of BC-section

The following are the specimen characterizations at peak load;

$\varepsilon_{FRP\ @\ ultimate\ load}$ (average of both the grooved and the flat sides) = 9576.59 micro strain,

$\varepsilon_{FRP\ @\ ultimate\ load}$ (short side) = 1337.5 micro strain

$P_{ult.}$ = 496.65 KN,

$P_{confined}$ = 539.22 KN

f'_c = 22.56 N/mm^2 , and f_{cu} = 20.78 N/mm^2

Solving the free body diagram along the short side (Section I-I), the confinement pressure f_{r2} can be given by the following equation;

$$f_{r2} = 2 \text{ x } f_{j2} \text{ / length of short side}$$

Therefore,

f_{r2} = 2 x 2.45 x 10^5 x 9576.59 x 10^{-6} x 0.111 / 130 = 4.01 N/mm/mm'

Applying in Equation (6.1);

K_2 = (22.56-20.78) / 4.01 = **0.44**

By applying the same procedure along the long side (Section II-II);

f_{r1} = 2 x 2.45 x 10^5 x 1337.5 x 10^{-6} x 0.111 / 200 = 0.36 N/mm/mm'

K_1 = (22.56-20.78) / 0.36 = **4.94**

6.6 ESTIMATION OF THE EFFECTIVENESS VALUE FOR GROOVED SECTIONS

From the previous analysis, two things were noted; 1) the smaller the "K" factor, the higher probability for failure to occur through this section, 2) the above mentioned effectiveness factor "K" for circular and rectangular sections are not applicable in the case of grooved sections; and thus an equivalent expression should be established.

It was also believed that the estimation of the ultimate load could only be based on the section where the crack could possibly occur (corresponding to the minimum "K"). The following analysis will be conducted or I-section column, after assuming 5% enhancement in the section loading capacity after wrapping, C-sections and BC-sections columns. It was suggested to carry the analysis based only on the section I-I which cuts the groove. In contrary, the possibility of crack to occur along section II-II is lower than section I-I and consequently the calculation will be based only on section I-I.

Equation (6.9) was suggested by Richart et al. (1928) to estimate the ultimate strength of confined columns. Many researchers have adjusted the effectiveness coefficient as per the confinement condition or the shape of the column. In this study, new effectiveness (K_{equiv}) coefficient was suggested and the formula was modified as follow;

$$f_c' = f_{cu} + K_{equiv} . f_r \tag{6.9}$$

$$K_{equiv} = f(n, A_{groove}, A_{total}) \tag{6.10}$$

Where,
n: number of existing grooves
A_{groove}: Area of grooves existing in the column
A_{total}: total area of column

The following equation was found best fitting C-column and BC-column for fully wrapped condition:

$$f_c' = f_{cu} + K.(\frac{1}{n})(\frac{A_{total} - A_{groove}}{A_{groove}})^{-0.43} f_r \tag{6.11}$$

Where K, is the effectiveness coefficient for an equivalent column with dimensions equal to the external dimensions of the grooved section. In this study, it was taken constant with a value equal to 2 for both sections (Lam and Teng, 2001)

The application of this to columns with I-section, C-section and BC-section gives an acceptable percentage error values 3.4%, 1.5%, and 4.2%, respectively. It was however, suggested to carry on the study on larger number of grooved columns to confirm the reasonability of Equation (6.11).

6.7 CONCLUSION

In this chapter, rectangular prisms containing grooves were tested under compressive loads. Different combinations of strengthening conditions were conducted. The following were among the important findings of this chapter:

(1) The efficiency of strengthening of circular columns by CFRP was much higher than rectangular columns.

(2) For grooved columns, the depth of groove has great influence on the section capacity of columns. Relatively the more the depth length, the higher the bonding efficiency; it is however noticed that the ratio between the depth of groove to the total depth of specimen play also important role; the higher the ratio, the higher the possibility to observe cracks

nearby the groove inner corners, and consequently the lower the load carrying capacity.

(3) The best assumption for the confinement coefficient "K" to calculate the ultimate load for CFRP wrapped concrete columns were 4 for circular columns, 2 for rectangular section with reasonable fillet radius, and a value less than 2 in case of grooved columns.

(4) New expression was suggested to predict the ultimate loads of grooved rectangular columns wrapped with CFRP.

(5) For grooved columns, the overall strength is not significantly affected by the variation in the strengthening condition.

(6) In general, the full specimen length wrapping followed by the strips confinement achieved the higher section loading capacity with reasonable ductility.

(7) As the ratio between the bearing plate of the machine and the cross-sectional area of the column increases, the loading efficiency decreases.

(8) For the same groove area, CFRP wrapping was more effective in cases where the groove was lumped in one side than cases where groove area was distributed on the two opposite sides.

CHAPTER 7

7. SUMMARY, CONCLUSION, AND RECOMMENDATIONS FOR FURTHER WORK

7.1 SUMMARY

Worldwide, concrete is considered one of the most widely used materials for construction purpose. In Egypt, concrete is being used in a broad range for residential, industrial, and hydraulic constructions. Many concrete structures in Egypt had already exceeded their designed life spans. For example, some concrete hydraulic structures have exceeded hundred years of age and still in operation up to date, other residential buildings are more than 50 years old. Thus, Egypt is now posing a big challenge for keeping their concrete structures healthy and extending their life time spans to a further longer time. It is also known that as the age of a structure increases, so do its maintenance and needs for repair. The very hot climate in arid and semi-arid regions along with various environmental and structural problems led to accelerate the deterioration of these structures. It can be generally said that, it is less expensive to maintain, repair, or even rehabilitate the deteriorated structure rather than to build a replacement structure. Thus, strengthening and retrofitting of the deteriorated structures are of great concern in both research and practical disciplines. Sufficient experience is also required for selecting the proper way and materials necessary for the repair.

Nowadays, Egypt is setting plans as well as encouraging researchers to conduct useful studies for strengthening and rehabilitation of deteriorated concrete structures in general and hydraulic structures in particular. The use of conventionally materials is no longer suitable, thus modern techniques should be adopted. The repairing materials should satisfy the following conditions: 1) preserve the geometry of the structures, 2) should not increase the weight of the structure, 3) should be compatible with the base material, 4) easy to apply, 5) should be of suitable cost.

In this thesis, engineered cementitious composites (ECC) was selected as repair material due to: ECC is one of the high performance fiber reinforced composites (HPFRC) having a pseudo tensile strain hardening behavior, ECC has a very high tensile strength along with high ductility. ECC has also many advantages such as protecting the reinforcement from corrosion due to the presence of very fine crack size and therefore enhances the durability of concrete structures. Moreover, ECC minimizes the penetration of water to the inner parts of the structure. Carbon fiber reinforced polymers (CFRP) was also used simultaneously in this study due to: CFRP have a very high strength to weight ratio, high resistance to corrosion and chemical attacks, ease of installation, and at the same time did not significantly affect the geometry of the structures.
The main objectives of the thesis were therefore to identify new ways for evaluating the concrete condition in situ as well as to investigate new and modern techniques for strengthening and

repairing of concrete structures. The study mainly concentrated on two main points: 1) utilizing the ultrasonic pulse velocity (UPV) test for detection of cracks in concrete, and 2) strengthening of different concrete elements using combinations of ECC, and CFRP sheets. The investigations involved the examination of selective structural elements such as; beams, columns, and arched specimens.

The study includes the development of a new technique for determining the size and position of embedded cracks in concrete structures. The new method is UPV test based. The new method depends on forming a single ellipse corresponding to each UPV reading. The generated ellipse is therefore considered a locus of points that can represent one edge of the crack. By solving equations of ellipses generated from different UPV readings, it would be easy to determine the crack edges. The method was found superior over the conventional used methods for crack detection due to; 1) the transducers can be placed over any available surfaces of the structure and not a must to be placed in a surface perpendicular to the crack plane, 2) the method is applicable along curved surfaces as well, and 3) the method is able to identify inclined and embedded cracks in concrete. The new method was experimentally verified by identifying surface crack in different sizes of plain concrete beams and arched specimen. The results were of acceptable values and were found comparatively better than those obtained by means of the conventional methods.

The study also utilized ECC for the purpose of strengthening of concrete beams. Comparison between ECC and CFRP for the purpose of strengthening of concrete beams was conducted. First, a group of beams were strengthened using ECC by partial replacement of concrete at the beam soffit with 10%, 30%, and 50% of the beam depth by ECC. Another group of beams was strengthened using the conventional CFRP sheets externally pasted at the soffit of beams. The results showed that beams strengthened with ECC were in general effective in enhancing the ductility with pure flexure mode of failure. It was also shown that the strength of the beam increased proportionally with the ECC thickness. Whereas, those strengthened directly with CFRP were able to achieve higher strength with the occurrence of the undesirable interfacial debonding mode of failure.

Furthermore, combinations to simultaneously use ECC and CFRP were conducted on both small scale prisms and large scale reinforced concrete beams. The study showed that both the ductility and strength of beams were significantly increased. It was also shown that pasting CFRP over a relatively thin layer of ECC, almost twice the covering depth in case of reinforced concrete beams, was found significant in decelerating or even preventing the interfacial debonding mode of failure. Moreover, the bonding strength between ECC and CFRP was studied, contrast between concrete and ECC strengthened with CFRP was also illustrated. The ductility of ECC along with the generation of many but very small size cracks prevented the stress concentration at the vicinity of cracks and consequently, the debonding mode of failure was minimized. For the brittle concrete, the stress concentration around the single developed crack allowed the debonding to start from nearby the crack position and continue directly till the cut-off position.

The study was also extended to use ECC as a repair material for initially cracked beams. Plain concrete beams with predefined crack located at the mid-span of the beams with depth equal to half the beam depth were prepared. The beams were mainly repaired by layers of ECC with different thickness placed over the crack position and extended to the beam supports. Further combinations of repair were done by pasting CFRP over the added ECC layer. The repair took place after 28 days of curing of the concrete beams. ECC was found superior in bridging the internal forces between the crack edges as well as restoring the beams to a condition better than their original state. The investigation also showed that the difference in the casting time of ECC and CFRP did not affect the repair. Additionally, good bonding between ECC and concrete was observed. The experiment ended-up with a recommendation to use a relatively small layer of ECC before the application of CFRP; this might be significantly effective in the field of repair and retrofitting of deteriorated structures.

CFRP sheets were used for strengthening of arched bridges. Scaled-down models typically used in Egypt for connecting piers of hydraulic structures were prepared. Different strengthening conditions including soffit, sides, and combination between both sides and soffit strengthening were conducted. The study showed that strengthening of arched bridges with soffit strengthening with a length equal to one third of the total soffit length was optimum in achieving high section capacity and increasing the member ductility as well. The sides strengthening mainly enhanced the structure ductility without significant increase in the structure loading capacity. Strut and tie models were also adopted in this study for determining the best locations to paste CFRP and to determine the expected failure mode corresponding to each combination.

Finally, CFRP was again used for strengthening of rectangular columns with grooves. These types of structures are often being seen in columns of bridges for architecture reasons as well as in hydraulic structures in positions of water logs. The discontinuities in the geometry of the column make it difficult to be wrapped with continuous fiber sheets.
Many researchers have been examined the behavior of confined cylinders with CFRP, few dealt with rectangular sections, but it was found that strengthening of rectangular columns with grooves had rarely been studied. In the study, prisms with different groove sizes and locations were prepared, different combinations for strengthening were suggested and the prisms were destructively examined. New expression was suggested for predicting the ultimate load of the confined columns with grooves.

7.2 CONCLUSIONS

The thesis ended-up with many useful conclusions that might be suitable for practical application; UPV was utilized for crack detection in concrete, combinations of ECC, and CFRP were found effective in enhancing the structural performance of the examined different concrete elements. The following are among the important findings of the thesis:

1- UPV test was used in new formulation to determine the location and size of cracks in concrete members.

2- The new UPV approach has many advantages over the conventionally used methods such as, the ability to place the transducers in different planes or along curved surfaces.

3- ECC and CFRP were first used alone to strengthen concrete beams. The tests showed that CFRP can increase significantly the loading capacity of beams while ECC was able to enhance the beam ductility with reasonable improvement to the loading capacity.

4- The bonding between ECC and CFRP was better than concrete and CFRP. This was utilized in using thin layer of ECC before strengthening of concrete beams with CFRP. This combination allowed having a section of higher section capacity and ductility at the same time.

5- Using thin layer of ECC before CFRP strengthening was able to prevent or delay the occurrence of the undesired debonding mode of failure of CFRP.

6- ECC was utilized for repairing of cracked concrete beams and was found excellent to bridge the internal forces among the crack edges. The repaired beams were restored to a condition better than their original condition.

7- In general, as ECC thickness laid at the soffit position of the beams increases, the ductility and beam flexure strength increase.

8- Strengthening of arched shape structures with CFRP was conducted. Different combinations such as soffit, sides, and combination between both sides and soffit strengthening were conducted.

9- For arched structures, soffit strengthening was good in achieving high section capacity while sides' strengthening was good in enhancing the section ductility. Combination between soffit and sides' strengthening was good in achieving both high loading capacity and ductility at the same time.

10- Different strengthening conditions for grooved columns with different shapes were examined. The strengthening showed that full wrapping followed by strips confinement were the best in achieving higher loading capacities.

11- New expression was introduced to estimate the ultimate loading capacity of grooved columns with CFRP wrapping. Comparison with other formulas suggested by some researchers for rectangular and circular columns was done as well.

7.3 RECOMMENDATIONS FOR FURTHER WORK

Further complementary studies should be done to evaluate the dynamic behavior of concrete elements to confirm the static results obtained during this research; it is thought that the dynamic analysis might give the same conclusions without destructive testing of the strengthened beams. Moreover, numerical analysis is also required for the purpose of increasing the number of the strengthening combinations and scale of structures as well as to compare the results with the laboratory test results. The following are among the necessary recommendations:

1- Application of UPV method in-situ with massive concrete sections.
2- Determination of correction factors if UPV method is applied under the water level.
3- Strengthening of full scale beams including higher shear reinforcement percentage with ECC and CFRP.
4- Application of dynamic analysis to determine the enhancement in the rigidity of beams strengthened with ECC non-destructively.
5- Studying the interfacial shear flow more deeply and set up governing equation to help prediction of the failure load.
6- Utilizing the ductile ECC for enhancing the dynamic behavior of massive hydraulic structures like dams against burst forces or heavy earthquakes.
7- Conduct further configurations with large scale columns confined with CFRP.
8- Conduction of a feasibility study for using ECC in developing countries.

CHAPTER 8

8. SUMMARY IN JAPANESE

まとめ

コンクリートは世界で最も幅広く使われている建設材料である。エジプトでもコンクリートは各種構造物に大規模に使われている。エジプトにおける多くのコンクリート構造物は既に設計寿命を越えており，あるコンクリート水利構造物の年数は百年を越えて現在までなお供用され，建築物も 50 年以上経過している。エジプトではこのようなコンクリート構造物を健全に保ち，さらに延命させるプロジェクトが提案されている。構造物の経過年数が増せばそれだけ維持管理と補修が必要になる。乾燥・半乾燥地域では様々な環境・構造的問題によってコンクリートの劣化が進行しやすい。一般的には劣化した構造物を更新するよりも維持管理し，補修・補強するほうが廉価であるので，劣化した構造物の補修・補強は研究及び実務上の関心事となっている。勿論，補強・補修に必要な材料と適切な手段を選ぶには豊かな経験が求められる。

今日，エジプトでは劣化した水利施設の補修・補強に必要な調査が計画実施されているが，ベース材料にマッチングし，適用しやすく，廉価である新しい技法を採用すべきである。このような意味から，本論文では，次の理由から ECC と CFRP を選んでいる；

① ECC は引張ひずみ硬化挙動を有する HPFRC の一つである。
② ECC は高い延性と共に高い引張強度を有する。
③ ECC はひび割れ分散性により鉄筋の腐食を抑制する。
④ コンクリート構造物の耐久性を高める。
⑤ ひび割れが発生しても透水性が抑制される。
⑥ CFRP は非常に高い強度重量比を有する。
⑦ CFRP は耐食性及び耐化学抵抗性が高い。
⑧ CFRP は適用が容易である。
⑨ ECC 及び CFRP とも構造物の形状への影響が少ない。

論文の主目的は，コンクリートの劣化状態を評価する新しい方法と，コンクリート構造物を補強・補修する新しい考え方を示すことである。研究は次の２点に重点をおいている；

１）コンクリート中のクラック位置を調べる UPV 試験
２）ECC と CFRP シートを組み合わせたコンクリート部材の補修・補強

研究ではコンクリート構造物中のクラックの大きさと位置を定める新しい方法を示した。これは UPV 読取値を１つの楕円方程式で表すもので，得られた楕円はクラックの一端を表す点を通る。複数の楕円方程式を連立させて解けば，クラックの両端を決めることができる。この方法はクラックの位置を決める従来の方法よりも以下の点で数段優れている；

① クラックに平行な面に発信・受信子を置かなくても適用できる。

② 曲面に沿っても適用できる。
③ コンクリート中の傾いたクラックも同定できる。

コンクリート梁の補強には ECC と，ECC 及び CFRP を併用した場合の比較も行った。先ず，一つの梁試験体グループの梁下端（ｼﾀﾊﾞ）の一部を ECC で梁深さの 10，30，50％置換した。もう一方の梁試験体グループは梁下端に CFRP シートを貼付け補強した。ECC 補強梁は，純曲げ破壊でかなり延性を示すことが分かった。さらに ECC の厚さに比例して梁の強度が増大することも分かった。一方，CFRP で直接補強された梁は接着面で剥離破壊を生じるものの，かなり高い強度を示すことが分かった。

ECC と CFRP を併用した実験を，サイズの小さい角柱供試体とサイズの大きい鉄筋補強コンクリート梁について行った。それによると梁の延性および強度ともかなり増大することが分かった。さらに鉄筋補強コンクリート梁の場合，かぶりのほぼ２倍の比較的薄い ECC 層に CFRP を貼り付けると接着面の剥離破壊をかなり抑制できることが分かった。また CFRP で補強されたコンクリートと ECC との間の違いも示された。多数で微細なクラックを生じる ECC の機能でクラック近傍の応力集中が抑制される結果，剥離破壊が極めて生じにくくなった。通常の脆性材料であるコンクリートの場合，１つのクラック周辺の応力集中は，クラック近傍から始まり端点まで直接続く剥離現象となってしまう。

初期段階からクラックに入った梁の補修材として ECC を用いたケースも検討した。梁の中央に梁高さの半分までクラックを入れた無筋コンクリート梁を作製し，クラック全体を ECC で覆う形で補修した。ECC と CFRP の組み合わせ補修も行った。補修は試験体の材齢 28 日に実施した。ECC はクラック端間の内部力を連結させ，梁を元の状態よりも強い状態に回復させることが分かった。さらに ECC と CFRP の貼付時期の違いは補修に影響せず，ECC とコンクリートは十分に結合することが分かった。CFRP を適用する前に ECC の比較的薄い層を適用したほうがよいことも分かった。このことは劣化した構造物の修復及び改修の点でかなり効果的であろう。

CFRP を溝付き矩形柱の補強にも適用した。この種の構造体は水に浸かる橋脚や水利構造物によく見かける。柱の幾何形状から連続した繊維シートの貼り付けは難しい。

CFRP を巻き付けた円柱の挙動研究は多くの研究者が行っており，また矩形断面の研究は若干見られるが，溝付き矩形柱の補強問題はほとんど研究されてきていない。本研究では，いろいろな場所にいろいろなサイズの溝を持つ角柱を作成し，いろいろな組み合わせの補強を考え，破壊試験を行った。そして溝付き角柱の限界荷重を予測する新しい推定式を提案した。

最後に，CFRP シートをアーチ形の橋の補強に使用した。エジプトでよく見られるアーチ形状を持った水利構造物をモデル化した。補強条件は，下端，両側，そして両側と下端の補強を組み合わせたモデルが実験に供された。全下端長さの 1/3 を補強したアーチ形橋は高い断面耐力と部材の延性を得るのに最適であった。両側の補強によって，載荷力はさほど大きくは成らなかったが構造的な延性が向

上した。CFRP 貼付最適位置の決定と各補強組み合わせに応じた破壊モードの推定にストラットータイモデルを適用した。

本論文では実用化できる多数の有益な結論を提示することができた。

① UPV はコンクリートのクラック探査に利用できる。

② ECC と CFRP の組み合わせ利用はいろいろなコンクリート部材の構造的な耐力を高めるのに効果的である。

本研究実験で得られた静的な実験結果を一層強固なものにするには，コンクリート部材の動的挙動の研究が必要である。動的解析によって補強された梁の破壊試験をせずとも同じ様な結論が得られると考えている。さらに，多様な補強組み合わせを増やし，構造物モデルのサイズを大きくし，その結果を実験室の試験結果と比較するために，数値解析も必要である。

REFERENCES

A. Caporale et al.: Limit analysis of masonry arches with externally bonded FRP reinforcements. Computer methods in applied mechanics and engineering, Vol. 196, pp. 247 – 260 (2006)

ACI Committee 211: Standard practice for selecting proportions for Normal, Heavyweight, Mass concrete (ACI 211.1-32), ACI manual of concrete practice (1982)

ASTM C 597-83: Test for Pulse Velocity Through Concrete. ASTM, U.S.A. (1991)

ASTM C 928/C 928M Standard Specification for Packaged, Dry, Rapid-Hardening Cementitious Materials for Concrete Repairs

ASTM C42 / C42M, Obtaining and Testing Drilled Cores and Sawed Beams of concrete, (2004)

ASTM, Standard test method for Flexural strength of concrete (using simple beam with third-point loading), C 78 – 02, and Standard test method for compressive strength of cylindrical concrete specimens, C 39/C 39 M – 03 (2004)

Alexander, A.M.,. "Impacts on a source of Acoustic Pulse-Echo Energy for Nondestructive testing of concrete structures", Technical report REMR-CS-40, U.S. Army Engineer Waterways Experiment Station, Vicksburg, MS., April (1993)

Ali Ural, Seref Oruc, Adam Dogangun, and O. Iskender Tuluk, "Turkish historical arch bridges and their deteriorations and failure" Engineering failure analysis, Vol. 15, pp. 43-53 (2008)

Amir M. Malek, Hamid Saadatmanesh and Mohammad R. Ehsani, "Prediction of Failure Load of R/C Beams Strengthened with FRP Plate Due to Stress Concentration at the Plate End", ACI Structural Journal, 95(1), pp. 142–152 (1998)

Amir Mirmiran and Mohsen Shahawy, "Behavior of Concrete Columns Confined by Fiber Composites", J. of Structural Engineering, ASCE, Vol. 123, No. 5, pp. 583 – 590 May (1997)

Aprile A, Spacone E, Limkatanyu S., "Role of Bond in RC Beams Strengthened with Steel and FRP Plates" ASCE, J. Structure Eng., 127, No. 12, 1445 – 1452 (2001)

B. Doran, H.O. Koksal, T. Turgay, "Nonlinear finite element modeling of rectangular of rectangular/square concrete columns confined with FRP", J. Materials and Design (2009) (Accepted). *Doi: 10.1016/J.matdes.2008.12.007*

B. Doran, “Numerical Simulation of conventional RC columns under concentric loading”, J. Materials and Design, (2008) (Accepted). *Doi: 10.1016/J.matdes.2008.08.033*

BS 1881-Part 203: Measurement of Velocity of Ultrasonic Pulses in Concrete. BSI, U.K.(1986)

Bo Gao, Jang-Kyo Kim and Christopher K.Y. Leung, “Strengthening Efficiency of Taper Ended FRP Strips Bonded to RC Beams”, Composites Science and Technology, 66, pp. 2257-2264 (2006)

Busby Associates, Inc., “Undersea vehicles directory”, Arlington, TX (1987)

Carino, Nicholas J., “Recent Developments in Nondestructive testing of concrete”, Advances in Concrete Technology, Canada center for mineral and Energy Technology, Ottawa, Canada, pp. 281 – 328, Jan. (1992)

Emmons, P. H., Concrete repair and maintenance illustrated, R.S. Means Co., Inc., Kingston, MA, pp. 295 (1993)

Fardis MN, Khalili H., “FRP-encased concrete as a structural material”, Magazine of construction Res., 34 (121), pp. 191 – 202 (1982)

G. Wu, Z.T. Lu, Z.S. Wu, “Strength and ductility of Concrete cylinders confined with FRP composites”, Composites and Building Material, 20, pp. 134 – 148, (2006)

G.J. Xiong, X. Jiang, J.W. Liu and L. Chen, “A Way for Preventing Tension Delamination of Concrete Cover in Midspan of FRP Strengthened Beams”, Construction and Building Materials, 21, pp. 402-408 (2007)

Giuseppe Campione, “Influence of FRP wrapping techniques on the compressive behavior of concrete prisms”, Cement and concrete composites, 28, 497 – 505 (2006)

Guide to Durable Concrete,” ACI 201.2R, “A Guide to the Use of Waterproofing, Dampproofing, Protective, and Decorative Barrier Systems for Concrete,” ACI 515.lR

Guoqiang Li, and Amanuel Ghebreyesus: Fast repair of damaged RC beams using UV curing FRP composites. Composite Structures, Vol. 72, pp. 105-110 (2006)

Hisham Y. Qasrawi, “Concrete strength by combined nondestructive methods simply and reliably predicted” Cement and Concrete Research, Vol. 30, pp. 739-746 (2000)

Houssam A. Toutanji, and William Gomez, “Durability Characteristics of Concrete Beams Externally Bonded with FRP Composite sheets” Cement and Concrete Composites, Vol. 19, pp. 351-358 (1997)

Islam, M.R., M.A. Mansur, M. Maalej, “Shear strengthening of RC deep beams using externally bonded FRP systems” Cem. & Conc. Composites, vol. 27, pp. 413-420 (2005)

J.F. Berthet, E. Ferrier, P. Hamelin, “Compressive behavior of concrete externally confined by compressive jackets. Part A: experimental study”, Construction and building materials, 19, pp. 223 – 232 (2005)

JCI TC952, Technical Report on continuous fiber reinforced concrete, JCI, September (1998)

Jun Zhang, Christopher K.Y. Lenung, Yin Nee Cheung, “Flexure Performance of Layered ECC-Concrete Composite Beam”, Composites Science and Technology, 66, 1501 – 1512, (2006)
Kajima Technical Research Institute, Japan: www.Kajima.co.jp/tech/katri/general/index.html

Keeney, C.A., “Procedures and Devices for Underwater cleaning of civil works structures”, Technical report REMR-CS-8, U.S. Army Engineer Water-ways experiment station, Vicksburg, MS, Nov (1987)

Koksal HO, Doran B, Ozsoy E, Alacah SN, “Nonlinear modeling of concentrically loaded reinforced blockwork masonry columns. Canadian J. Civil Eng, 31 (6), pp. 1012 – 1023 (2004)

Koksal HO, Karakoc C, Polat Z, Turgay T, Akgun S., “Evaluation of experimental procedures for confined concrete columns using 3D finite element analyses”, Computational methods and experimental measurements XIII, WIT transactions on modeling and simulation, WIT press 46, pp. 233 – 242, (2007)

Lam L, Teng JG, “A new stress-strain model for FRP-confined concrete”, Proceedings of the international conference on FRP composites in civil Engineering, Hong Kong, China, pp. 283 – 292, (2001)

Li C. Victor, “Reflections on the Research and Development of Engineered Cementitious Composites (ECC)”, Proceedings of the JCI International Workshop on Ductile Fiber Reinforced Cementitious Composites (DFRCC) – Application and Evaluation, pp. 1-21, (2002)

Li Victor, Lim YM, Foremsky DJ, “Interfacial Fracture Toughness of Concrete Repair Materials” Proceeding of the Fracture Mechanics of Concrete Structures II, 1329 – 1344 (1995)

Lim YM, Li Victor, “Durable Repair of Aged Infrastructures Using Trapping Mechanism of Engineered Cementitious Composites”, J. Cement and Conc. Comp., 19, No 4, 373 – 385, (1997) Maalej M., and Leong K.S., “Effect of beam size and FRP thickness on interfacial shear stress concentration and failure mode of FRP- strengthened beams”, Composites Science and Technology, vol. 65, pp. 1148-1158 (2005a)

Maalej M., Leong K.S., “Engineered Cementitious Composites for Effective FRP-Strengthening of RC beams” Composites Science and Technology, 65, pp. 1120–1128, (2005b)

Manish A. Kewalramani and Rajiv Gupta, “Concrete compressive strength prediction using ultrasonic pulse velocity through artificial neural networks”, Automation in Construction, Vol. 15, pp. 374-379 (2006)

Masato Abe, Toyota Fujioka, and Yoshifumi Nagata, “Location of a defect in a concrete block by a non-destructive technique”, J. Acoustic Science and Technology, Vol. 23, pp.308-312, June (2002)

Miyauchi K, Inoue S, Kuroda T, Kobayashi A., “Experimental study on the confinement effect of concrete cylinders confined by carbon fiber sheets”, Proceeding of Japan Concrete Institute, JCI, 23 (1), 865 – 870 (2001) (***in Japanese***).

Naaman, A.E. and Jeong, S.M., “Structural ductility of concrete beams with FRP tendons” Proceeding of the second international RILEM symposium on non-metallic reinforcement for concrete structures, pp. 379-386 (1995)

Neville A.M.: Properties of Concrete. Textbook, pp. 581-587 (1981)

Ogata, H., Hattori, K., and Hirashi, T, “Consideration of the Estimating Method of crack Depth of Concrete by USPV Method” JSIDRE, Japan, No. 246, Volume 74, pp. 833-839, December (2006) ***(in Japanese)***

Omar Chaallal, Mohsen Shahawy, and Munzer Hassan, “Performance of Axially Loaded short Rectangular Columns Strengthened with Carbon Fiber-Reinforced Polymer Wrapping”, Journal of Composites for Construction, Vol. 7, No.3, pp. 200-208, August (2003)

Popovics, S., and McDonald, W. E., “Inspection of the Engineering Condition of Underwater Concrete Structures”, Technical Report REMR-CS-9, U.S. Army Engineer Waterways Experiment Station, Vicksburg, MS., Apr. (1989)

Practices for Evaluation of Concrete in Existing Massive Structures for Service Conditions,” ACI 207.3R-94, 1994 (re-approved 2008).

Richart, F. E., Brandtzeaeg, A., and Brown, R. L., “A study of the failure of concrete under combined compressive stresses”, Engineering Experimental Station Bull. No. 85, University of Illinois, Urbana, I11, (1928)

S.T. Smith, J. G. Teng, “Interfacial Stresses in Plated Beams”, Eng. Structure, 23, pp. 857–871 (2001)

Saafi M, Toutanji HA, Li Z, “Behavior of concrete columns confined with fiber reinforced Polymer tubes”, ACI Struct J., 96(4), pp. 500–509, (1999)

Shamim, A. Sheikh, David DeRose, and Jamil Mardukhi, “Retrofitting of concrete structures for shear and flexure with Fiber-Reinforced Polymers, ACI Structural Journal, pp. 451-459, July – August (2002)

Shaun Hay, Kenton Thiessen, Dagmar Svecova, and Baidar Bakht, “Effectiveness of GFRP sheets for shear strengthening of timber”, J. of Composites for construction, ASCE, Volume 10, No.6, pp. 483-491, Nov./Dec., (2006)

Stowe, R. L., and Thornton, H. T., “Engineering Condition survey of Concrete in Service”, Technical Report REMR-CS-1, U.S. Army Engineer Waterways Experiment Station, Vicksburg, MS. Sep (1984)

TaeHoon Hong and Makarand Hastak, “Construction, Inspection, and Maintenance of FRP Deck Panels”, Journal of Composites for Construction, ASCE, Vol. 10, Number 6, pp. 561-572, November/December (2006)

Tawfik A. E., “Old, and new Esna Barrage and its hydro-power station”, Ministry of water resources and Irrigation, Egypt, July (2003) (in Arabic).

Tetsushi Kanda, Shiro Tomoe, Satoru Nagai, Makoto Maruta, Toshiyuki Kanakubo, “Full Scale Processing Investigation for ECC Pre-cast Structural Element”, Journal of Asian Architecture and Building Engineering, JAABE, 5(2), pp. 333–340, (2006).

Tetsushi Kanda, Tadashi Saito, Noburu sakata, Masanori Hiraishi, “Fundemental Properties of Direct Sprayed ECC”, JCI International Workshop on Ductile Fiber Reinforced Cementitious Composites (DFRCC) – Application and Evaluation, pp. 133-141, (2002).

Theriault M, Neale KW, Claude S. Fiber-reinforced polymer confined circular concrete columns investigation of size and slenderness effects. J Compos Constr, ASCE; 8(4): 323–31, (2004)

Thornton H.T., and Alexander, A.M., “Development of Nondestructive Testing systems for In Situ Evaluation of Concrete Structures”, Technical Report REMR-CS-10, U.S. Army Engineer

Waterways Experiment Station, Vicksburg, MS., Dec (1987)

Toshiro Kamada, Victor C. Li the effects of Surface Preparation on the Fracture Behavior of ECC/Concrete Repair System. Cement and Concrete Composites, 22, 423 – 431, (2000)

Toutanji HA., “Stress–strain characteristics of concrete columns externally confined with advanced fiber composite sheets” ACI Mater J;96(3):397–404, (1999)

U.S. Army Engineer corps, EM 385-1-1 Safety and Health Requirements Manual.

U.S. Army corps of Engineers, “Evaluation and repair of concrete structures”, (EM 1110-2-2002), Washington DC, June (1995)

Underwood S. and Y.R. Kim, “Determination of Depth of Surface Cracks in Asphalt Pavements”, J. of the Transportation Research Board, No. 1853, National Research Council, Washington, D.C., pp. 143-149 (2003)

V.M. Malhotra and N.J. Cairno, “Handbook on Non-Destructive Testing of Concrete”, CRC Press, Florida, pp. 169-188 (1991)

Waleed A. Thanoon, M.S. Jaafar, Razali A. Kadir, J. Noorzari, “Repair and Structural Performance of Initially Cracked Reinforced Concrete Slabs”. Construction and Building Materials, 19, 595 – 603, (2005).

Weisstein Eric W.: Ellipse. From MathWorld – A Wolfram Web Resource. http://mathworld.wolfram.com/Ellipse.html.

LIST OF PUBLICATIONS

A- Journal Papers

1- Anwar A. M., Hattori K., Ogata H., and Goyal A., "Evaluation of Using CFRP for Strengthening of Hydraulic Arched Structures" Cement Science and Concrete Technology, No. 61, Japan, pp. 509-516, 2007. [**Chapter 5**]

2- Anwar A. M., Hattori K., Ogata H., and Goyal A., "Crack Detection in Concrete Structure Using UPV test Incorporated Ellipse properties", Cement Science and Concrete Technology, No. 62, Japan, pp. 565-572, 2008. [**Chapter 2**]

3- A.M. Anwar, Hattori K., Ogata H, M. Ashraf, and Mandula, "Engineered Cementitious Composites for Repair of Initially Cracked Concrete Beams", Asian Journal of applied science, Vol. 2 (3), Malaysia, pp. 223-231, 2009. [**Chapter 4**]

4- Anwar A.M., Hattori, K., Ogata, H., Mandula "Comparative Study on Using CFRP with Both ECC and Concrete Substrates", J. of Housing and Building Research Center, HBRC, Egypt, Vol. 5, No. 1, April 2009, pp. 38 – 45. [**Chapter 3**]

B- Conference Papers

1- Anwar A.M., Hattori K., Ogata H., Ashraf M., and Goyal A., "Strut and Tie Model for Evaluation of Arch Structures Strengthened with CFRP", International Conference on Advances in Cement Based Materials and Applications to Civil Infrastructure, (ACBM-ACI), Lahore, Pakistan, December 12-14, 2007. [**Chapter 5**]

2- Anwar A.M., Hattori K., Ogata H., "Crack Detection in Concrete Structures – Their Strengthening Using CFRP", The First Egypt Japan International Symposium on Science and Technology, Tokyo, Japan, June 8-10, 2008. [**Chapter 2**]

3- Anwar A. M., Hattori K., and Ogata H., "Effect of ECC Thickness at Soffit of Concrete Beams before Strengthening With CFRP", Proceeding of the 3rd International Conference on Concrete Repair, Venice/Padua. Italy, 29th June to 2nd July 2009. [**Chapter 3**]

4- Anwar, A.M., Mandula, Hattori K., and Ogata H., "Utilizing ECC for better flexural performance of beams strengthened with CFRP", 63rd National conference of Japanese Society of Irrigation, Drainage and Reclamation Engineering, JSIDRE, Hiroshima, Japan, October 20-21, 2008. [**Chapters 3 & 4**]

LIST OF AWARDS

1- Rotary Yoneyama memorial Foundation, INC. Rotary Yoneyama Memorial Doctoral Course Scholarship（YD）from April 2009 – September 2010. (2^{nd} and 3^{rd} year PhD).

2- Tottori University Encouragement Fund for outstanding scientific performance and research achievements – 2008 (1^{st} year PhD).

3- EJISST2008 Award Certificate, June 2008, for an outstanding paper presented in the EJISST2008 conference. Awarded by the Culture, Education, and Science Bureau – The Embassy of Egypt in Japan.

4- The Kubuta Fund from Nihon Koei, financial subsidy from April 2008 – March 2009. (1^{st} year PhD).